

Continuous-Time Analog Circuits for Statistical Signal Processing

by

Benjamin Vigoda

Submitted to the Program in Media Arts and Sciences,
School of Architecture and Planning
in partial fulfillment of the requirements for the degree of

Doctor of Philosophy

at the

MASSACHUSETTS INSTITUTE OF TECHNOLOGY

September 2003

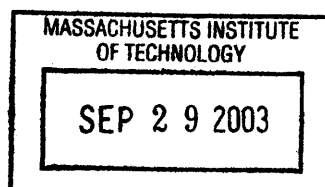
© Massachusetts Institute of Technology 2003. All rights reserved.

Author
Program in Media Arts and Sciences,
School of Architecture and Planning
August 15, 2003

Certified by
Neil Gershenfeld
Associate Professor
Thesis Supervisor

Accepted by
Andrew B. Lippman
Chair, Department Committee on Graduate Students

ROTCH



Continuous-Time Analog Circuits for Statistical Signal Processing

by

Benjamin Vigoda

Submitted to the Program in Media Arts and Sciences,
School of Architecture and Planning
on August 15, 2003, in partial fulfillment of the
requirements for the degree of
Doctor of Philosophy

Abstract

This thesis proposes an alternate paradigm for designing computers using continuous-time analog circuits. Digital computation sacrifices continuous degrees of freedom. A principled approach to recovering them is to view analog circuits as propagating probabilities in a message passing algorithm. Within this framework, analog continuous-time circuits can perform robust, programmable, high-speed, low-power, cost-effective, statistical signal processing. This methodology will have broad application to systems which can benefit from low-power, high-speed signal processing and offers the possibility of adaptable/programmable high-speed circuitry at frequencies where digital circuitry would be cost and power prohibitive.

Many problems must be solved before the new design methodology can be shown to be useful in practice: Continuous-time signal processing is not well understood. Analog computational circuits known as “soft-gates” have been previously proposed, but a complementary set of analog memory circuits is still lacking. Analog circuits are usually tunable, rarely reconfigurable, but never programmable.

The thesis develops an understanding of the convergence and synchronization of statistical signal processing algorithms in continuous time, and explores the use of linear and nonlinear circuits for analog memory. An exemplary embodiment called the Noise Lock Loop (NLL) using these design primitives is demonstrated to perform direct-sequence spread-spectrum acquisition and tracking functionality and promises order-of-magnitude wins over digital implementations. A building block for the construction of programmable analog gate arrays, the “soft-multiplexer” is also proposed.

Thesis Supervisor: Neil Gershenfeld
Title: Associate Professor

Continuous-Time Analog Circuits for Statistical Signal Processing

by Benjamin Vigoda

Dissertation in partial fulfillment of the degree of Doctor of Philosophy
at the Massachusetts Institute of Technology, September 2003

Benjamin Vigoda

Author

Program in Media Arts and Sciences

August 14, 2003

Neil Gershenfeld

Thesis Advisor

Professor of Media Arts and Sciences

MIT Media Laboratory

Hans-Andrea Loeliger

Thesis Reader

Professor of Signal Processing

Signal Processing Laboratory of ETH

Zurich, Switzerland

Anantha Chandrakasan

Thesis Reader

Associate Professor

Department of Electrical Engineering and Computer Science, MIT

Jonathan Yedidia

Thesis Reader

Research Scientist

Mitsubishi Electronics Research Laboratory

Cambridge, MA

Acknowledgments

Thank you to the Media Lab for having provided the most interesting context possible in which to conduct research. Thank you to Neil Gershenfeld for providing me with the direction opportunity to study what computation means when it is analog and continuous-time; a problem which has intrigued me since I was 13 years old. Thank you to my committee, Anantha Chandrakasan, Hans-Andrea Loeliger, and Jonathan Yedidia for their invaluable support and guidance in finishing the dissertation. Thank you to professor Loeliger's group at ETH in Zurich, Switzerland for many of the ideas which provide prior art for this thesis, for your support, and especially for your shared love for questions of time and synchronization. Thank you to the Physics and Media Group for teaching me how to make things and to our fearless administrators Susan Bottari and Mike Houlihan for their work which was crucial to the completion of the physical implementations described herein. Thank you to Bernd Schoner for being a role model and to Matthias Frey, Justin Dauwels, and Yael Maguire for your collaboration and suggestions.

Thank you to Saul Griffith, Jon Feldman, and Yael Maguire for your true friendship and camaraderie in the deep deep trenches of graduate school. Thank you to Bret Bjurstrom, Dan Paluska, Chuck Kemp, Nancy Loedy, Shawn Hershey, Dan Overholt, John Rice, Rob McCuen and the Flying Karamazov Brothers, Howard, Kristina, Mark, Paul and Rod for putting on the show. Thank you to my parents for all of the usual reasons and then some.

Much of the financial resources for this thesis were provided through the Center for Bits and Atoms NSF research grant number NSF CCR-0122419.

Contents

1	Introduction	25
1.1	A New Way to Build Computers	25
1.1.1	Digital Scaling Limits	25
1.1.2	Analog Scaling Limits	26
1.2	Statistical Inference and Signal Processing	27
1.3	Application: Wireless Transceivers	29
1.4	Road-map: Statistical Signal Processing by Simple Physical Systems .	31
1.5	Analog Continuous-Time Distributed Computing	32
1.5.1	Analog VLSI Circuits for Statistical Inference	33
1.5.2	Analog, Un-clocked, Distributed	34
1.6	Prior Art	39
1.6.1	Entrainment for Synchronization	39
1.6.2	Neuromorphic and Translinear Circuits	41
1.6.3	Analog Decoders	42
1.7	Contributions	43
1.7.1	Reduced Complexity Synchronization of Codes	43
1.7.2	Theory of Continuous-Time Statistical Estimation	44
1.7.3	New Circuits	45
1.7.4	Probabilistic Message Routing	45
2	Probabilistic Message Passing on Graphs	47
2.1	The Uses of Graphical Models	47
2.1.1	Graphical Models for Representing Probability Distributions .	47

2.1.2	Graphical Models in Different Fields	48
2.1.3	Factor Graphs for Engineering Complex Computational Systems	50
2.1.4	Application to Signal Processing	51
2.2	Review of the Mathematics of Probability	52
2.2.1	Expectations	52
2.2.2	Bayes' Rule and Conditional Probability Distributions	53
2.2.3	Independence, Correlation	53
2.2.4	Computing Marginal Probabilities	53
2.3	Factor Graph Tutorial	55
2.3.1	Soft-Inverter	56
2.3.2	Factor Graphs Represent a Factorized Probability Distribution	57
2.3.3	Soft-xor	58
2.3.4	General Soft-gates	60
2.3.5	Marginalization on Tree: The Message Passing Metaphor	61
2.3.6	Marginalization on Tree: Variable Nodes Multiply Incoming Messages	62
2.3.7	Joint Marginals	63
2.3.8	Graphs with Cycles	64
2.4	Probabilistic Message Passing on Graphs	66
2.4.1	A Lower Complexity Way to Compute Marginal Probabilities	66
2.4.2	The Sum-Product Algorithm	68
2.5	Other Kinds of Probabilistic Graphical Models	70
2.5.1	Bayesian Networks	71
2.5.2	Markov Random Fields	73
2.5.3	Factor Graphs	74
2.5.4	Forney Factor Graphs (FFG)	74
2.5.5	Circuit Schematic Diagrams	76
2.5.6	Equivalence of Probabilistic Graphical Models	76
2.6	Representations of Messages: Likelihood Ratio and Log-likelihood Ratio	79
2.6.1	Log-Likelihood Formulation of the Soft-Equals	79

2.6.2	Log-Likelihood Formulation of the Soft-xor	79
2.7	Derivation of Belief Propagation from Variational Methods	81
3	Examples of Probabilistic Message Passing on Graphs	83
3.1	Kalman Filter	83
3.2	Soft Hamming Decoder	86
3.2.1	Encoding	87
3.2.2	Decoding with Sum Product Algorithm	90
3.3	Optimization of Probabilistic Routing Tables in an Adhoc Peer-to-Peer Network	93
4	Synchronization as Probabilistic Message Passing on a Graph	101
4.1	The Ring Oscillator	101
4.1.1	Trellis Decoding for Ring Oscillator Synchronization	103
4.1.2	Forward-only Message Passing on the Ring Oscillator Trellis	106
4.2	Synchronization to a Linear Feedback Shift Register (LFSR)	108
4.2.1	LFSRs Generate PN-Sequences	108
4.2.2	Applications of LFSR Synchronization	110
4.3	Maximum Likelihood LFSR Acquisition	113
4.3.1	Trellis for Maximum-Likelihood LFSR Synchronization	113
4.3.2	Converting a the Trellis to a Factor Graph	114
4.3.3	The Sum Product (Forward-Backward) Algorithm on the LFSR Trellis	115
4.3.4	The Max Product (Viterbi's) Algorithm	117
4.4	Low-Complexity LFSR Acquisition	117
4.4.1	The LFSR Shift Graph	117
4.4.2	"Rolling Up the Shift Graph: The Noise Lock Loop	118
4.4.3	Performance of the Noise Lock Loop (NLL)	119
4.5	Joint Marginals Generalize Between the NLL and the trellis	121
4.6	Scheduling	126
4.7	Routing	127

5	Analog VLSI Circuits for Probabilistic Message Passing	131
5.1	Introduction: The Need for Multipliers	131
5.2	Multipliers Require Active Elements	133
5.3	Active Elements Integrated in Silicon: Transistors	135
5.3.1	BJTs	135
5.3.2	JFETs	136
5.3.3	MOSFETs	137
5.4	Single-Quadrant Multiplier Circuits	138
5.4.1	Multiply by Summing Logarithms	138
5.4.2	Multiply by Controlling Gain: The Differential Pair	139
5.5	General Theory of Multiplier Circuits	141
5.5.1	Nonlinearity Cancellation	141
5.5.2	The Translinear Principle	145
5.5.3	Companding Current-Mirror Inputs	146
5.6	Soft-Gates	147
5.7	Figures of Merit	148
5.7.1	Resolution and Power Consumption of Soft-Gates at 1GHz	151
6	The Sum Product Algorithm in Continuous-Time	155
6.1	Differential Message Passing	155
6.1.1	Damping	157
6.1.2	Von Neuman Stability Analysis of Finite Differences	157
6.1.3	Filtering Probabilities and Likelihoods is Equivalent to Damping	160
6.1.4	Filtering Log-Likelihoods	161
6.2	Analog Memory Circuits for Continuous-Time Implementation	162
6.2.1	Active Low-Pass Filters	164
6.3	Continuous-Time Dynamical Systems	166
6.3.1	Simple Harmonic Oscillators	166
6.3.2	Ring Oscillator	168
6.3.3	Continuous-Time LFSR Signal Generator	169

6.4	Continuous-Time Synchronization by Injection Locking as Statistical Estimation	174
6.4.1	Synchronization of Simple Harmonic Oscillator by Entrainment	174
6.4.2	Noise Lock Loop Tracking by Injection Locking	177
7	Systems	183
7.1	Extending Digital Primitives with Soft-Gates	183
7.1.1	Soft-Multiplexer (soft-MUX)	184
7.1.2	Soft Flip-Flop	186
7.2	Application to Wireless Transceivers	191
7.2.1	Conventional Wireless Receiver	191
7.2.2	Application to Time-Domain (Pulse-based) Radios	194
8	Biographies	201
8.1	Anantha P. Chandrakasan, MIT EECS, Cambridge, MA	201
8.2	Hans-Andrea Loeliger, ETH, Zurich, Switzerland	202
8.3	Jonathan Yedidia, Mitsubishi Electronics Research Lab, Cambridge, MA	202
8.4	Neil Gershenfeld, MIT Media Lab, Cambridge, MA	203
8.5	Biography of Author	204

List of Figures

1-1	Analog, distributed and un-clocked design decisions reinforce each other	35
1-2	A design space for computation. The partial sphere at the bottom represents digital computation and the partial sphere at the top represents our approach.	39
1-3	Chaotic communications system proposed by Mandal et al. [30] . . .	41
2-1	Gaussian distribution over two variables	48
2-2	Factor graph for computer vision	49
2-3	Factor graph model for statistical physics	50
2-4	Factor graph for error correction decoding	51
2-5	Visualization of joint distribution over random variables x_1, x_2, x_3 . .	54
2-6	Visualization of marginalization over random variables x_2, x_3 to find $p(x_1 = 1)$	55
2-7	Visualization of marginalization over 2-dimensional gaussian distribution	56
2-8	Factor graph expressing that binary variables x and y are constrained to be opposite in value	56
2-9	Factor graph expressing that binary variables $x, y,$ and z are constrained to sum to zero mod 2	59
2-10	Factor graph with more than one kind of constraint node	61
2-11	Factor graph containing a variable node more than one incident edge	62
2-12	Factor graph with incomplete marginalization leaving a “region” node: The basis of Generalized Belief Propagation	63
2-13	Factor graph with a frustrated cycle	65

2-14	Factor graph with a frustrated cycle and a local evidence node	65
2-15	Simple acyclic graph	66
2-16	Left to right: factor graph, MRF, Bayesian network	70
2-17	The fictional “Asia” example of a Bayesian network, taken from Lauritzen and Spiegelhalter 1988	71
2-18	Message passing with a single equals gate	75
2-19	Converting a factor graph to a pairwise MRF	76
2-20	Converting a a factor graph to a Bayesian network	77
2-21	Converting a MRF to a factor graph	78
2-22	Converting a Bayesian network to a factor graph	78
3-1	System state update	84
3-2	System state update combined with measurements	84
3-3	Kalman filter update	85
3-4	A communications system	86
3-5	Graph representing the codeword constraints	89
3-6	Graph representing the same codeword constraints	89
3-7	Mod 2 sum	90
3-8	Receiver graph implementing the codeword constraints	91
3-9	Symbol for the soft-xor gate	91
3-10	Random ad hoc peer-to-peer network. There are four interfaces $\{1, 2, 3, 4\}$ on nodes 1 and 4, and three interfaces $\{1, 2, 3\}$ on nodes 2 and 3.	93
3-11	Factor graph derived from ad hoc peer-to-peer network.	97
3-12	Factor graph derived from ad hoc peer-to-peer network. There are four interfaces $\{1, 2, 3, 4\}$ on nodes 1 and 4, and three interfaces $\{1, 2, 3\}$ on nodes 2 and 3.	98
4-1	Schematic diagram for a ring (relaxation) oscillator	102
4-2	Factor graph for a ring (relaxation) oscillator	102
4-3	Factor graph for trellis for synchronization of a ring oscillator	103
4-4	Trellis section for a ring oscillator	104

4-5	Factor graph for transmit and receive ring oscillators	107
4-6	4-bin, 2-tap LFSR	108
4-7	State cycle of a 4-bin, 2-tap LFSR	110
4-8	Mod 2 sum	111
4-9	DS/CDMA <i>modulation</i> with PN-sequence generated by an LFSR . .	113
4-10	DS/CDMA <i>demodulation</i> with PN-sequence generated by an LFSR .	113
4-11	Trellis section for a 4-bin, 2-tap LFSR	114
4-12	Factor graph for a trellis	115
4-13	Shift graph for a linear feedback shift register	118
4-14	Forward-only message passing on shift graph for a linear feedback shift register	119
4-15	Section of the shift graph for a linear feedback shift register	120
4-16	System to recursively implement section of the shift graph	120
4-17	The Noise Lock Loop (NLL)	121
4-18	The Noise Lock Loop (NLL)	122
4-19	2 time-step joint message on the LFSR shift graph	123
4-20	3 time-step joint message on the LFSR shift graph (recovers the trellis)	124
4-21	Block diagram for a binary counter	128
4-22	Shift graph for a binary counter	129
5-1	Signal consisting of successive analog samples represented by, respec- tively, NRZ analog levels with smooth transitions, RZ analog levels with a soliton-like waveform, and RZ antipodal soliton waveforms . .	132
5-2	Resistor divider performs scalar multiplication, $V_{out} = V_{in}(R_1/R_1 + R_2)$.	133
5-3	Bipolar Transistors	135
5-4	MOSFET transistors	137
5-5	Logarithmic Summing Circuit	138
5-6	Logarithmic Summing Circuit	139
5-7	Differential pair	140
5-8	multiplier using a nonlinearity	142

5-9	operational transconductance amplifier (OTA)	142
5-10	OTA with additional bias current i_2	143
5-11	Controlling i_2 from v_2	143
5-12	cancelling k_2v_1 with a third transconductor	144
5-13	fully differential design	144
5-14	Translinear Loop Circuit	146
5-15	Current Controlled Current Divider	146
5-16	Gilbert Multiplier Implements Softxor Function	147
5-17	Modified Gilbert Multiplier Implements Softequals Function	148
5-18	2 transistor multiply single-quadrant multiply (component of a soft-gate)	152
6-1	A two-tap FIR filter with tap weights a_1 and a_2	160
6-2	Schematic of sample-and-hold delay line circuit	163
6-3	Sample-and-hold delay line circuit operating on sinusoidal signal	163
6-4	Spice simulations of serial delay line composed of 10 Chebyshev filters	165
6-5	Oscilloscope traces of input to (top) and output from (bottom) a fifth order Chebychev filter delay line	166
6-6	Schematic diagram of Chebychev continuous-time delay circuit	166
6-7	Poles of Chebychev delay filter	167
6-8	Frequency response of Chebychev delay filter	168
6-9	Phase response of Chebychev delay filter	169
6-10	Group delay of Chebychev delay filter	170
6-11	“W” shaped (nonlinear) energy potential with ball trapped in one minima	170
6-12	Continuous-time LFSR	171
6-13	Output of continuous-time LFSR circuit	171
6-14	Continuous-time LFSR circuit with mapper and limiter	172
6-15	Block diagram of noise lock loop (NLL) transmit system	172
6-16	Output of filter 1 and XOR in NLL transmit system	173
6-17	Phase space lag plot of output of filter1 in NLL transmit system	174
6-18	Factor graph for two coupled simple harmonic oscillators	176

6-19	Block diagram of noise lock loop (NLL) receiver system	178
6-20	Performance of NLL and comparator to perform continuous-time estimation of transmit LFSR in AWGN. The comparator (second line) makes an error where the NLL (third line) does not. The top line shows the transmitted bits. The fourth line shows the received bits with AWGN. The fifth line shows the received bits after processing by the channel model. The other lines below show aspects of the internal dynamics of the NLL.	180
6-21	Block diagram of Spice model of noise lock loop (NLL) receiver system	181
7-1	One bit multiplexer	184
7-2	A modified soft-and gate for the soft-MUX	186
7-3	RS flip flop	187
7-4	D flip-flop	187
7-5	Edge-triggered D flip-flop	188
7-6	Time course of outputs Q and \bar{Q} with inputs $(R,S) = (1,1)$ and initial internal states = $(.5,.5)$	189
7-7	Time course of outputs Q and \bar{Q} with inputs $(R,S) = (1,0)$ and initial internal states = $(.5,.5)$	190
7-8	Time course of outputs Q and \bar{Q} with inputs $(R,S) = (0,1)$ and initial internal states = $(.5,.5)$	191
7-9	Time course of outputs Q and \bar{Q} with inputs $(R,S) = (.5,.5)$ and initial internal states = $(.5,.5)$	192
7-10	Map of final output Q for all possible inputs (R,S) and initial internal states = $(1,1)$	193
7-11	Map of final output Q for all possible inputs (R,S) and initial internal states = $(0,1)$	193
7-12	Map of final output Q for all possible inputs (R,S) and initial internal states = $(1,0)$	194

7-13	Map of final output Q for all possible inputs (R,S) and initial internal states = $(0,0)$	194
7-14	Map of final output Q for all possible inputs (R,S) and initial internal states = $(.5,.5)$	195
7-15	Conventional radio receiver signal chain	195
7-16	Conceptual sketch of CT softgate array in a radio receiver	196
7-17	Time-domain (pulse) radio communications system	197
7-18	Chaotic communications system proposed by Mandal et al. [30]	197
8-1	Benjamin Vigoda	204

“From discord, find harmony.”

-Albert Einstein

“It’s funny funny funny how a bear likes honey,
Buzz buzz buzz I wonder why he does?”

-Winnie the Pooh

Chapter 1

Introduction

1.1 A New Way to Build Computers

This thesis suggests a new approach to building computers using analog, continuous-time electronic circuits to make statistical inferences. Unlike the digital computing paradigm which presently monopolizes the design of useful computers, this new computing methodology does not abstract away from the continuous degrees of freedom inherent in the physics of integrated circuits. If this new approach is successful, in the future, we will no longer debate about “analog vs. digital” circuits for computing. Instead we will always use “continuous-time statistical” circuits for computing.

1.1.1 Digital Scaling Limits

New paradigms for computing are of particular interest today. The continued scaling of the digital computing paradigm is imperiled by severe physical limits. Global clock speed is limited by the speed-of-light in the substrate, power consumption is limited by quantum mechanics which determines that energy consumption scales linearly with switching frequency $E = hf$ [18], heat dissipation is limited by the surface-area-to-volume ratio given by life in 3-dimensions, and on-off ratios of switches (transistors) are limited by the classical (and eventually quantum) statistics of fermions (electrons).

But perhaps the most immediate limit to digital scaling is an engineering limit not

a physical limit. Designers are now attempting to place tens of millions of transistors on a single substrate. In a digital computer, every single one of these transistors *must* work perfectly or the entire chip must be thrown away. Building in redundancy to avoid catastrophic failure is not a cost-effective option when manufacturing circuits on a silicon wafer, because although doubling every transistor would make the overall chip twice as likely to work, it comes at the expense of producing half as many chips on the wafer: a zero-sum game. Herculean efforts are therefore being expended on automated design software and process technology able to architect, simulate and produce so many perfect transistors.

1.1.2 Analog Scaling Limits

In limited application domains, analog circuits offer solutions to some of these problems. When performing signal processing on a smooth waveform, digital circuits must, according to the Nyquist sampling theorem, first discretize (sample) the signal at a frequency twice as high as the highest frequency component that we ever want to observe in the waveform [37]. Thereafter, all downstream circuits in the digital signal processor must switch at this rate. By contrast, analog circuits have no clock. An analog circuit transitions smoothly with the waveform, only expending power on fast switching when the waveform itself changes quickly. This means that the effective operating frequency for analog circuit tends to be lower than for a digital circuit operating on precisely the same waveform. In addition, a digital signal processor represents a sample as a binary number, requiring a separate voltage and circuit device for every significant bit while an analog signal processing circuit represents the waveform as a single voltage in a single device. For these reasons analog signal processing circuits tend to use ten to a hundred times less power and several times higher frequency waveforms than their digital equivalents. Analog circuits also typically offer much greater dynamic range than digital circuits.

Despite these advantages, analog circuits have their own scaling limits. Analog circuits are generally not fully modular so that redesign of one part often requires redesign of all the other parts. Analog circuits are not easily scalable because a new

process technology changes enough parameters of some parts of the circuit that it triggers a full redesign. The redesign of an analog circuit for a new process technology is often obsolete by the time human designers are able to complete it. By contrast, digital circuits are modular so that redesign for a new process technology can be as simple as redesigning a few logic gates which can then be used to create whatever functionality is desired. Furthermore, analog circuits are sometimes tunable, rarely reconfigurable and never truly programmable so that a single hardware design is generally limited to a single application. The rare exception such as “Field-Programmable Analog Arrays”, tend to prove the rule with limited numbers of components (ten or so), low-frequency operation (10-100kHz), and high power consumption limiting them to laboratory use.

Perhaps most importantly, analog circuits do not benefit from device scaling the same way that digital circuits do. Larger devices are often used in analog even when smaller devices are available in order to obtain better noise performance or linearity. In fact, one of the most ubiquitous analog circuits, the analog-to-digital converter has lagged far behind Moore’s Law, doubling in performance only every 8 years [47]. All of these properties combine to make analog circuitry expensive. The trend over the last twenty to thirty years has therefore been to minimize analog circuitry in designs and replace as much of it as possible with digital approaches. Today, extensive analog circuitry is only found where it is mission critical, in ultra-high-frequency or ultra-low-power signal processing such as battery-powered wireless transceivers or hearing aids.

1.2 Statistical Inference and Signal Processing

Statistical inference algorithms involve parsing large quantities of noisy (often analog) data to extract digital meaning. Statistical inference algorithms are ubiquitous and of great importance. Most of the neurons in your brain and a growing number of CPU cycles on desk-tops are spent running statistical inference algorithms to perform compression, categorization, control, optimization, prediction, planning, and learning.

The data set would consist of a long character string drawn from an alphabet of 4 symbols $\{G, C, T, A\}$ along with (hopefully) confidence information indicating how accurate each symbol in the string is thought to be. For example we may be given a DNA data set measured from a gene sequencer:

DNA Sequence:	T	A	T	A	T	G	G	G	C	G	...
Measurement certainty:	.9	.9	.9	.9	.1	.9	.9	.9	.9	.9	...

The goal of inference is to look for subsequences or groups of subsequences within this data set which code for a protein. For example we might be looking for a marker which identifies a gene such as “TATAA”. In the case, we can see from inspection that it is quite likely that this gene marker is present in the DNA measurements.

An inference algorithm is able to do this, because it has a template or *model* that encodes expectations about what a protein subsequence looks like [26]. The algorithm compares its model to the measured data to make a digital decision about which protein was seen or if a protein was seen. A model is often expressed in terms of a set of constraints on the data. Statistical inference is therefore actually a constraint satisfaction problem. Recent work in machine learning and signal processing has led to the generalization of many of these algorithms into the language of probabilistic message passing algorithms on *factor graphs*.

Increasingly, digital signal processors (DSP) are being called upon to run statistical inference algorithms. In a DSP, an analog-to-digital converter (ADC) first converts an incoming analog waveform into a time-series of binary numbers by taking discrete samples of the waveform. Then the processor core of the DSP applies the model to the sampled data.

But the ADC in effect makes digital decisions about the data, before the processor core applies the model to analyze the data. In so doing the ADC creates a huge number of digital bits which must be dealt with, when really we are only interested in a few digital bits - namely the answer to the inference problem.

The ADC operates at the interface between analog information coming from the world and a digital processor. One might think that it would make more sense to apply

the model before making digital decisions about it. We could envision a smarter ADC which incorporates a model of the kind of signals it is likely to see into its conversion process. Such an ADC could potentially produce a more accurate digital output while consuming less resources. For example, in a radio receiver, we could model the effects of the transmitter system on the signal such as compression, coding, and modulation and the effect of the channel on the signal such as noise, multi-path, multiple access interference (MAI), etc. We might hope that the performance of the ADC might then scale with the descriptive power (compactness and generality) of our model.

1.3 Application: Wireless Transceivers

In practice replacing digital computers with an alternative computing paradigm is a risky proposition. Alternative computing architectures, such as parallel digital computers have not tended to be commercially viable, because Moore's Law has persistently enabled conventional von Neumann architectures to render alternatives unnecessary. Besides Moore's Law, digital computing also benefits from mature tools and expertise for optimizing performance at all levels of the system: process technology, fundamental circuits, layout and algorithms. Many engineers are simultaneously working to improve every aspect of digital technology, while alternative technologies like analog computing do not have the same kind of industry juggernaut pushing them forward. Therefore, if we want to show that analog, continuous-time, distributed computing can be viable in practice, we must think very carefully about problems for which it is ideally well-suited.

There is one application domain which has persistently resisted the allure of digital scaling. High-speed analog circuits today are used in radios to create, direct, filter, amplify and synchronize sinusoidal waveforms. Radio transceivers use oscillators to produce sinusoids, resonant antenna structures to direct them, linear systems to filter them, linear amplifiers to amplify them, and an oscillator or a phase-lock loop to synchronize them. Analog circuits are so well-suited to these tasks in fact, that it is a fairly recent development to use digital processors for such jobs, despite the incredible

advantages offered by the scalability and programmability of digital circuits. At lower frequencies, digital processing of radio signals, called *software radio* is an important emerging technology. But state-of-the-art analog circuits will always tend to be five to ten times faster than the competing digital technology and use ten to a hundred times less power. For example, at the time of writing, state-of-the-art analog circuits operate at approximately 10GHz while state-of-the-art digital operate at approximately 2GHz. Radio frequency (RF) signals in wireless receivers demand the fastest possible signal processing. Portable or distributed wireless receivers need to be small, inexpensive, and operate on an extremely limited power budget. So despite the fast advance of digital circuits, analog circuits have continued to be of use in radio front-ends.

Despite these continued advantages, analog circuits are quite limited in their computational scope. Analog circuits have a difficult time producing or detecting arbitrary waveforms, because they are not programmable. Furthermore, analog circuit design is limited in the types of computations it can perform compared to digital, and in particular includes little notion of stochastic processes.

The unfortunate result of this inflexibility in analog circuitry is that radio transmitters and receivers are designed to conform to industry standards. Wireless standards are costly and time-consuming to establish, and subject to continued obsolescence. Meanwhile the Federal Communications Commission (FCC) is overwhelmed by the necessity to perform top-down management of a menagerie of competing standards. It would be an important achievement to create radios that could adapt to solve their local communications problems enabling bottom-up rather than top-down management of bandwidth resources. A legal radio in such a scheme would not be one that broadcasts within some particular frequency range and power level, but instead would “play well with others”. The enabling technology required for a revolution in wireless communication is programmable statistical signal processing with the power, cost and speed performance of state-of-the-art analog circuits.

1.4 Road-map: Statistical Signal Processing by Simple Physical Systems

When oscillators hang from separate beams, they will swing freely. But when oscillators are even slightly coupled, such as by hanging them from the same beam, they will tend to synchronize their respective phase. The moments when the oscillators instantaneously stop and reverse direction will come to coincide. This is called *entrainment* and it is an extremely robust physical phenomena which occurs in both coupled dissipative linear oscillators as well as coupled nonlinear systems.

One kind of statistical inference - statistical signal processing - involves estimating parameters of a transmitter system when given a noisy version of the transmitted signal. One can actually think of entraining oscillators as performing this kind of task. One oscillator is making a decision about the phase of the other oscillator given a noisy received signal.

Oscillators tend to be stable, efficient building blocks for engineering, because they derive directly from the underlying physics. To borrow an analogy from computer science, building an oscillator is like writing “native” code. The outcome tends to execute very fast and efficiently, because we make direct use of the underlying hardware. We are much better off using a few transistors to make a physical oscillator than simulating an oscillator in a digital computer language running in an operating system on a general purpose digital processor. And yet this circuitous approach is precisely what a software radio does.

All of this might lead us to wonder if there is a way get the efficiency and elegance of a native implementation combined with the flexibility of a more abstract implementation. Towards this end, this dissertation will show how to generalize a ring-oscillator to produce native nonlinear dynamical systems which can be programmed to create, filter, and synchronize arbitrary analog waveforms and to decode and estimate the digital information carried by these waveforms. Such systems begin to bridge the gap between the base-band statistical signal processing implemented in a digital signal processor and analog RF circuits. Along the way, we learn how to understand the

synchronization of oscillators by entrainment as an optimum statistical estimation algorithm.

The approach I took in developing this thesis was to first try to design oscillators which can create arbitrary waveforms. Then I tried to get such oscillators to entrain. Finally I was able to find a principled way to generalize these oscillators to perform general-purpose statistical signal processing by writing them in the language of probabilistic message-passing on factor graphs.

1.5 Analog Continuous-Time Distributed Computing

The digital revolution with which we are all familiar is predicated upon the digital abstraction, which allows us to think of computing in terms of logical operations on zeros and ones (or bits) which can be represented in any suitable computing hardware. The most common representation of bits, of course, is by high and low voltage values in semiconductor integrated circuits.

The digital abstraction has provided wonderful benefits, but it comes at a cost; The digital abstraction means discarding all of the state space available in the voltage values *between* a low voltage and a high voltage. It also tends to discard geographical information about where bits are located on a chip. Some bits are actually, physically stored next to one another while other bits are stored far apart. The von Neumann architecture requires that any bit is available with any other bit for logical combination at any time; All bits must be accessible within one operational cycle. This is achieved by imposing a clock and globally synchronous operation on the digital computer. In an integrated circuit (a chip), there is an lower bound on the time it takes to access the most distant bits. This sets the lower bound on how short a clock cycle can be. If the clock were to switch faster than that, a distant bit might not arrive in time to be processed before the next clock cycle begins.

But why should we bother? Moore's Law tells us that if we just wait, transis-

tors will get smaller and digital computers will eventually become powerful enough. But Moore’s Law is not a law at all, and digital circuits are bumping up against the physical limits of their operation in nearly every parameter of interest: speed, power consumption, heat dissipation, “clock-ability”, “simulate-ability” [17], and cost of manufacture [45]. One way to confront these limits is to challenge the digital abstraction and try to exploit the additional resources that we throw away when we use what are inherently analog CT distributed circuits to perform digital computations. If we make computers analog then we get to store on the order of 8 bits of information where once we could only store a single bit. If we make computers asynchronous the speed will no longer depend on worst case delays across the chip [12]. And if we make use of geographical information by storing states next to the computations that use them, then the clock can be faster or even non-existent [33]. The asynchronous logic community has begun to understand these principles. Franklin writes,

“In clocked digital systems, speed and throughput is typically limited by worst case delays associated with the slowest module in the system. For asynchronous systems, however, system speed may be governed by actual executing delays of modules, rather than their calculated worst case delays, and improving predicted average delays of modules (even those which are not the slowest) may often improve performance. In general, more frequently used modules have greater influences on overall performance [12].”

1.5.1 Analog VLSI Circuits for Statistical Inference

Probabilistic message-passing algorithms on factor graphs tend to be distributed, asynchronous computations on continuous valued probabilities. They are therefore well suited to “native” implementation in *analog, continuous-time* Very-Large-Scale-Integrated (VLSI) circuitry. As Carver Mead predicted, and Loeliger and Lustenberger have further demonstrated, such analog VLSI implementations may promise more than two orders of magnitude improvement in power consumption and silicon

area consumed [29].

The most common objection to analog computing is that digital computing is much more robust to noise, but in fact all computing is sensitive to noise. Analog computing is not robust because it never performs error correction in this way and so tends to be more sensitive to noise. Digital computing avoids errors by performing ubiquitous local error correction - every logic gate always thresholds its inputs to 0s and 1s even when it is not necessary. The approach advocated here and first proposed by Loeliger, Lustenberger offers more “holographic” error correction; the factor graph implemented by the circuit imposes constraints on the likely outputs of the circuit. In addition, by representing all analog values differentially (with two wires) and normalizing these values in each “soft-gate”, there is a degree of ubiquitous local error correction as well.

1.5.2 Analog, Un-clocked, Distributed

Philosophically it makes sense that if we are going to recover continuous degrees-of-freedom in state we should also try to recover continuous degrees-of-freedom in time. But it also seems that analog CT and distributed computing go hand in hand since each of these design choices tends to reinforce the others. If we choose not to have discrete states, we should also discard the requirement that states occur at discrete times, and independently of geographical proximity.

Analog Circuits imply Un-clocked

Clocks tend to interfere with analog circuits. More generally, highly discrete time steps are incompatible with analog state, because sharp state transitions add glitches and noise to analog circuits.

Analog Circuits imply Distributed

Analog states are more delicate than digital states so they should not risk greater noise corruption by travelling great distances on a chip.

Un-clocked implies Analog Circuits

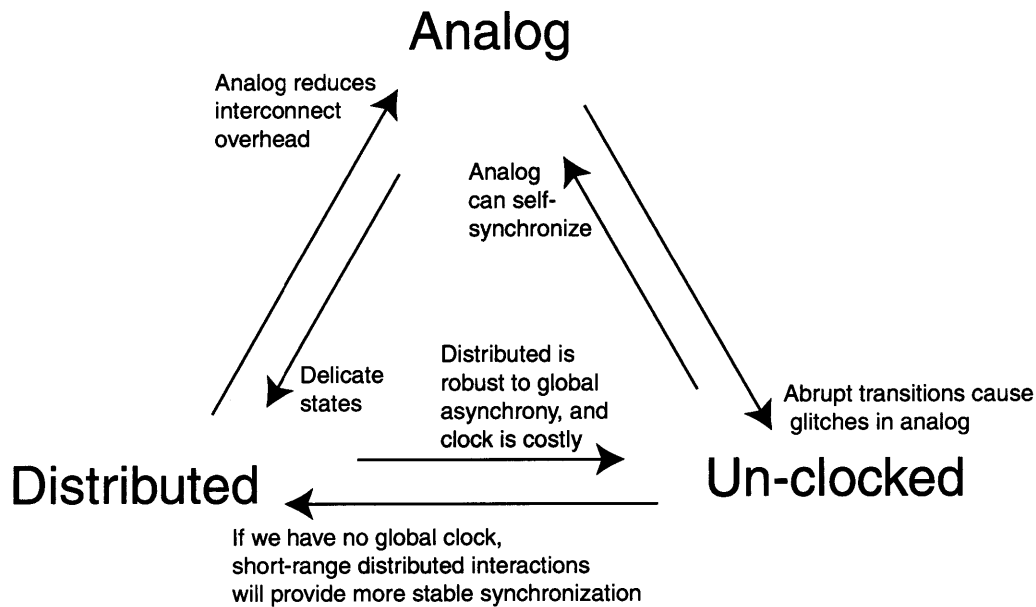


Figure 1-1: Analog, distributed and un-clocked design decisions reinforce each other

Digital logic designs often suffer from *race conditions* where bits reach a gate at different times. Race conditions are a significant problem which can be costly in development time.

By contrast, analog computations tend to be robust to distributed asynchrony, because state changes tend to be gradual rather than abrupt, and as we shall see, we can design analog circuits that tend to locally self-synchronize.

Un-clocked implies Distributed

Centralized computing without a clock is fragile. For example, lack of a good clock is catastrophic in a centralized digital Von Neumann where bits need to be simultaneously available for computation but are coming from all over the chip across heterogeneous delays. Asynchronous logic, an attempt to solve this problem without a clock by inventing digital logic circuits which are robust to bits arriving at different times (so far) requires

impractical overhead in circuit complexity. Centralized digital computers therefore need clocks.

We might try to imagine a centralized analog computer without a clock using emergent synchronization via long-range interactions to synchronize distant states with the central processor. But one of the most basic results from control theory tells us that control systems with long delays have poor stability. So distributed short-range distributed interactions are more likely to result in stably synchronized computation. To summarize this point: if there isn't a global synchronizing clock, then longer delays in the system will lead to larger variances in timing inaccuracies.

Distributed weakly implies Analog Circuits

Distributed computation does not necessarily imply the necessity of analog circuits. Traditional parallel computer architectures for example, are collections of many digital processors. However, extremely fine grained parallelism can often create a great deal of topological complexity for the computer's interconnect compared to a centralized architecture with a single shared bus. (A centralized bus is the definition of centralized computation - it simplifies the topology but creates the so called von Neumann "bottleneck").

For a given design, Rents Rule characterizes the relationship between the amount of computational elements (e.g. logic blocks) and the number of wires associated with the design. Rent's rule is

$$N = KG^p, \tag{1.1}$$

where N is the number of wires emanating from a region, G is the number of circuit components (or logic blocks), K is Rent's constant, and p is Rent's exponent. Lower N means less area devoted to wiring. For message passing algorithms on relatively "flat" graphs with mostly local

interconnections, we can expect $p \approx 1$. For a given amount of computational capacity G , the constant K (and therefore N) can be reduced by perhaps half an order of magnitude by representing between 5 and 8 bits of information on a single analog line instead of on a wide digital bus.

Distributed weakly implies Un-clocked

Distributed computation does not necessarily imply the necessity of un-clocked operation. For example, parallel computers based on multiple Von Neumann processor cores generally have either global clocks or several local clocks. But a distributed architecture makes clocking less necessary than in a centralized system and combined with the costliness of clocks, this would tend to point toward their eventual elimination.

The clock tree in a modern digital processor is very expensive in terms of power consumption and silicon area. The larger the area over which the same clock is shared, the more costly and difficult it is to distribute the clock signal. An extreme illustration of this is that global clocking is nearing the point of physical impossibility. As Moore's law progresses, digital computers are fast approaching the fundamental physical limit on maximum global clock speeds imposed by the minimum time it takes for a bit to traverse the entire chip travelling at the speed of light on a silicon dielectric.

A distributed system, by definition, has a larger number of computational cores than a centralized system. Fundamentally, each core need not be synchronized to the others in order to compute, as long as they can share information when necessary. Sharing data, communication between two computing cores always in some sense requires synchrony. This thesis demonstrates a very low-complexity system in which multiuser communication is achieved by the receiver adapting to the rate at which data is sent, rather than by a shared clock. Given this technology, multiple cores

could share common channels to accomplish point-to-point communication without the aid of a global clock. In essence, processor cores could act like nearby users in a cell phone network. The systems proposed here make this thinkable.

Let us state clearly that this is not an argument against synchrony in computing systems, just the opposite. Synchronization seems to increase information sharing between physical systems. The generalization of synchrony, coherence may even be a fundamental resource for computing, although this is a topic for another thesis. The argument here is only that coherence in the general sense may be achieved by systems in other ways besides imposing an external clock.

Imagine a three dimensional space with axes representing continuous (un-clocked) vs. discrete (clocked) time, continuous (analog) vs. discrete (digital) state, and distributed vs. centralized computation. Conventional digital computing inhabits the corner of the space where computing is digital, DT, and centralized. Digital computing has been so successful and has so many resources driving its development, that it competes extremely effectively against alternative approaches which are not alternative *enough*. If we are trying to find a competitive alternative to digital computing, chances are that we should try to explore parts of the space which are as far as possible from the digital approach. So in retrospect, perhaps it should not come as a surprise that we should make several simultaneous leaps of faith in order to produce a compelling challenge to the prevailing digital paradigm. This thesis therefore moves away from several aspects of digital computing at once, simultaneously becoming continuous state, CT, and highly distributed.

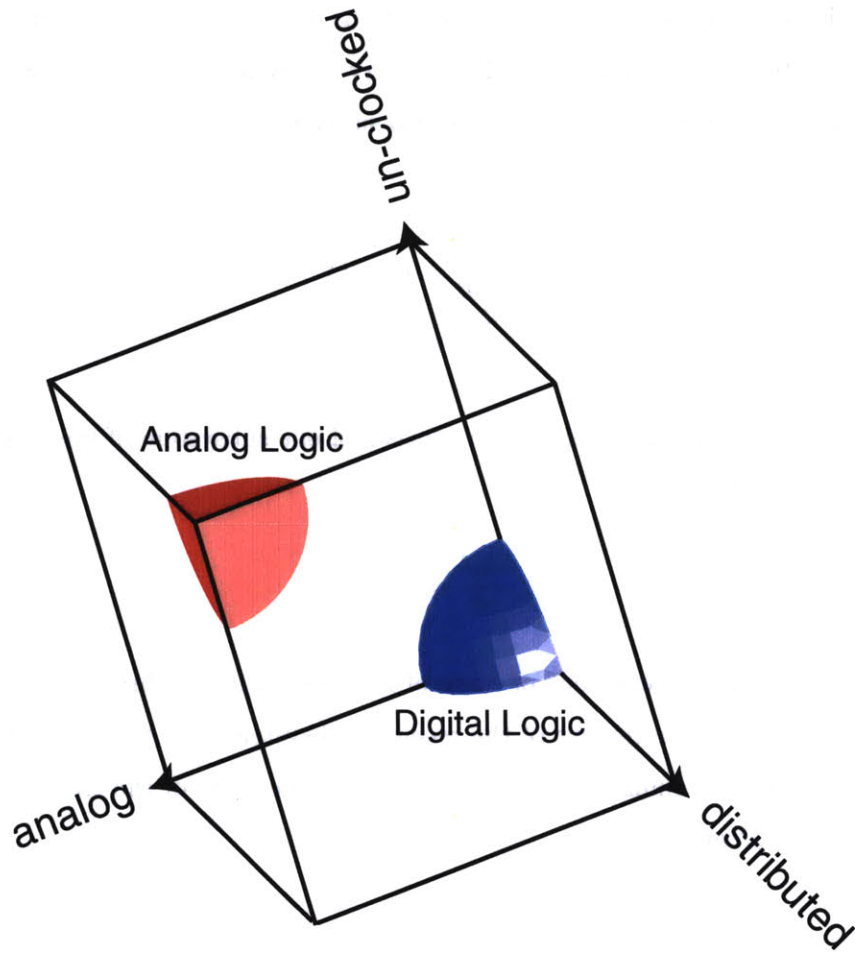


Figure 1-2: A design space for computation. The partial sphere at the bottom represents digital computation and the partial sphere at the top represents our approach.

1.6 Prior Art

1.6.1 Entrainment for Synchronization

There is vast literature on coupled nonlinear dynamic systems - whether just periodic or chaotic. The work presented in this dissertation originally drew inspiration, but ultimately departed from research into coupled chaotic nonlinear dynamic systems for communications. Several canonical papers were authored by Cuomo and Oppenheim [7].

This literature generally presents variations on the same theme. There is a transmitter system of nonlinear first order ordinary differential equations. The transmitter system can be arbitrarily divided into two subsystems, g and h ,

$$\begin{aligned}\frac{dv}{dt} &= g(v, w) \\ \frac{dw}{dt} &= h(v, w).\end{aligned}$$

There is a receiver system which consists of one subsystem of the transmitter,

$$\frac{dw'}{dt} = h(v, w')$$

The transmitter sends one or more of its state variables through a noisy channel to the receiver. Entrainment of the receiver subsystem h to the transmitter system will proceed to minimize the difference between the state of the transmitter, w and the receiver w' at a rate

$$\frac{d\Delta w'}{dt} = J[h(v, w')] \cdot \Delta w$$

where J is the Jacobian of the subsystem, h and $\Delta w = w - w'$.

There is also an extensive literature on the control of chaotic nonlinear dynamical systems. The basic idea there is essentially to push the system when it is close to a bifurcation point to put it in one part of its state space or another. Recently, there has been a rapidly growing number of chaotic communication schemes based on exploiting these principles of chaotic synchronization and/or control [9]. Although several researchers have been successful in implementing transmitters based on chaotic circuits, the receivers in such schemes generally consist of some kind of matched filter. For example, Mandel et al. proposed a transmitter based on a controlled chaotic system and a receiver with a correlator as shown in figure 1-3. They called this

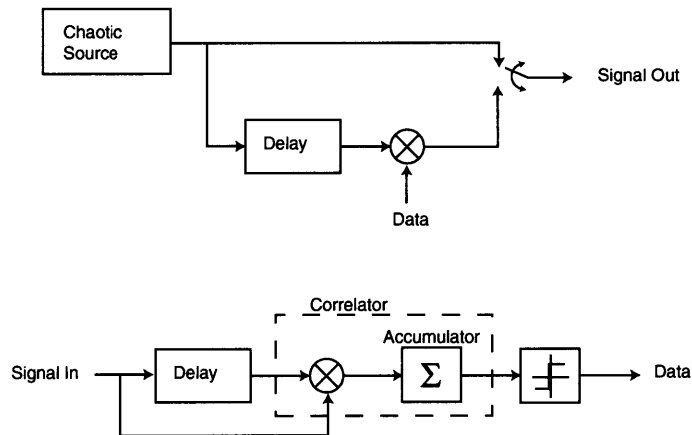


Figure 1-3: Chaotic communications system proposed by Mandal et al. [30]

scheme modified differential chaos shift keying (M-DCSK) [30].

Chaotic systems have some major disadvantages as engineering primitives for communication systems. They are non-deterministic which makes it hard to control and detect their signals. Chaotic systems are also not designable in that we do not have a principled design methodology for producing a chaotic nonlinear dynamic system which has particular desired properties such as conforming to a given spectral envelope.

1.6.2 Neuromorphic and Translinear Circuits

Carver Mead first coined the term “neuromorphic” to mean implementing biologically inspired circuits in silicon. There is a long history and broad literature on neuromorphic circuits including various kinds of artificial neural networks for vision or speech processing as well as highly accurate silicon versions of biological neurons, for example, implementing the frog’s leg control circuitry.

In 1975, Barrie Gilbert coined the term translinear circuits to mean circuits that use the inherent nonlinearity available from the full dynamic range of a semiconductor junction. The most useful and disciplined approaches to neuromorphic circuits have generally been based on translinear circuits. Applications of translinear circuits have

included hearing aids and artificial cochlea (Sarpeshkar et al.), low level image processing vision chips (Carver Mead et al., Dan Seligson at Intel), Viterbi error correction decoders in disk drives (IBM, Loeliger et al., Hagenauer et al.), as well as multipliers [21], oscillators, and filters for RF applications such as a PLL [35]. Translinear circuits have only recently been proposed for performing statistical inference. Loeliger and Lustenberger have demonstrated BJT and sub-threshold CMOS translinear circuits which implement the sum-product algorithm in probabilistic graphical models for soft error correction decoding [29]. Similar circuits were simultaneously proposed by Hagenauer et al. [19] and are the subject of recent research by Dai [8].

1.6.3 Analog Decoders

When analog circuits settle to an equilibrium state, they minimize an energy or action, although this is not commonly how the operation of analog circuits has been understood. One example where this was made explicit, is based on Minty's elegant solution to the shortest problem path problem. The decoding of a trellis code is equivalent to the shortest path problem in a directed graph. Minty assumes a net of flexible, variable length strings which form a scale model of an undirected graph in which we must find the shortest path. If we hold the source node and the destination node and pull the nodes apart until the net is tightened, we find the solution along the tightened path.

“An analog circuit solution to the shortest-path problem in directed graph models has been found independently by Davis and much later by Loeliger. It consists of an analog network using series-connected diodes. According to the individual path section lengths, a number of series connected diodes are placed. The current will then flow along the path with the least number of series-connected, forward biased diodes. Note however that the sum of the diode threshold voltages fundamentally limits practical applications. Very high supply voltages will be needed for larger diode networks, which makes this elegant solution useless for VLSI implementations. [29]”

There is a long history and large literature on analog implementations of error correction decoders. Lustenberger provides a more complete review of the field in his doctoral thesis [29]. He writes, “the new computationally demanding iterative decoding techniques have in part driven the search for alternative implementations of decoders.” Although there had been much work on analog implementations of the Viterbi algorithm [43], Wiberg et al. were the first to think about analog implementations of the more general purpose sum-product algorithm. Hagenauer et al. proposed the idea of an analog implementation approach for the maximum a posteriori (MAP) decoding algorithm, but apparently did not consider actual transistor implementations.

1.7 Contributions

1.7.1 Reduced Complexity Synchronization of Codes

Continuous-Time Analog Circuits for Arbitrary Waveform Generation and Synchronization

This thesis generally applies statistical estimation theory to the entrainment of dynamical systems. This research program resulted in

- Continuous-time dynamical systems that can produce designable arbitrary waveforms.
- Continuous-time dynamical systems that perform maximum-likelihood synchronization with the arbitrary waveform generator.
- A principled methodology for the design of both from the theory of finite state machines

Reduced-Complexity Trellis Decoder for Synchronization

By calculating joint messages on the shift graph formed from the state transition constraints of any finite state machine, we derive a hierarchy of state estimators of

increasing complexity and accuracy.

Since convolutional and turbo codes employ finite state machines, this directly suggests application to decoding. The method described shows us how to “dial a knob” between quality of decoding versus computational complexity.

Low-Complexity Spread Spectrum Acquisition

I derive a probabilistic graphical model for performing maximum-likelihood estimation of the phase of a spreading sequence generated by an LFSR. Performing the sum-product algorithm on this graph performs improved spread spectrum acquisition in terms of acquisition time and tracking robustness when bench-marked against conventional direct sequence spread spectrum acquisition techniques. Furthermore, this system will readily lend itself to implementation with analog circuits offering improvements in power and cost performance over existing implementations.

Low-Complexity Multiuser Detection

Using CT analog circuits to produce faster, lower power, or less expensive statistical signal processing would be useful in a wide variety of applications. In this thesis, I demonstrate analog circuits which perform acquisition and tracking of a spread spectrum code and lay the groundwork for performing multiuser detection the same class of circuits.

1.7.2 Theory of Continuous-Time Statistical Estimation

Injection Locking Performs Maximum-Likelihood Synchronization

Continuous-Time

not just soft logic but smooth logic - cont. time operation

1.7.3 New Circuits

Analog Memory: Circuits for Continuous-Time Analog State Storage

Programmability: Circuit for Analog Routing/Multiplexing, *soft-MUX*

Design Flow for Implementing Statistical Inference Algorithms with Continuous-Time Analog Circuits

- Define data structure and constraints in language of factor graphs (MATLAB)
- Compile to circuits
- Layout or Program gate array

1.7.4 Probabilistic Message Routing

**Learning Probabilistic Routing Tables in ad hoc Peer-to-Peer Networks
Using the Sum Product Algorithm**

**Propose “Routing” as a new method for low complexity approximation of
joint distributions in probabilistic message passing**

Chapter 2

Probabilistic Message Passing on Graphs

“I basically know of two principles for treating complicated systems in simple ways; the first is the principle of *modularity* and the second is the principle of *abstraction*. I am an apologist for computational probability in machine learning, and particularly for graphical models and variational methods, because I believe that probability theory implements these two principles in deep and intriguing ways – namely through *factorization* and through *averaging*. Exploiting these two mechanisms as fully as possible seems to me to be the way forward in machine learning.”

Michael I. Jordan Massachusetts Institute of Technology, 1997.

2.1 The Uses of Graphical Models

2.1.1 Graphical Models for Representing Probability Distributions

When we have a probability distribution over one or two random variables, we often draw it on axes as in figure 2-1, just as we might plot any function of one or two variables. When more variables are involved in a probability distribution, we can-

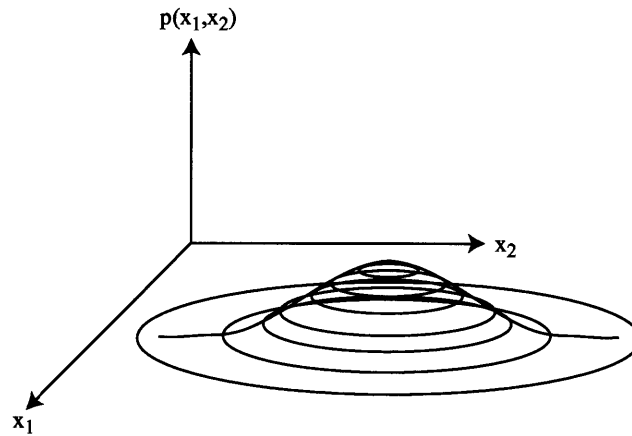


Figure 2-1: Gaussian distribution over two variables

not easily draw the distribution on paper. If we cannot visually represent the shape of the entire distribution over many variables, we can at least represent the dependencies between the random variables, ie. which variables depend on which others. Probabilistic graphical models such as factor graphs do just that.

2.1.2 Graphical Models in Different Fields

The mathematics of probabilistic message passing on graphs is perhaps most often applied to the problem of extracting information from large data sets. Since many different research fields deal with large data sets, probabilistic message passing on graphs has been independently reinvented several times in different research communities. Many well known algorithms from different research communities are actually examples of probabilistic message passing algorithm on different graph topologies or with different kinds of random variables. In the machine inference and learning community the graphs are called Bayesian networks and probabilistic message passing is known as belief propagation. In machine vision, researchers deal with pixels and so use graphs with a lattice structure called Markov Random Fields (MRF). In the signal processing community, Kalman filters or Hidden Markov Model algorithms can be very helpfully represented as graphs. When so represented, the Baum-Welch and

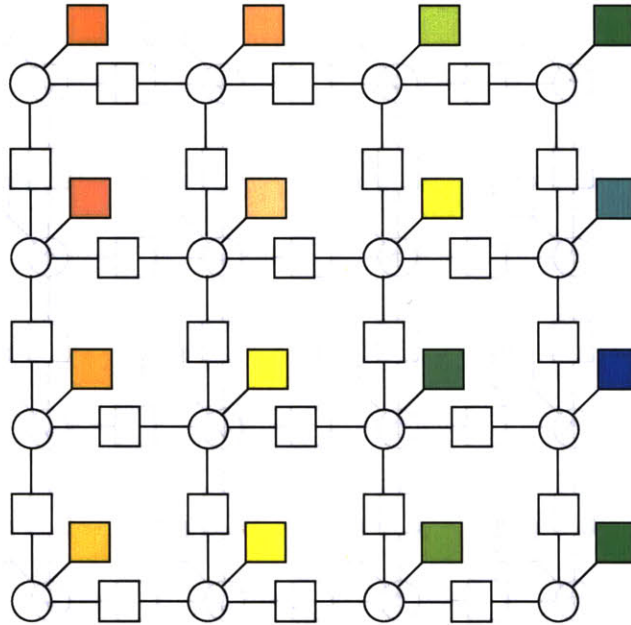


Figure 2-2: Factor graph for computer vision

Forward-Backward algorithms constitute probabilistic message passing. In the communication and coding community, the graphs were called a trellis, a Tanner graph, or a factor graph and the algorithm is known as Viterbi's algorithm, BCJR, or sum product/max product respectively. Finally, the spin glass model in statistical physics is a lattice graphical model which closely resembles an MRF, and the variational methods for solving them are closely related to message passing.

The ability to understand all of these algorithms within a single mathematical framework has been very helpful for catalyzing cross-fertilization between these ordinarily separate research communities. Previously disparate research communities have been able to share algorithms and extend them. Furthermore studying how probabilistic message passing algorithm perform on different graph topologies has provided information about the conditions under which message passing works well and how it may be extended to work better.

But all of these algorithms took years to develop in their respective research communities. Researchers painstakingly developed and proved algorithms for each

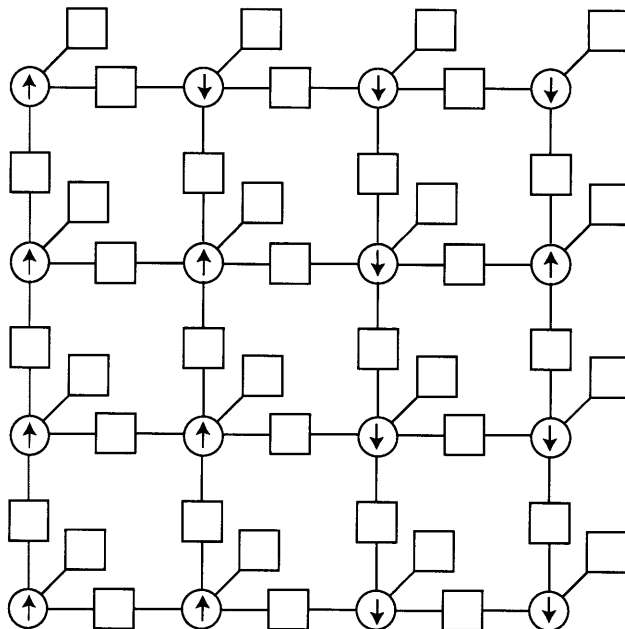


Figure 2-3: Factor graph model for statistical physics

particular problem of interest. As we will see, if we know the random variables we are dealing with and their mutual constraints, then it is a simple matter to draw the factor graph which represents the constrained joint probability over the variables. We then derive the messages for every node in the graph. Implementing the inference algorithm then becomes simply iteratively passing messages on the graph. In other words, if we know the structure of the problem, we get the algorithm for free. This is one of the most important contributions of message passing on graphs.

2.1.3 Factor Graphs for Engineering Complex Computational Systems

Digital design offers us abstraction and modularity. Abstraction means that we don't need to know how a component actually works, we can specify everything about it by its inputs and outputs. The related principle of modularity means that the system can be decomposed into subsystems which can be abstracted. These modules can be combined without affecting one another except via their inputs and outputs.

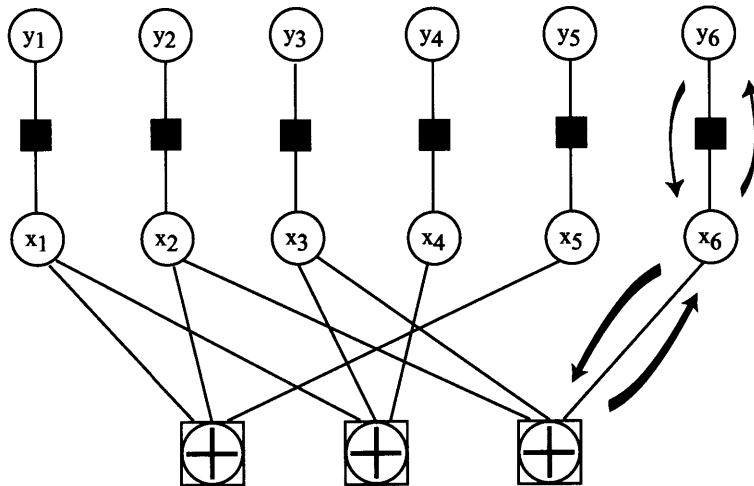


Figure 2-4: Factor graph for error correction decoding

Modularity and abstraction are enable engineers to design robust complex systems.

As the quote by Michael Jordan at the beginning of the chapter indicates, and as we will begin to see in this chapter, factor graphs also offer these properties. In fact factor graphs can represent not only statistical inference algorithms but any constraint satisfaction problem. Factor graphs are therefore promising as a new way of representing rather general-purpose, complex computing architectures.

2.1.4 Application to Signal Processing

Statistical signal processing algorithms involve parsing large quantities of noisy *analog* data to extract digital meaning. In this thesis, the data sets from which we wish to extract information are analog electrical signals, the kinds of signals for example, that a cell phone receives with its antenna. Signal processing often involves making educated guesses from data; a signal processor sees an incoming signal and makes a guess about what the signal is saying. A signal processor that performs speech recognition, for example, receives an audio signal from a person speaking into a microphone and decides what words have been spoken. The decision is an educated guess, because the signal processor is programmed in advance with an internal *model* of speech. A speech model might contain information about how particular words

sound when they are spoken by different people and what kinds of sentences are allowed in the English language [38]. The model encapsulates information such as, you are more likely to see the words, “signal processing” in this document than you are to see the words “Wolfgang Amadeus Mozart.” Except of course, for the surprising occurrence of the words “Wolfgang Amadeus Mozart” in the last sentence.

This kind of information, the relative likelihoods of occurrence of particular patterns is expressed by the mathematics of probability theory. Probabilistic graphical models provide a general framework for expressing the web of probabilities of a large number of possible inter-related patterns that may occur in the data. Before we describe probabilistic graphical models, we will review some essentials of probabilities.

2.2 Review of the Mathematics of Probability

2.2.1 Expectations

The probability that a random value x falls between a and b is

$$\int_a^b p(x)dx. \quad (2.1)$$

An expectation is defined as

$$\langle f(x) \rangle \equiv \int f(x)p(x)dx. \quad (2.2)$$

The most trivial example of an expectation is the normalization condition where $f(x) = 1$,

$$\langle 1 \rangle = \int p(x)dx = 1. \quad (2.3)$$

Perhaps the most common expectation is the mean or first moment of a distribution,

$$\mu = \langle x \rangle = \int xp(x)dx = 1. \quad (2.4)$$

2.2.2 Bayes' Rule and Conditional Probability Distributions

Bayes' Rule,

$$p(x|y) = \frac{p(x, y)}{p(y)} \quad (2.5)$$

expresses the probability that event x occurs given that we know that event y occurred in terms of the joint probability that both events occurred. The rule can be extended to more than two variables. For example,

$$\begin{aligned} p(x, y, z) &= p(x|y, z)p(y, z) \\ &= p(x|y, z)p(y|z)p(z) \\ &= p(x, y|z)p(z). \end{aligned} \quad (2.6)$$

2.2.3 Independence, Correlation

If x and y are independent then, $p(x, y) = p(x)p(y)$ and therefore $p(x|y) = p(x)$, since by Bayes' rule, $p(x|y) = p(x, y)/p(y) = p(x)p(y)/p(y) = p(x)$.

For uncorrelated variables, $\langle xy \rangle = \langle x \rangle \langle y \rangle$. Independent variables are always uncorrelated, but uncorrelated variables are not always independent. This is because independence says there is NO underlying relationship between two variables and so they must appear uncorrelated. By contrast, two variables which appear uncorrelated, may still have some underlying causal connection.

2.2.4 Computing Marginal Probabilities

We often want to compute the probability that a particular event will occur, given the occurrence of many other related events. The goal of a radio receiver for example, is to find the probability that a given symbol was transmitted, given the noisy values that were received via the channel. In a probabilistic graphical model, answering this question means we are asking for the distribution of probability over the possible states of a particular variable (node), given probability distributions for each of the other nodes. This is called finding the *marginal* probability distribution for a par-

ticular variable. Marginalization and related computations pop up as sub-routines in many statistical computations, and are important in many applications.

Let $p(x)$ be a joint distribution over variables $x = \{x_1, x_2, \dots, x_n\}$. Let x_S denote a subset of these the variables. Then the marginal distribution for the variable nodes in x_S is given by

$$p_{x_S}(x_S) = \sum_{x \setminus x_S} p(x), \quad (2.7)$$

where $x \setminus x_S$ is the sum over the states of all of the variable nodes *not* in x_S .

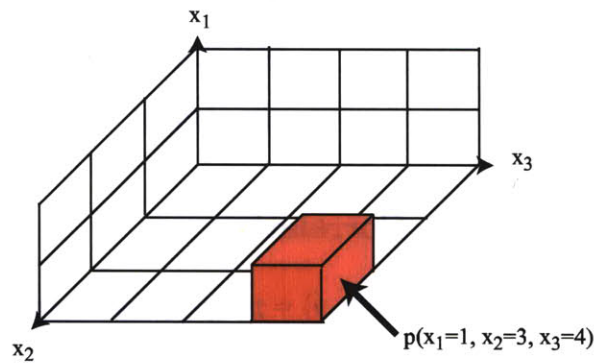


Figure 2-5: Visualization of joint distribution over random variables x_1, x_2, x_3

If $p(x)$ is a joint distribution over variables x_1, x_2, \dots, x_n , then the computational complexity of this sum is exponential in the number of variables not in S . This is perhaps easiest to see by an illustration. Figure 2-5 represents a joint distribution over discrete random variables $\{x_1, x_2, x_3\}$. Each axis of the volume in the figure is labelled by a variable and divided into spaces for each possible state of that variable. x_1 has possible states $\{1, 2\}$, x_2 has possible states $\{1, 2, 3\}$, and x_3 has possible states $\{1, 2, 3, 4\}$. The joint distribution over all three variables $\{x_1, x_2, x_3\}$ contains a probability for every entry in this volume with the total probability in all entries summing to 1. In the figure, x_1 has two possible states, so finding the marginal distribution $p(x_1)$ requires finding $p(x_1 = 1)$ and $p(x_1 = 2)$. As shown in figure 2-6, each of these requires summing over x_2 and x_3 by summing over all 12 entries contained in a 3×4 horizontal plane.

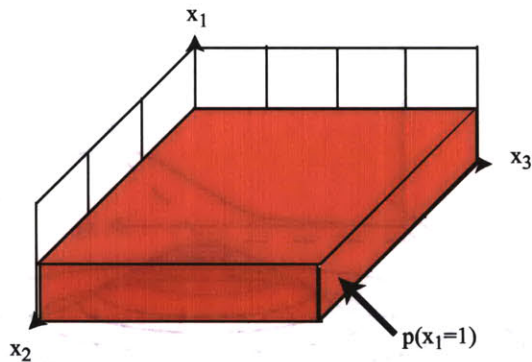


Figure 2-6: Visualization of marginalization over random variables x_2, x_3 to find $p(x_1 = 1)$

Observe the exponential growth of the problem; For every additional variable not in S , the plane we must sum over gains a dimension and the number of entries we must sum over is multiplied by the number of states of the new variable. If we added another variable x_4 with 5 states for example, calculating $p(x_1 = 1)$ would require summing over all 60 entries in a $3 \times 4 \times 5$ hyper-plane. We can also marginalize over distributions of continuous variables of course, with sums becoming integrals. Figure 2-7 illustrates marginalization of a 2-dimensional gaussian distribution onto each dimension x_1

$$p(x_1) = \int e^{C^T \bar{x} C / \sigma^2} dx_2, \quad (2.8)$$

and x_2 ,

$$p(x_2) = \int e^{C^T \bar{x} C / \sigma^2} dx_1. \quad (2.9)$$

Figure 2-7 also illustrates how marginalization is in essence a projection of a probability distribution into a smaller number of dimensions.

2.3 Factor Graph Tutorial

Let us get our feet wet by looking at some simple examples of factor graphs.

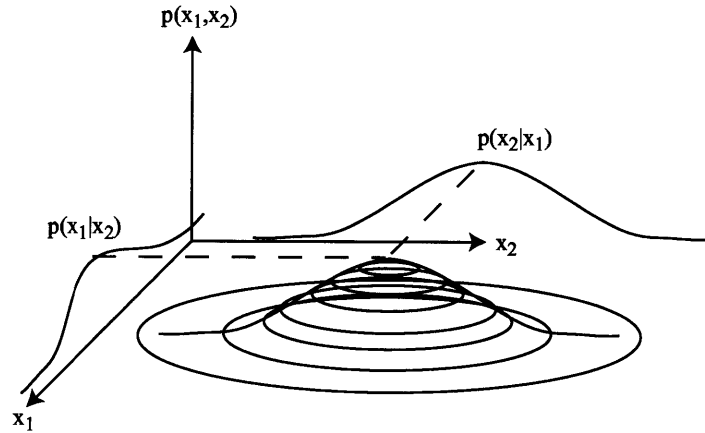


Figure 2-7: Visualization of marginalization over 2-dimensional gaussian distribution

2.3.1 Soft-Inverter

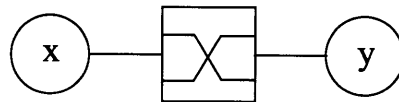


Figure 2-8: Factor graph expressing that binary variables x and y are constrained to be opposite in value

Let x and y be binary random variables which are constrained to be opposites $y = \sim x$. For example, we might flip a coin to generate x , and then generate y by taking the opposite of x . We could also write this constraint in terms of a mod 2 sum, $x \oplus y = 1$. If x and y are opposite, then their probabilities are also opposite, $p_X(1) = 1 - p_Y(1)$. In other words, if we are pretty certain that $x = 1$, then we are equally certain that $y = 0$. So,

$$\begin{aligned}
 p_X(1) &= p_Y(0) \\
 p_X(0) &= p_Y(1).
 \end{aligned}
 \tag{2.10}$$

For example if $[p_X(0), p_X(1)] = [.8, .2]$, then $[p_Y(0), p_Y(1)] = [.2, .8]$. This relation between the probability distribution of x and y is called a soft-inverter. The soft inverter constraint applied over x and y can be represented pictorially by a factor graph as shown in figure 2-8. The *variable nodes* for x and y are represented by circles, while the constraint is represented by a square *factor node*.

2.3.2 Factor Graphs Represent a Factorized Probability Distribution

A factor graph should be thought of imposing constraints on a joint probability distribution over the variables represented in the graph. The joint probability distribution over binary variables x and y above, $p(x, y)$ can be represented by a four-vector

$$\begin{aligned} p_{X,Y}(00) \\ p_{X,Y}(01) \\ p_{X,Y}(10) \\ p_{X,Y}(11). \end{aligned} \tag{2.11}$$

The inverter constraint, however, imposes the condition that states 00 and 11 are not allowed. The probabilities of those states occurring is therefore zero, $p_{X,Y}(00) = 0$ and $p_{X,Y}(11) = 0$. The total probability mass must therefore be spread over the remaining probabilities $p_{X,Y}(01)$ and $p_{X,Y}(10)$ of the allowed states, 01 and 10.

More generally, a factor graph represents a factorized probability distribution of the form

$$p(x_1, x_2, \dots, x_N) = \frac{1}{Z} \prod_{a=1}^M f_a(x_a). \tag{2.12}$$

Factor graphs are bipartite, meaning they have two kinds of nodes, variable nodes and factor nodes. There is always a variable node between any two factor nodes and there is always a factor node between any two variable nodes. In figure 2-16 and

throughout this document, the *variable nodes* are denoted by circles and the *factor nodes* are denoted by black squares. A factor graph has a variable node for each variable x_i , and a factor node for each function f_a with an edge connecting variable node i to factor node a if and only if x_i is an argument of f_a .

2.3.3 Soft-xor

x	y	z
0	0	0
0	1	1
1	0	1
1	1	0

(2.13)

There could be other kinds of constraints on variables besides forcing them to be opposite. For example, we could impose a parity check constraint so that $(x \oplus y \oplus z) \bmod 2 = 0$. The truth table for a parity check constraint is given in table 4.19. Parity check constraints such as this will be important for error correction codes.

According to the constraint, if x and y are opposite, then z must be a 1. Otherwise, z must be 0. We can calculate the $p_Z(1)$ by summing the probabilities of all the ways that x and y can be different. Similarly, we can calculate the $p_Z(0)$ by summing the probabilities of all the ways that x and y can be the same. In both calculations it is necessary to normalize afterwards.

$$\begin{aligned}
 p_Z(1) &= p_X(0)p_Y(1) + p_X(1)p_Y(0) \\
 p_Z(0) &= p_X(0)p_Y(0) + p_X(1)p_Y(1)
 \end{aligned}
 \tag{2.14}$$

So now we know how to calculate $p_Z(z)$ when we are given $p_X(x)$ and $p_Y(y)$ and

we know that x, y, z constrained by $(x \oplus y \oplus z) \bmod 2 = 0$. Let's try it for some actual probabilities. If

$$\begin{aligned} p_X(1) &= .8 \\ p_X(0) &= .2 \end{aligned} \tag{2.15}$$

and

$$\begin{aligned} p_Y(1) &= .3 \\ p_Y(0) &= .7 \end{aligned} \tag{2.16}$$

then,

$$\begin{aligned} p_Z(1) &= (.2)(.3) + (.8)(.7) = .62 \\ p_Z(0) &= (.2)(.7) + (.8)(.3) = .38. \end{aligned} \tag{2.17}$$

Finally we must check to make sure that our final answer is normalized, $.62 + .38 = 1$.

This kind of factor node is called a *soft-xor* gate. It is visualized as the factor graph shown in figure 2-9.

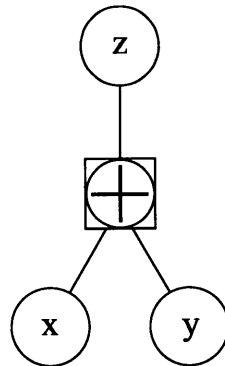


Figure 2-9: Factor graph expressing that binary variables x , y , and z are constrained to sum to zero mod 2

2.3.4 General Soft-gates

We appealed to a specialized arguments to derive the soft-inverter and soft-xor. But more generally, one way we can think of soft-gates is as the probabilistic equivalent of logic gates. For example, the soft-xor is the probability version of the logical XOR function. Thought of this way, the output from a soft-gate tells us how likely it would be for a distribution of input strings to satisfy its corresponding logic gate.

In fact, given any logic gate there is a principled way to find the output of the corresponding soft-gate. The output from a soft-gate over three variables x, y, z is given in general by

$$p_Z(z) = \gamma \sum_{x \in X} \sum_{y \in Y} p_X(x) p_Y(y) f(x, y, z) \quad (2.18)$$

where $f(x, y, z)$ is the constraint function within a delta function which we will consider to be zero except when its argument is true. If we substitute the constraint function for the XOR, $f(x, y, z) = \delta(x \oplus y \oplus z = 0)$ into equation (2.18), we find that

$$\begin{aligned} p_Z(1) &= \sum_{x, y = \{0, 1\}} p_X(x) p_Y(y) \delta(x \oplus y \oplus 1 = 0) \\ p_Z(0) &= \sum_{x, y = \{0, 1\}} p_X(x) p_Y(y) \delta(x \oplus y \oplus 0 = 0) \end{aligned} \quad (2.19)$$

To calculate $p_Z(1)$, we sum over all possible (binary) values of x and y . The constraint within a dirac delta serves to include some probability terms and exclude others. So in calculating $p_Z(1)$, the $p_X(0)p_Y(1)$ and $p_X(1)p_Y(0)$ terms are included because

$$\begin{aligned} \delta(0 \oplus 1 \oplus 1 = 0) &= 1 \\ \delta(1 \oplus 0 \oplus 1 = 0) &= 1. \end{aligned} \quad (2.20)$$

While the $p_X(0)p_Y(0)$ and $p_X(1)p_Y(1)$ terms are zero because

$$\begin{aligned} \delta(0 \oplus 0 \oplus 1 = 0) &= 0 \\ \delta(1 \oplus 1 \oplus 1 = 0) &= 0. \end{aligned} \quad (2.21)$$

Similarly, in calculating $p_Z(0)$, we use the fact that

$$\begin{aligned}
 f(0, 0, 0) &= 1 \\
 f(0, 1, 0) &= 0 \\
 f(1, 0, 0) &= 0 \\
 f(1, 1, 0) &= 1.
 \end{aligned}
 \tag{2.22}$$

2.3.5 Marginalization on Tree: The Message Passing Metaphor

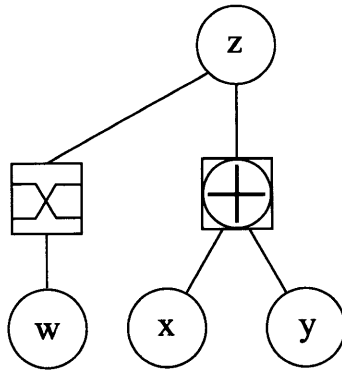


Figure 2-10: Factor graph with more than one kind of constraint node

So far we have only seen factor graphs containing a single type of factor node. Figure 2-10 shows a factor graph with both a soft-xor and soft-inverter node along with variable nodes, w, x, y, z . Remember that the factor graph actually represents a constrained joint probability distribution over all variables in the graph,

$$p_{w,x,y,z}(w, x, y, z) = \delta(x \oplus y \oplus z = 0) \delta(w \oplus x = 1) p_W(w) p_X(x) p_Y(y) p_Z(z). \tag{2.23}$$

Suppose we want to calculate the marginal probability $p(z)$ given $p(w), p(y)$. First we find $p(x)$ from $p(w)$ by using the equation for the soft-inverter. Then we find $p(z)$ from $p(x)$ and $p(y)$ using the equations for the soft-xor. It may occur to us, that we can imagine that the nodes act as if they are sending messages along the edges between them. This is the metaphor which leads to the notion of *probabilistic message*

passing on graphs.

2.3.6 Marginalization on Tree: Variable Nodes Multiply Incoming Messages

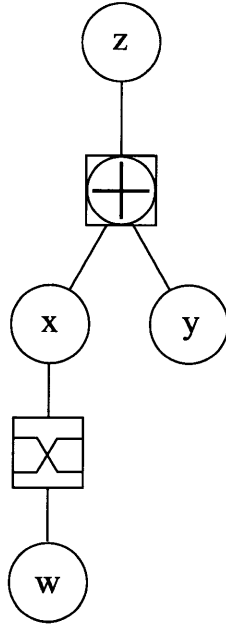


Figure 2-11: Factor graph containing a variable node more than one incident edge

We know now how to generate messages from factor nodes, but so far we have only seen variable nodes with one incident edge. The variable node for z in figure 2-11 has two incident edges. Suppose that we would like to calculate the marginal probability $p(z)$ given $p(w)$, $p(x)$, $p(y)$ and of course $p(w, x, y, z)$ which is given by the form of the factor graph.

- Find $p(z)$ message from $p(w)$ using the soft-inverter
- Find $p(z)$ message from $p(x)$ and $p(y)$ using the soft-xor
- Multiply $p(z)$ messages together
- Normalize

Factor nodes are responsible for placing constraints on the joint probability distribution. So a variable node with two incident edges can treat the messages it receives on those edges as if they are statistically independent. If the z node has only two incident edges from x and y , then the joint probability distribution for z must be in terms of only x and y , $p(z) = p(x, y)$. Since the messages containing $p(x)$ and $p(y)$ can be considered independent from the point of view of z , $p(z) = p(x, y) = p(x)p(y)$. So variable nodes simply multiply probabilities.

We now are in a position to understand the motivation behind equation (2.18). It essentially allows for any statistical dependence over the variables to which it is applied. Equation (2.18) can be generalized by allowing fewer or more variables and even non-binary functions for $f(x, y, z)$.

2.3.7 Joint Marginals

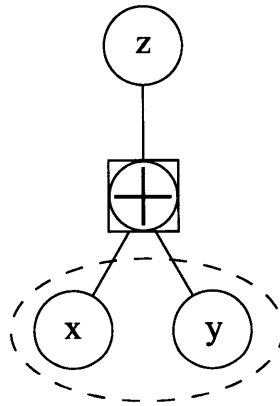


Figure 2-12: Factor graph with incomplete marginalization leaving a “region” node: The basis of Generalized Belief Propagation

We don't have to marginalize over all of the variables but one in a factor graph. For example given the factor graph in figure 2-12, we could calculate the joint probability $p(x, y)$ given $p(z)$. By modifying equation (2.18), we can write the proper

message for $p(x, y)$

$$p_{X,Y}(x, y) = \gamma \sum_{z \in Z} p_Z(z) f(x, y, z). \quad (2.24)$$

So that,

$$\begin{aligned} p_{X,Y}(0, 0) &= p_Z(0) \\ p_{X,Y}(0, 1) &= p_Z(1) \\ p_{X,Y}(1, 0) &= p_Z(1) \\ p_{X,Y}(1, 1) &= p_Z(0). \end{aligned} \quad (2.25)$$

It is important to note that the probability distribution $p_{X,Y}(x, y)$ requires us to store four numbers. It contains twice as much data than $p(x)$ or $p(y)$ alone. If we had a joint probability distribution over three binary variables, for example $p_{X,Y,Z}(x, y, z)$ it would contain eight numbers. Each additional variable in a joint distribution increases the size of the data structure exponentially. This is the essential idea in generalized belief propagation (GBP) [56]. In GBP we form “region” nodes which represent joint probabilities over more than one variable. We can perform message passing between these new region nodes just as we would on any factor graph, at the expense of exponentially increasing the computational complexity of the algorithm. GBP has a number of uses. In this document we will show a novel way to use GBP to effectively trade-off the quality of statistical estimates in a decoder against the computational complexity of decoding. GBP can also be used to improve the answers that we get from message passing on graphs with cycles.

2.3.8 Graphs with Cycles

So far, all of the graphs we have examined have had a tree topology. For graphs that are trees, probabilistic message passing is guaranteed to give us the correct answers for the marginal probability or joint marginal probability of any variables in the graph. Graphs with cycles (“loopy graphs”) are a different story. Message passing

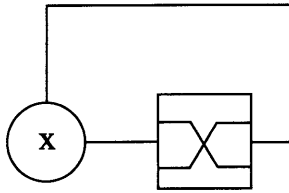


Figure 2-13: Factor graph with a frustrated cycle

may not converge in if the graph contains cycles. For example, the graph in figure 2-13 has a single cycle. If $p(x)$ is initialized to $p_X(1) = 1, p_X(0) = 0$, then message passing around the loop through the soft-inverter will cause the messages to simply oscillate $(0,1)^*$. This can be solved by *damping*. Damping essentially low-pass filters or smooths the message passing algorithm. If we add damping in the example above, the inverting loop will settle to $p_X(1) = .5, p_X(0) = .5$. We will discuss damping in greater depth later in this document.

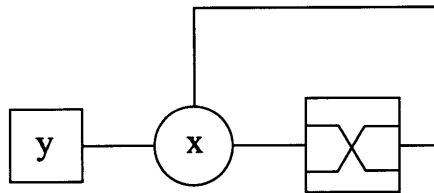


Figure 2-14: Factor graph with a frustrated cycle and a local evidence node

For some graphs with loops, message passing may never settle to an answer even with damping. The graph in figure 2-14 shows such a graph. The local evidence node y (evidence nodes are squares or shaded circles by convention) continues to perturb the variable x away from equilibrium $p_X(1) = .5, p_X(0) = .5$ which continues to cause oscillations no matter how long we wait.

Even if message passing does settle to an answer on a loopy graph, the answer may be wrong, but if it does the solution will be a stationary point of the “Bethe free energy” [22].

We can convert a graph with the cycles to a tree with GBP by choosing to form messages which are joint distributions over more than one variable. GBP allows us

to assure that message passing will converge even on a graph with cycles at the cost of increasing the computational complexity of calculating some of the messages.

2.4 Probabilistic Message Passing on Graphs

We have seen that probabilistic graphical models can be handy visual aids for representing the statistical dependencies between a large number of random variables. This can be very helpful for organizing our understanding of a given statistical problem. The real power of probabilistic graphical models become obvious however, when we begin to use them as data structures for algorithms. As we will see, by understanding the independencies (factorizations) in the probability distributions with which we are working, we can greatly reduce the computational complexity of statistical computations.

2.4.1 A Lower Complexity Way to Compute Marginal Probabilities

By factoring the global probability distribution $p(x)$ into the product of many functions as in equation, and distributing the summations into the product as far as possible, the number of operations required to compute $p(x_1)$ can be greatly reduced. For example, let us compute the marginal distribution $p(x_1)$ for the factorized distribution represented by the graph in figure 2-15.

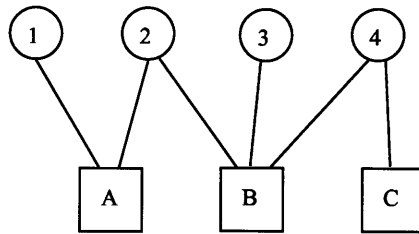


Figure 2-15: Simple acyclic graph

We index the factor nodes in our graph with letters $a = \{A, B, C, \dots\}$ and the

variable nodes with numbers $i = \{1, 2, 3, \dots\}$. For convenience, we speak of a factor node a as if it is synonymous with the function f_a which it represents and likewise for a variable node i which represents a variable x_i . A factor node is connected to any variable node of which it is a function. Those variable nodes will in turn be connected to other factor nodes. Then the factorization represented by the graph in figure 2-15 can be written as

$$p(x) = \frac{1}{Z} f_A(x_1, x_2) f_B(x_2, x_3, x_4) f_C(x_4), \quad (2.26)$$

Computing the marginal for x_1 requires summing over all of the other variables

$$p(x_1) = \frac{1}{Z} \sum_{x_2, x_3, x_4} f_A(x_1, x_2) f_B(x_2, x_3, x_4) f_C(x_4) \quad (2.27)$$

Because of the factorization of $p(x)$ and because the graph has no cycles (loops), we can actually arrange these summations in a more computationally efficient manner. By pushing each summation as far as possible to the right in our calculation, we reduce its dimensionality

$$p(x_1) = \frac{1}{Z} \sum_{x_2} f_A(x_1, x_2) \sum_{x_3} \sum_{x_4} f_B(x_2, x_3, x_4) f_C(x_4). \quad (2.28)$$

In this example, I simply ordered the terms in a way that seemed like it would help. For a small graph without loops this was not difficult. It would be nice however, to have a way to accomplish this efficient arrangement of summations for any arbitrary factor graph. If you try to produce a nice ordering of summations and probability terms like the one I have constructed in equation (2.4.1), you will find that the summations tend to “push to the right” until they bump up against a particular factor node containing the variable in the summation. This means that we could imagine each summation happening locally at its particular factor node. The factor graph itself is providing a hint as to how to organize the computations in a marginalization. We can compute locally at each factor node and then pass our local answer on for

aggregation into the final answer. This is known as a probabilistic message passing algorithm.

Many statistical computations are like marginalization in the sense that they require computation over a factored joint distribution to compute a statistic of interest on a subset of variables and therefore lend themselves to a distributed message passing approach. First we show how to perform marginalization by probabilistic message passing. This is often called the sum product algorithm.

2.4.2 The Sum-Product Algorithm

Let us continue to suppose that we want to find the marginal probability distribution $p(x_1)$ on the graph in figure 2-15. In many applications we deal with random variables which are described by a discrete probability distribution, so the marginal distribution for a variable node is actually a vector representing the relative probabilities that variable i is in each of its various possible states. The message $n_{i \rightarrow a}(x_i)$ from a variable node i to a factor node a is also a vector containing the relative probabilities of the states of variable i given all the information available to node i except the information from the factor node f_a

$$n_{i \rightarrow a}(x_i) = \prod_{b \in N(i) \setminus a} m_{b \rightarrow i}(x_i). \quad (2.29)$$

Similarly, the message $m_{a \rightarrow i}(x_i)$ from a factor node f_a to a neighboring variable node i is a vector containing the relative probabilities of the states of variable i given the information available to f_a

$$m_{a \rightarrow i}(x_i) = \sum_{x_a \setminus x_i} f_a(x_a) \prod_{j \in N(a) \setminus i} n_{j \rightarrow a}(x_j). \quad (2.30)$$

Using the message passing rules we see that

$$\begin{aligned} p_1(x_1) &\propto m_{A \rightarrow 1}(x_1) \\ &\propto \sum_{x_2} f_A(x_1, x_2) n_{2 \rightarrow A}(x_2) \end{aligned}$$

$$\begin{aligned}
&\propto \sum_{x_2} f_A(x_1, x_2) m_{B \rightarrow 2}(x_2) \\
&\propto \sum_{x_2} f_A(x_1, x_2) \sum_{x_3} \sum_{x_4} f_B(x_2, x_3, x_4) n_{3 \rightarrow B}(x_3) n_{4 \rightarrow B}(x_4) \\
&\propto \sum_{x_2} f_A(x_1, x_2) \sum_{x_3} \sum_{x_4} f_B(x_2, x_3, x_4) m_{C \rightarrow 4}(x_4) \\
&\propto \sum_{x_2} f_A(x_1, x_2) \sum_{x_3} \sum_{x_4} f_B(x_2, x_3, x_4) f_C(x_2, x_4) \tag{2.31}
\end{aligned}$$

which is exactly the desired marginal distribution.

The sum product algorithm provides a general method for computing marginal probability efficiently in this way. It iterates on *local* estimates of the marginal probabilities of the variables by using probability information only from neighboring (connected) factor nodes. Nodes are said to share information with adjacent nodes by “passing a message” along the edge that connects them. Although messages are only passed between neighboring nodes of the graph at each step of the algorithm, over many steps information can traverse the graph in an attempt to find a globally consistent estimate of the marginal probabilities.

Message passing is a kind of dynamic programming, storing intermediate approximations to the true marginals and iterating on them. If the graph has no cycles, the sum product algorithm will find the exact maximum likelihood estimate for the marginal probability distributions for the state variables and is guaranteed to converge. If a graph is “loopy” (has cycles), as in our coding example, then the messages can potentially continue to traverse the graph forever searching in vain for a globally consistent answer and the algorithm may never converge. In practice, however, the sum product algorithm will often arrive at a good approximation of the exact marginal distributions even on loopy graphs. Much recent work has been centered on understanding under what circumstances this is so and the accuracy of the approximations made by the sum product and related algorithms.

2.5 Other Kinds of Probabilistic Graphical Models

So far we have focused on factor graphs. There are, however, other types of graphs for representing constrained probability distributions. In this section we introduce these other kinds of probabilistic graphical models, draw some comparisons, and show that they are all equivalent to factor graphs.

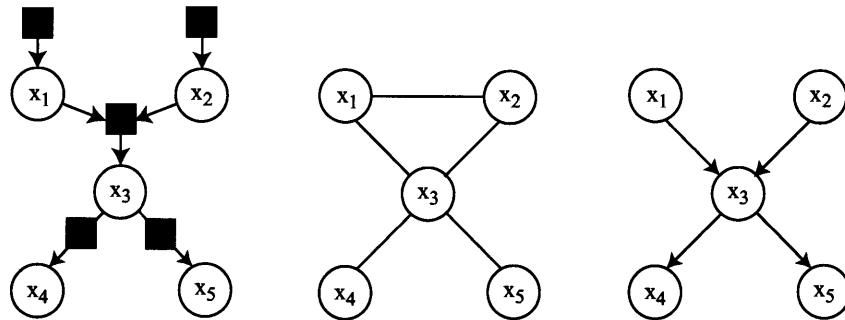


Figure 2-16: Left to right: factor graph, MRF, Bayesian network

Directed acyclic graphical models (Bayesian networks), undirected probabilistic graphical models (Markov Random Fields), and bipartite graphical models (factor graphs) are all ways to visually represent the dependencies among a set of random variables. An example of each kind of graphical model is shown in figure 2-16. Bayesian networks, Markov Random Fields (MRFs), and factor graphs are all formally equivalent in that any of them can be used to represent any probability distribution, however they tend to be appropriate in different situations. Bayesian networks with their directed edges are useful for representing conditional probability distributions and the conditional dependencies between variables. MRFs with their undirected edges are useful for representing unconditional probability distributions where the overall joint distribution is represented by the model factors into so called “potential” functions over pairs of random variables.

A factor graph like an MRF is an undirected graph. It can be advantageous to use a factor graph instead of an MRF when a model factors into potential functions of more than two variables. In such cases, it is often clearer to explicitly represent these functions of three or more variables by adding a node for such a function and

connecting to each of the three or more variable nodes thereby creating a factor graph. A factor graph can also represent conditional relationships between random variables like a Bayesian network. Factor graphs have begun to gather favor for representing signal processing systems.

2.5.1 Bayesian Networks

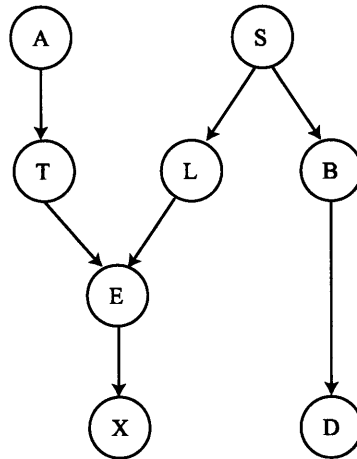


Figure 2-17: The fictional “Asia” example of a Bayesian network, taken from Lauritzen and Spiegelhalter 1988

Bayesian networks are probably the most widely known type of probabilistic graphical model. They are useful for modelling expert knowledge for applications such as medical diagnosis, natural language understanding, etc. The graph above illustrates a Bayesian network for medical diagnosis. We are given information about a patient such as risk factors, symptoms and test results, and we are asked to infer the probability that a given disease is the cause. The Bayesian network encodes statistical dependencies between symptoms, test results, and diseases which have been gathered in advance by for example asking medical experts or studying epidemiological research. The graph in figure 2-17 is from a fictional example which was presented by Lauritzen and Spiegelhalter and recounted in a very useful paper by Yedidia, Freeman, and Weiss [55]. The nodes represent random variables: A recent trip to Asia

“A” increases the probability of tuberculosis “T”. Smoking “S” increases the risk of both lung cancer “L” and bronchitis “B”. “E” represents the presence of either tuberculosis or lung cancer. They are both detectable by an X-ray “X”, but the X-ray alone is not enough to distinguish them. “D” is dyspnoea (shortness of breath) which may be caused by bronchitis, tuberculosis or lung cancer

x_i is the (discrete) state of a given node i . Arrows on edges indicate that there is a conditional probability of a node’s state given the state of its “parent” node. For example $p(x_L|x_S)$ is the conditional probability that a patient has lung cancer given that he or does not smoke. When a node has two parents, its state depends on both, for example $p(x_D|x_E, x_B)$. Nodes which have no parents have probabilities which are not conditional, like $p(x_S)$ or $p(x_A)$. If we have some absolute information about the state of a particular “observable” node, then we can set the probability of that state to 100%, for example if we “know for a fact” that someone smokes or did not ever visit Asia. The graph defines the dependency of some variables on some others, and is useful when there is structure in these dependencies. If every variable depended on every other, we might as well just write the equation for the joint over all the variables and dispense with drawing a graph at all. The graph expresses the fact that the joint probability distribution that the patient has some combination of symptoms, test results, risk factors and diseases can be written as the product of many distributions over just a few variables,

$$p(x_A, x_B, x_S, x_L, x_T, x_D, x_E, x_X) = p(x_A)p(x_S)p(x_T|x_A)p(x_L|x_S)p(x_B|x_S)p(x_E|x_L, x_T)p(x_D|x_B, x_E)p(x_X|x_E). \quad (2.32)$$

The Bayesian network on the right of figure 2-16 represents the factorization,

$$p(x_1, x_2, x_3, x_4, x_5) = p(x_1)p(x_3|x_1, x_2)p(x_4|x_3)p(x_5|x_3). \quad (2.33)$$

In general, a Bayesian network represents a factorization of a conditional distribution,

$$p(x_1, x_2, \dots, x_N) = \prod_{i=1}^n p(x_i | \text{parents}(x_i)). \quad (2.34)$$

2.5.2 Markov Random Fields

An MRF is an undirected graph G , with vertices and edges (V, E) . Each vertex V corresponds to a random variable in the model. Every node has neighbor nodes which are the nodes to which it is directly connected by an edge. Every variable in an MRF is independent of all the other variables in the model given its neighbors so that

$$(\forall x \in V) p(x | V \setminus \{x\}) = p(x | n(x)) \quad (2.35)$$

where $n(x)$ is the set of neighbors of x . An MRF is a graphical representation of how a global probability distribution over all of the random variables can be “factored” into a product of several lower dimensional probability distributions. Recall that the probability of an event A is equal to the product of the events that cause A so long as the causes are independent from one another; Independent probabilities simply multiply. An MRF is a pictorial representation of a product of potential functions. Once we normalize the product of the potential functions we have a joint probability distribution over all the random variables in the system,

$$p(x_1, x_2, \dots, x_N) = \frac{1}{Z} \prod_a f_a(V_a), \quad (2.36)$$

where a is an index labelling M functions, $f_A, f_B, f_C, \dots, f_M$, where the function $f_a(x_a)$ has arguments x_a that are some subset of $\{x_1, x_2, \dots, x_N\}$, and Z is a normalization pre-factor.

An edge connecting two nodes in an MRF represents the fact that those two random variables are NOT always independent. It turns out that if each function, $f_a(V_a)$, is identified with a completely inter-connected group of variable nodes known as a “clique,” then it is always possible to draw an MRF graph for any product of $f_a(V_a)$ ’s. The converse is also true; if we choose non-overlapping cliques to correspond to $f_a(V_a)$ ’s, then it is always possible to find a product of $f_a(V_a)$ ’s that corresponds to

any MRF that we can draw. This correspondence between a graph and a factorization of a probability distribution is called the Hammersley-Clifford Theorem.

2.5.3 Factor Graphs

Just like an MRF, the factor graph represents a product of potential functions. Unlike an MRF, potential functions in a factor graph are not defined over more than two nodes - so that there are no cliques in a factor graph which contain more than two nodes. In a factor graph, potential functions over more than two variables are represented by connecting all of the variables in the potential to a single factor node. Factor graphs make it easy to identify each potential function with a corresponding node which is not always immediately obvious in an MRF.

This is especially useful in the context of graphs for representing error correcting codes (ECC). In error correction coding, it is useful to make a distinction between variable nodes, which represent measured data from the channel or guesses by the decoder about symbols sent by the transmitter, and factor nodes which represent constraint functions (checksum operations or sub-codes). In error correction coding, the constraint functions act to impose the limitation that there can be no probability mass over certain values of the domain of the joint distribution. In other words, the constraint functions zero out the joint probability distribution for certain values of the state variables. Mathematically, we could have treated variables and constraint functions alike, as factors in the joint probability distribution represented by the overall graph, but in practice they play different roles and it is useful to represent this difference visually.

2.5.4 Forney Factor Graphs (FFG)

In a factor graph, variable nodes store values while factor nodes compute functions on them and unlike other graphical models, there is a one to one correspondence between functions and the factor nodes which represent them. This means that we don't really need to represent the variables explicitly in the graph. The functions are

the important part. They can simply pass values to each other along edges.

Forney showed how to create factor graphs without variable nodes by replacing internal variable nodes of degree ≥ 3 by a special kind of soft-gate called a soft-equals whose job it is to insist that all (3 or more) incident edges have equal values. Variable nodes of degree 2 have no processing task to fulfill since they simply pass a value on from one edge to the other. They can therefore be removed just leaving the edge. External variable nodes (leaf nodes) in this scheme are still included in the factor graph and have degree = 1.

A soft-equals node with incoming messages $p_X(x)$ and $p_Y(y)$ computes

$$p_Z(z) = \gamma \int_x \int_y f(x, y, z) p_X(x) p_Y(y) \quad (2.37)$$

where $f(x, y, z) = \delta(x - y)\delta(x - z)$. A soft-equals for *binary* variables and three incident edges is given by

$$\begin{aligned} p_Z(1) &= p_X(1)p_Y(1) \\ p_Z(0) &= p_X(0)p_Y(0). \end{aligned} \quad (2.38)$$

where $f(x, y, z) = 1$ if $x = y = z$, and otherwise $f(x, y, z) = 0$.

Let us examine the sum product algorithm for a single soft-equals gate with three attached leaf nodes. The Forney factor graph is shown in figure 2-18. Recall that in a Forney factor graph, even as we remove all internal variable nodes, variable nodes which are leaf nodes are allowed to remain.

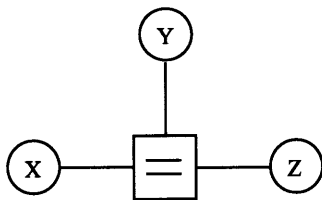


Figure 2-18: Message passing with a single equals gate

Let X, Y, Z be binary variables, each receiving some evidence. The soft-gate imposes a constraint requiring them to be equal. For example, if the local evidence for X was $[\cdot 7, \cdot 3]$, for Y was $[\cdot 6, \cdot 4]$, and for Z was $[\cdot 2, \cdot 8]$, then we would find that the beliefs at X, Y , and Z would be equal and would be equal to $[(\cdot 7)(\cdot 6)(\cdot 2), (\cdot 3)(\cdot 4)(\cdot 8)]$ normalized appropriately. X would send in a message to the soft-equals, $[\cdot 7, \cdot 3]$ and Y would send in a message to the equal that was $[\cdot 6, \cdot 4]$. The soft-equals would then send out a message to Z , $[(\cdot 7)(\cdot 6), (\cdot 3)(\cdot 4)]$. Combining that with its local evidence, Z would conclude that its belief was $[(\cdot 7)(\cdot 6)(\cdot 2), (\cdot 3)(\cdot 4)(\cdot 8)]$.

2.5.5 Circuit Schematic Diagrams

In an factor graph we can think of edges as wires, and function nodes as computational elements, directly suggesting circuit implementations. Later, we will discuss circuit implementations of probabilistic message passing at great length. But if we forget for a moment about the messages being probability distributions, factor graphs should already appear rather familiar. They are just diagrams of functions and how they are connected. Schematic diagrams of circuits are technically a kind of factor graph.

2.5.6 Equivalence of Probabilistic Graphical Models

Converting from a Factor Graph to a Markov Random Field

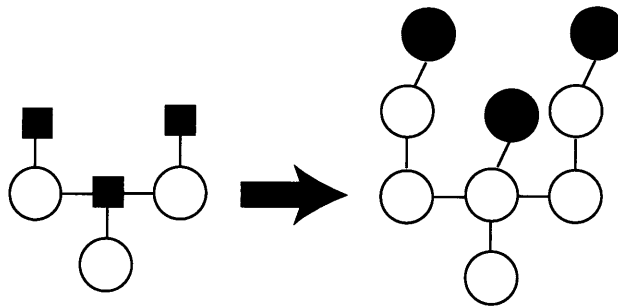


Figure 2-19: Converting a factor graph to a pairwise MRF

It is easy to convert a factor graph into an equivalent MRF. Let $F(S, Q)$ be a

factor graph and let F^2 be a graph with the same set of vertices as F but with edges between any two vertices, x and x' only if they are connected by a path of length two in F . Since F is bipartite like all factor graphs, F^2 is actually at least two graphs, one with only variable nodes and one with only factor nodes. As long as $F(S, Q)$ is a factor graph that represents a product of non-negative functions as in equation (2.36), then the graph in F^2 with only variable nodes is an MRF. For example, the factor graph on the left in figure 2-16 reduces to the MRF to its right. Notice that states x_1 and x_2 are now connected, because in the factor graph they were separated by a path of length two.

We lost nothing when we removed the factor nodes from the factor graph to produce the MRF. We didn't remove potentials from our product of potentials. However the correspondence between potential functions and nodes must be reinterpreted when we perform this operation. In the MRF, potential functions that used to be affiliated with factor nodes will now correspond to cliques of connected variable nodes.

Bayesian Networks and Converting a Factor Graph to a Bayesian Network

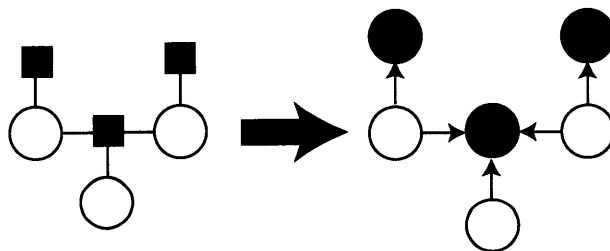


Figure 2-20: Converting a a factor graph to a Bayesian network

A Factor Graph can be thought of as the "square root" of a Bayes Net. As can be seen in the example in figure 2-16, to obtain a Bayesian network from the factor graph $F(S, Q)$, it is only necessary to remove the factor nodes from the factor graph.

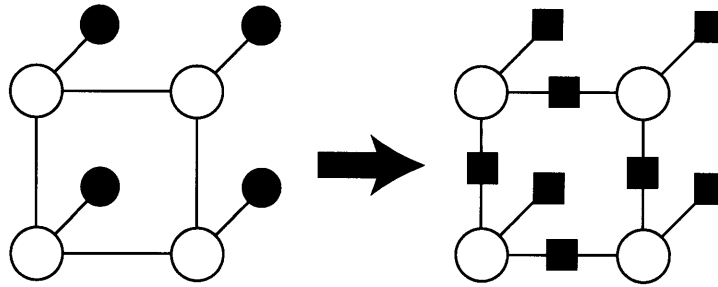


Figure 2-21: Converting a MRF to a factor graph

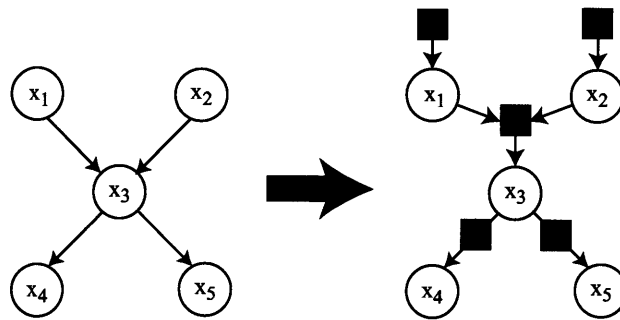


Figure 2-22: Converting a Bayesian network to a factor graph

Converting from Markov Random Fields and Bayesian Networks to Factor Graphs

It is also possible to go the other way, from a given MRF or Bayesian network to a factor graph. To convert an MRF to a factor graph, the two node functions in in the MRF are replaced by factor nodes. To convert a Bayesian network to a factor graph, we must insert a factor node to link a node and all of its parents, since that is the form of each conditional potential function. Every MRF and Bayesian network can be written as a number of different factor graphs, because we must make some arbitrary choices about how to break up cliques and consequently where to add factor nodes.

2.6 Representations of Messages: Likelihood Ratio and Log-likelihood Ratio

2.6.1 Log-Likelihood Formulation of the Soft-Equals

The definition of the log-likelihood ratio (log-likelihood) is

$$L_Z = \ln \left[\frac{p_Z(0)}{p_Z(1)} \right]. \quad (2.39)$$

In the log-likelihood representation, the product message from an soft-equals gate can be written as

$$L_Z = L_X + L_Y. \quad (2.40)$$

To see this, we begin by manipulating the definition of the log-likelihood,

$$L_Z = \ln \left[\frac{\mu_Z(0)}{\mu_Z(1)} \right] \quad (2.41)$$

$$= \ln \left[\frac{\mu_X(0)\mu_Y(0)}{\mu_X(1)\mu_Y(1)} \right] \quad (2.42)$$

$$= L_X + L_Y. \quad (2.43)$$

2.6.2 Log-Likelihood Formulation of the Soft-xor

In the log-likelihood representation, the product message from an soft-xor gate can be written as

$$\tanh(L_Z/2) = \tanh(L_X/2) \tanh(L_Y/2). \quad (2.44)$$

To see this, we begin by manipulating the definition of the log-likelihood,

$$L_Z = \ln \left[\frac{\mu_Z(0)}{\mu_Z(1)} \right] \quad (2.45)$$

$$= \ln \left[\frac{\mu_X(0)\mu_Y(0) + \mu_X(1)\mu_Y(1)}{\mu_X(1)\mu_Y(0) + \mu_X(0)\mu_Y(1)} \right] \quad (2.46)$$

$$= \ln \left[\frac{\frac{\mu_X(0) \mu_Y(0)}{\mu_X(1) \mu_Y(1)} + 1}{\frac{\mu_X(0)}{\mu_X(1)} + \frac{\mu_Y(0)}{\mu_Y(1)}} \right] \quad (2.47)$$

$$= \ln \left[\frac{\exp(L_X + L_Y) + 1}{\exp(L_X) + \exp(L_Y)} \right] \quad (2.48)$$

$$\exp(L_Z) = \left[\frac{\exp(L_X + L_Y) + 1}{\exp(L_X) + \exp(L_Y)} \right]. \quad (2.49)$$

Multiplying both sides by the denominator of the right side we obtain

$$\exp(L_X + L_Y) = \exp(L_X + L_Z) + \exp(L_Y + L_Z) - 1. \quad (2.50)$$

As can be seen by multiplying by the denominators of both sides of the following expression, the last equation is a simplification of the following

$$\frac{\exp(L_X + L_Y) - \exp(L_X) - \exp(L_Y) + 1}{\exp(L_X + L_Y) + \exp(L_X) + \exp(L_Y) + 1} = \frac{\exp(L_Z) - 1}{\exp(L_Z) + 1}. \quad (2.51)$$

The left hand side of this equation can be factored into

$$\frac{(\exp(L_X) - 1)(\exp(L_Y) - 1)}{(\exp(L_X) + 1)(\exp(L_Y) + 1)} = \frac{\exp(L_Z) - 1}{\exp(L_Z) + 1}. \quad (2.52)$$

remembering the definition of tanh

$$\tanh(x) = \frac{e^x - e^{-x}}{e^x + e^{-x}} = \frac{\exp(2x) - 1}{\exp(2x) + 1}, \quad (2.53)$$

we can finally write the message from soft-xor in terms of log-likelihoods as

$$\tanh(L_Z/2) = \tanh(L_X/2) \tanh(L_Y/2). \quad (2.54)$$

2.7 Derivation of Belief Propagation from Variational Methods

In the previous sections we derived the sum product algorithm by observing that marginalization could be simplified by performing local marginalization at each factor node and passing on the answer. Another way to understand message passing algorithms involves the calculus of variations. The sum product algorithm can be understood as minimizing a “free energy” function with Lagrangian constraints. In this scheme, each factor node is thought of as imposing a constraint on the shape of the joint distribution and therefore also constrains the marginal distribution that we are attempting to find. This is easier to understand in the context of an example and is presented in the next chapter in the example on routing in an adhoc peer-to-peer networks.

Chapter 3

Examples of Probabilistic Message Passing on Graphs

3.1 Kalman Filter

In this example we explore a practical example of the sum product algorithm on graphs with a one-dimensional “chain” topology. The operations are on probability distributions of continuous-valued variables. Message passing occurs in only one direction (forward) on the graph.

We use a Kalman filter when we have a good model for the update dynamics of a system but we cannot directly observe the (hidden) internal state of the system. Since we cannot directly observe the internal state of the system, we measure something about the system which we know is related to the internal state. Then, using successive measurements, we repeatedly update the state of our model of the system until it (hopefully) corresponds to the hidden internal state of the system we are observing.

The canonical example is the task of continuously estimating the position of an airplane. The airplane has a current state, \vec{x}_t given by its position, velocity and acceleration in three-space as well as the positions of its control surfaces. The state is updated in discrete-time according to a distribution function $p(\vec{x}_{t+1}|\vec{x}_t)$, which includes both deterministic influences (aerodynamics) and random influences (turbu-

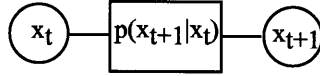


Figure 3-1: System state update

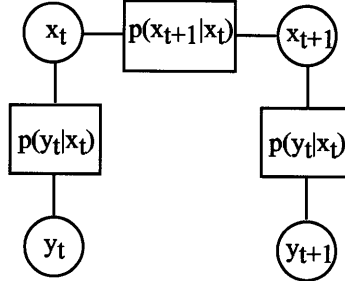


Figure 3-2: System state update combined with measurements

lence, control errors). For now, let us assume that the system update is linear with update matrix \mathbf{A} and Gaussian noise process η with covariance matrix \mathbf{Q} ,

$$\vec{x}_t = \mathbf{A}x_{t-1} + \mathbf{G}\vec{\eta}_t. \quad (3.1)$$

We don't actually know the current state of the airplane. We only infer it from a model which updates the last state according to $p(x_{t+1}|x_t)$. Our estimate would be better, if we combined this information with information from current measurements y_t from equipment such as airspeed sensors, global positioning devices, radar, and aileron position sensors. These sensor measurements are related to the actual state by a noise model $p(\vec{y}_t|\vec{x}_t)$. For now we assume a linear relationship between the sensor readings and the current state with Gaussian noise process ε ,

$$\vec{y}_t = \mathbf{B}x_t + \vec{\varepsilon}_t. \quad (3.2)$$

In Kalman filtering wish to calculate $P(x_t|y_0, \dots, y_t)$. In order to do this we must send messages from the current measurement nodes and the last state node to the current state node. The message passed along the horizontal edge from past state to current state is called the time update and calculates $P(x_t|y_0, \dots, y_t) \rightarrow$

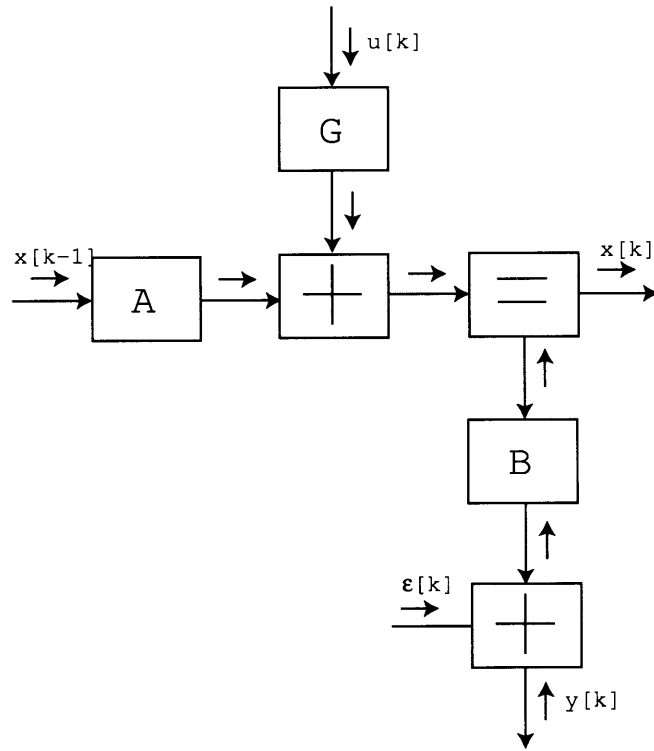


Figure 3-3: Kalman filter update

$P(x_{t+1}|y_0, \dots, y_t)$. The message passed along the vertical edge which incorporates a new measurement is called the measurement update and calculates, $y_{t+1}: P(x_{t+1}|y_0, \dots, y_t) \rightarrow P(x_{t+1}|y_0, \dots, y_t)$.

Let us use a more compact notation, so that the probability distribution for x_t conditioned on y_0, \dots, y_t has mean $\hat{x}_{t|t} \equiv E[x_t|y_0, \dots, y_t]$ and covariance $P_{t|t} \equiv E[(x_t - \hat{x}_{t|t})(x_t - \hat{x}_{t|t})^T|y_0, \dots, y_t]$. With this notation the time update step is

$$\hat{x}_{t+1|t} = \mathbf{A}\hat{x}_{t|t} \tag{3.3}$$

and

$$P_{t+1|t} = \mathbf{A}P_{t|t}\mathbf{A}^T + \mathbf{G}\mathbf{Q}\mathbf{G}^T. \tag{3.4}$$

So far we have used the Kalman filter proper to model a linear system. For a linear system, the Kalman filter obtains a provably maximum-likelihood estimate of

the system's state. In order to obtain this maximum-likelihood estimate, messages only need be passed forward along the graph, since we are only ever interested in an estimate of the current (hidden) state of the system given the most up-to-date measurements we have. In this application we have no reason need to go back to improve our estimates of past states. A Kalman filter with a linear approximation of a nonlinear system is called an extended Kalman filter, and is not provably optimum, but has been shown to behave well for many examples. A Kalman filter with a nonlinear model of a nonlinear system may behave just as well as the extended Kalman filter, but does not have a name. The Noise Lock Loop described in this thesis is just such a model.

3.2 Soft Hamming Decoder

In this example we explore a practical example of a the sum product algorithm on graphs of arbitrary topology, possibly with cycles. The operations are on probability distributions of discrete-valued variables.

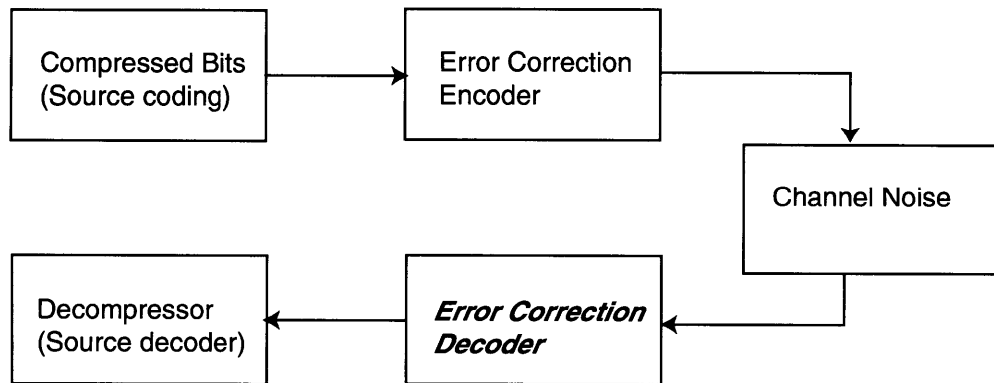


Figure 3-4: A communications system

Probabilistic graphical models have become essential for understanding communication systems. In a communication system, we wish to transmit information represented as bits across a noisy channel without losing any of the information. The

information to be communicated is encoded and then modulated before it is transmitted over a channel. Encoding is generally used to add redundancy to the information in order to make it robust against the channel noise. Modulation is generally thought of as being used to represent the information in such a way that is suited for transmission through the physical medium of the channel. Traditionally, coding was performed by a digital system while modulation was performed by an analog system, but the distinction is unimportant from a mathematical perspective.

3.2.1 Encoding

Let us examine a simple example of how probabilistic graphical models can be used in a communication system for error correction coding (ECC). Suppose we wanted to be able to send any possible 3 bit message, $\{(000), (001), \dots (111)\}$, over a noisy channel. In practice, to protect the message from corruption by channel noise we want to encode the message as a word containing more bits. Whenever we mean $\{001\}$ for example, we could actually send (001101) . To define such a code, we could make a list of 6-bit codewords, \vec{x} that we could transmit in lieu each of the 3-bit messages, \vec{m} . The extra bits are often called parity bits.

message	codeword
000	000000
001	001101
010	010011
011	011110
100	100110
101	101011
110	110101
111	111011

For long message words, such lists could quickly become memory intensive in the transmitter. This is a linear code which means we can create a generator matrix,

$$\mathbf{G} = \begin{bmatrix} 100110 \\ 010011 \\ 001101 \end{bmatrix}. \quad (3.5)$$

as a convenience for transmuting messages into codewords by the formula $\mathbf{M} \cdot \vec{m}$. Note that this is also a *systematic code* meaning that each message word is actually transmitted as part of the codeword - in this case the first part. The first three columns of the generator matrix therefore are the identity matrix.

The receiver can determine if any errors were introduced into the transmitted codeword by multiplying the received (hard-decision, possibly corrupt) codeword by the parity-check matrix $\mathbf{H} \cdot \vec{x}$, where

$$\mathbf{H} = \begin{bmatrix} 101100 \\ 110010 \\ 011001 \end{bmatrix}. \quad (3.6)$$

and seeing if the answer is 0. We can convert the generator matrix into its corresponding parity-check matrix by transposing unsystematic part of the generator matrix and concatenating it to the right with the appropriate sized (here 3×3) identity matrix.

The parity-check matrix is really checking the received codewords to see if they satisfy set of algebraic constraints that define the code. All of the above codewords satisfy the constraints:

$$\begin{aligned} x_1 \oplus x_2 \oplus x_5 &= 0 \\ x_2 \oplus x_3 \oplus x_6 &= 0 \\ x_1 \oplus x_3 \oplus x_4 &= 0. \end{aligned} \quad (3.7)$$

Defining the codewords in terms of a set of constraints is very helpful when we start to think about building a receiver which must recognize if a message is in error.

If the received signal does not satisfy the set of constraints, then the receiver knows that an error has been introduced by the channel. If the codewords are long enough for a given amount of noise, and thereby provide enough information, the receiver can even use the rules to make a good guess for what value was actually sent by the transmitter and restore the corrupted bit to its original uncorrupted value.

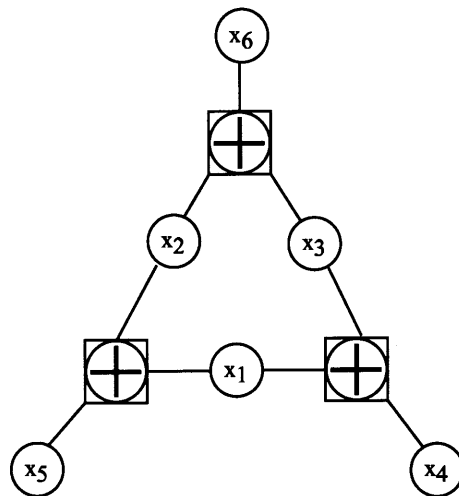


Figure 3-5: Graph representing the codeword constraints

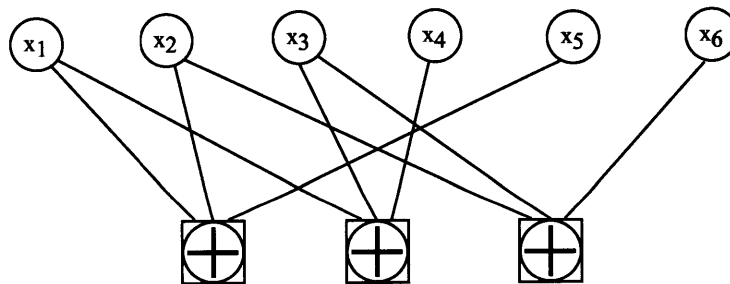


Figure 3-6: Graph representing the same codeword constraints

The constraints can be represented in graphical form as shown in figures 3-5 and 3-6. In these encoder graphs, the constraint nodes are mod 2 sums as defined by

<i>Edge1</i>	<i>Edge2</i>	<i>Edge3</i>	
0	0	0	
0	1	1	(3.8)
1	0	1	
1	1	0	

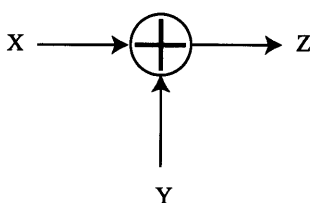


Figure 3-7: Mod 2 sum

and represented by the node in figure 3-7. Considering any two edges as the input to the mod 2 sum and the third edge as an output, it is evident that the output of the mod 2 sum is 1 when the inputs are different and 0 when the inputs are the same. The edges attached to the nodes in 3-8 are bidirectional, so that at any time we can choose two of the three edges into a node to consider as inputs, while the third edge will output the mod 2 sum of the values presented on these two edges. The check-sum constraint must be satisfied in every direction.

3.2.2 Decoding with Sum Product Algorithm

Representing the constraints in graphical form is helpful, because it enables us to immediately construct a graph for the receiver's decoder as in figure 3-8. In the receiver, we replace the mod 2 sum with its probabilistic equivalent, a "soft-xor" gate which was defined in equation (2.3.3). Just like the mod 2 check-sum nodes in the encoder graphs, the edges connected to the soft-xor nodes in the decoder graphs

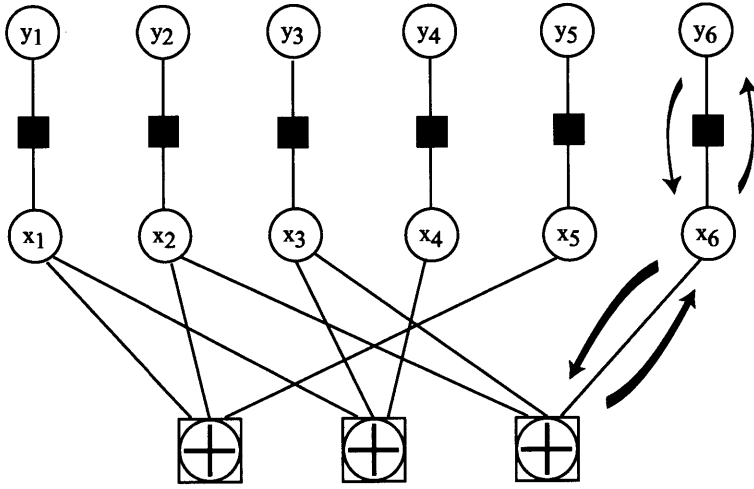


Figure 3-8: Receiver graph implementing the codeword constraints

are bidirectional.

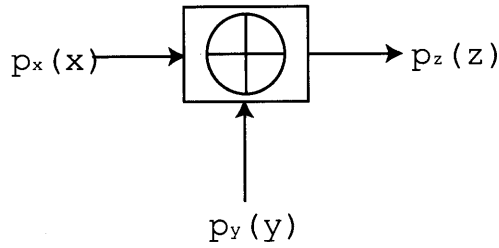


Figure 3-9: Symbol for the soft-xor gate

Now let us perform the sum-product algorithm on our larger decoder graph to again compute the marginal probability of variable x_1 .

$$\begin{aligned}
 p_1(x_1) &\propto m_{A \rightarrow 1}(x_1) m_{B \rightarrow 1}(x_1) m_{E \rightarrow 1}(x_1) \\
 &\propto \sum_{x_2, x_5} f_A(x_1, x_2, x_5) \sum_{x_3, x_4} f_B(x_1, x_3, x_4) \sum_{y_1} f_E(y_1) \cdot n_{2 \rightarrow A}(x_2) n_{5 \rightarrow A}(x_5) n_{3 \rightarrow B}(x_3) n_{4 \rightarrow B}(x_4) \\
 &\propto \sum_{x_2, x_5} f_A \sum_{x_3, x_4} f_B \sum_{y_1} f_E \cdot m_{C \rightarrow 2} m_{F \rightarrow 2} m_{I \rightarrow 5} m_{C \rightarrow 3} m_{G \rightarrow 3} m_{H \rightarrow 4}
 \end{aligned} \tag{3.9}$$

Already we can see that the single cycle in our decoder graph complicates matters,

since we must sum over the same variable more than once. It turns out that the sum-product algorithm yields the exact solution for the marginal probabilities on graphs with no cycles. On graphs with a single cycle it is guaranteed to still converge, but usually does not converge to the exact answer. With more than one cycle in this graph, we are not guaranteed that the algorithm will converge at all.

To implement the algorithm, the soft parity check functions are soft-gates. For example, f_A is a soft-xor,

$$\sum_{x_2, x_5} f_A(x_1, x_2, x_5) = \begin{pmatrix} p_{x_1}(0) \\ p_{x_1}(1) \end{pmatrix} = \begin{pmatrix} p_{x_2}(0)p_{x_5}(0) + p_{x_2}(1)p_{x_5}(1) \\ p_{x_2}(0)p_{x_5}(1) + p_{x_2}(1)p_{x_5}(0) \end{pmatrix}. \quad (3.10)$$

f_E is a conditional distribution which models the noise in the channel. Let us assume it is Gaussian with mean μ_1 and variance σ ,

$$p(y_1|x_1) = \frac{1}{2\sigma} e^{-(y_1-x_1)^2/2\sigma^2}. \quad (3.11)$$

Similarly, let

$$\begin{aligned} f_F &= p(y_2|x_2) \\ f_G &= p(y_3|x_3) \\ f_H &= p(y_4|x_4) \\ f_I &= p(y_5|x_5) \\ f_J &= p(y_6|x_6). \end{aligned} \quad (3.12)$$

$$(3.13)$$

are all functions of analogous form. Let \hat{y}_i be a received value, then for an *additive white Gaussian noise* (AWGN) channel, $p_{Y|X}(\hat{y}|x)$ is given by

$$\begin{aligned} p_{Y|X}(\hat{y}|x=1) &= \exp[-(\hat{y}-1)^2/2\sigma^2] \\ p_{Y|X}(\hat{y}|x=-1) &= \exp[-(\hat{y}+1)^2/2\sigma^2] \end{aligned} \quad (3.14)$$

3.3 Optimization of Probabilistic Routing Tables in an Adhoc Peer-to-Peer Network

In this example we explore a practical example of a the sum product algorithm on random graphs with an arbitrary topology, with cycles. The operations are on probability distributions of discrete-valued variables. We also show how to derive local constraint functions in general from a global property which we would like to optimize. Along the way show the connection of the sum product algorithm to variational methods for finding minima of a function.

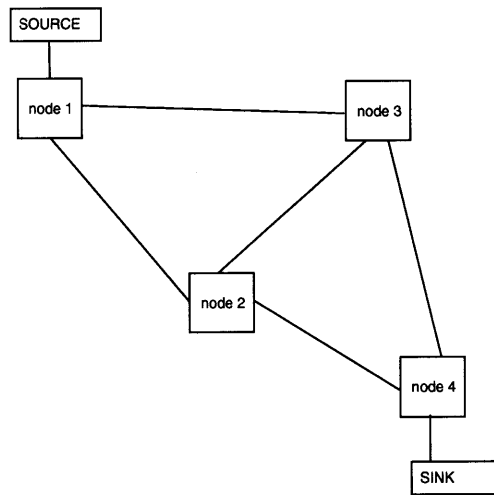


Figure 3-10: Random ad hoc peer-to-peer network. There are four interfaces $\{1, 2, 3, 4\}$ on nodes 1 and 4, and three interfaces $\{1, 2, 3\}$ on nodes 2 and 3.

We present a dynamic program for the optimization of probabilistic routing tables in an ad hoc peer-to-peer network. We begin with a random graph composed of $n = \{1 \dots N\}$ communication nodes each represented in figure 3-11 by a dashed square. Each node can have an arbitrary number of arbitrary interconnections. Each node will have some number of incident edges $n_i = \{n_1 \dots n_I\}$. In the figure, nodes are shown with either three or four incident edges. An incident edge n_i to a node n we call an interface. An interface is a port for a node n_i to communicate to another node

n_j along a connecting edge. Interfaces will serve as the fundamental data structure in our dynamic program, and are represented by circles in figure 3-12.

The goal is to route data packets across this random graph of communication nodes from an arbitrarily chosen *source* node to an arbitrarily chosen *sink* node via a path with the smallest possible number of intervening nodes. Let each interface i of each node n be associated with a random (binary) variable, *send* which has two states: the interface is a sender, denoted by s or a receiver denoted by r . Each interface therefore has an associated (normalized) probability distribution,

$$b_{n_i}(\textit{send}) = \begin{bmatrix} b(n_i = s) \\ b(n_i = r). \end{bmatrix} \quad (3.15)$$

When a node receives a packet it “flips a weighted coin” to decide which of its interfaces out of which it will route that packet according to a (normalized) distribution over its interfaces,

$$b_n(\textit{send}) = \begin{bmatrix} b(n_1 = s) \\ b(n_2 = s) \\ \vdots \\ b(n_I = s). \end{bmatrix} \quad (3.16)$$

To accomplish the goal of routing packets, we will optimize this probabilistic “routing table”, p_{n_i} for every node.

It is possible to write the (factorized) joint distribution over all of the random variables in our graph as the product of each of the local p_{n_i} ,

$$b_N = \prod_{n=1}^N p_{n_i} \quad (3.17)$$

This is a many dimensional distribution with as many dimensions as there are interfaces in the network. To pose the optimization problem, we imagine a goal distribution p_N which is the best choice of b_N and which will optimally route packets

through the network. The Kullback-Liebler (KL) divergence,

$$D(b(x)||p(x)) = \sum_x b(x) \ln \frac{b(x)}{p(x)}, \quad (3.18)$$

although not a true metric, is a useful measure for the difference between two probability distributions. If we define $p(x) = \frac{1}{Z} e^{-E(x)}$, we can rewrite the KL divergence as

$$D(b(x)||p(x)) = \sum_x b(x) E(x) + \sum_x b(x) \ln b(x) + \ln Z \equiv U(b(x)) - S(b(x)). \quad (3.19)$$

We call $U(b(x)) - S(b(x))$ the Gibbs free energy. Its minimum possible value is $-\ln Z$ (the Helmholtz free energy). The definition of an expectation of a function $f(x)$ is defined as

$$\langle f(x) \rangle \equiv \sum_x f(x) b(x), \quad (3.20)$$

so the first term in the Gibbs free energy, $U(b(x)) = \sum_x b(x) E(x)$ is called the average energy. The second term is the negative of the entropy of $b(x)$. To optimize our probabilistic routing table we must choose a form for our trial distribution $b(x)$, and substitute it into the Gibbs free energy and perform the minimization. We would like to optimize this $b(x)$ subject to some constraints which we might believe should be imposed to achieve efficient routing. We will choose the “flow” constraint,

$$F(x) = \delta[\sum_N \sum_I p(n_i = s) - \sum_N \sum_I p(n_i = r) = z] \quad (3.21)$$

where $z = \{\dots, -3, -2, -1, 0, 1, 2, 3, \dots\}$ is a “small” integer, based on the common-sense assumption that messages should be sent from nodes as often as they are received. This is essentially a conservation constraint. In a flow of water, for example, this would tend to say that water that enters somewhere, should on average tend to leave there. This constraint will be imposed by the average energy term, while the negative entropy term in the Gibbs free energy will tend to force the trial distribution $b(x)$ to have the maximum possible entropy (minimum negative entropy) while still

satisfying the constraint. Since the uniform distribution is the maximum entropy distribution, this will tend to spread probability over all of $p(x)$ as much as possible subject to the flow constraint, thereby tending to distribute satisfaction of the flow constraint across the network. We will impose the global flow constraint $f(x)$, by choosing an energy function of the form,

$$E(x) = \exp \left[\sum \ln f(x) \right]. \quad (3.22)$$

Optimizing this many-dimensional distribution would be computationally prohibitive. However, we can factorize the global flow constraint function into many local constraints in order to make the computation more tractable. This will require that we make some assumptions about which variables must be modelled as being directly dependent on one another. Once we decide what dependencies between variables are important to model, the dependencies can be conveniently represented in graphical form by a factor graph.

For example, we will begin by hoping that stable routing can be achieved with only nearest-neighbor connections. This means that we can derive the factor graph of dependencies graph from the ad hoc network itself as shown in figure 3-12. Other dependencies could also exist, but are a subject for future work.

Constraint functions in figure 3-12 are indicated by black squares. We will actually use two constraint functions, one between two interfaces connecting different nodes $f(b_i, b_j)$, and one between the multiple interfaces of a single node $g(b_k, b_l, b_m, b_n \dots)$. If two interfaces i and j from two different nodes are connected, this represents a path for packets to flow from node to node, so it makes sense that if one interface is the sender the other ought to be a receiver. This condition can be enforced by the constraint

$$f(x) = \delta(p_i(s) - p_j(r) = 0) \delta(p_j(s) - p_i(r) = 0). \quad (3.23)$$

If multiple interfaces $\{k, l, m\}$ belong to the same node, it makes sense that at least one should be a receiver and at least one should be a transmitter which can be enforced by the constraint

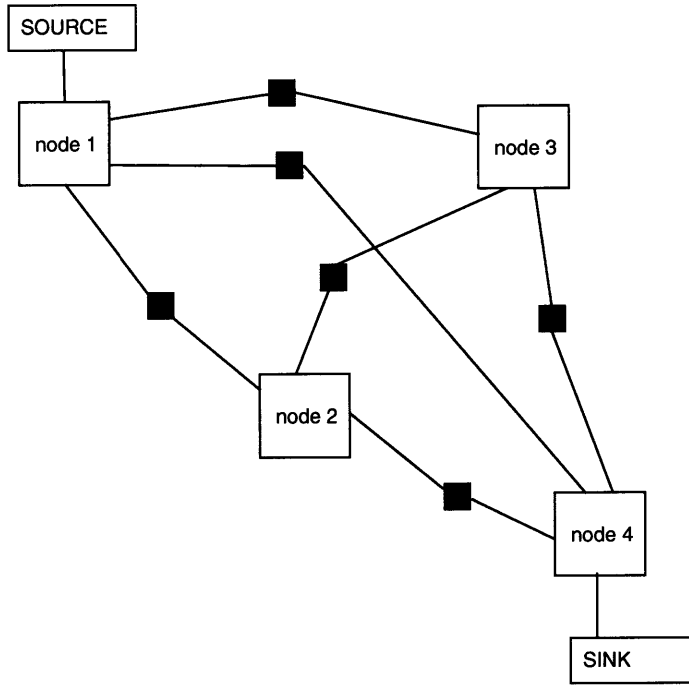


Figure 3-11: Factor graph derived from ad hoc peer-to-peer network.

$$\begin{aligned}
 g(x) &= \delta(p_k(s) + p_l(s) + p_m(s) - p_k(r) - p_l(r) - p_m(r) = 1) \cdot \\
 &\delta(p_k(s) + p_l(s) + p_m(s) - p_k(r) - p_l(r) - p_m(r) = 2). \quad (3.24)
 \end{aligned}$$

We can use the sum-product algorithm to minimize the Gibbs free energy under these constraints. In order to do this we must derive probabilistic messages to pass from function nodes f in our factor graph to interface nodes, from function nodes g to interface nodes, and from interface nodes to function nodes. Messages from function nodes f , connected to two interfaces are denoted by

$$\mu(i) = \sum_j p_J(j) f(i, j). \quad (3.25)$$

With the constraint that a sender sends to a receiver, the function between two

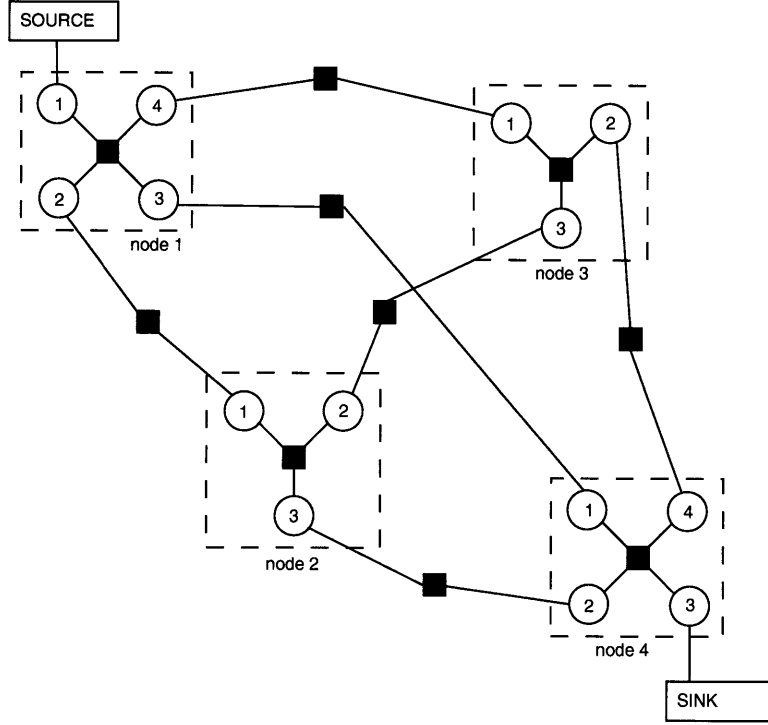


Figure 3-12: Factor graph derived from ad hoc peer-to-peer network. There are four interfaces $\{1, 2, 3, 4\}$ on nodes 1 and 4, and three interfaces $\{1, 2, 3\}$ on nodes 2 and 3.

interfaces from two different nodes is a soft-inverter so that,

$$\begin{bmatrix} \mu(i = s) \\ \mu(i = r) \end{bmatrix} = \begin{bmatrix} p_J(r) \\ p_J(s) \end{bmatrix}. \quad (3.26)$$

Messages from function nodes connected to three interfaces $\{k, l, m\}$ are given by

$$\mu(n_i) = \sum_{k,l} p_K(k) p_L(l) f(k, l, m). \quad (3.27)$$

which with the constraints we have chosen becomes,

$$\begin{bmatrix} \mu(k = s) \\ \mu(k = r) \end{bmatrix} = \begin{bmatrix} p_L(r) p_M(r) + p_L(r) p_M(s) + p_L(s) p_M(r) \\ p_L(s) p_M(s) + p_L(s) p_M(r) + p_L(r) p_M(s) \end{bmatrix}. \quad (3.28)$$

The derivation of messages from function nodes with more than three interfaces is

left as an exercise for the reader. The outgoing message from an interface with two incident edges is just a copy of the incoming message,

$$\begin{bmatrix} \mu(i = s) \\ \mu(i = r) \end{bmatrix} = \begin{bmatrix} p_J(s) \\ p_J(r) \end{bmatrix}. \quad (3.29)$$

In addition, we must also impose a normalization constraint on all messages so that $\mu(i = s) + \mu(i = r) = 1$ and $\nu(i = s) + \nu(i = r) = 1$.

Implementation of continuous-time message passing involves an asynchronous discrete-time approximation. We use a message passing schedule in which a node sends a message along an incident edge if and only if there are incoming messages pending on every other incident edge. We will further discuss scheduling in a later chapter.

Chapter 4

Synchronization as Probabilistic Message Passing on a Graph

In this chapter I apply message passing on graphs to the problem of synchronizing discrete-time periodic systems. We examine two examples, synchronization of a discrete-time ring oscillator in AWGN and of a Linear Feedback Shift Register (LFSR) in AWGN. From the ring oscillator example we learn that entraining oscillators perform maximum-likelihood phase estimation, if given the proper coupling. LFSR synchronization is an important problem in DS/CDMA multiuser communication.

4.1 The Ring Oscillator

A ring (relaxation) oscillator is a very simple circuit which is often used to test a new semiconductor fabrication process. It consists of an inverter with its output connected to its input in a feedback loop. The circuit will repeatedly switch from a zero to a one and back again as fast as the devices allow. The schematic diagram for a ring oscillator is shown in figure 4-1. For compliance reasons, a single inverter doesn't like to drive its own input so a larger (odd) number of inverters is generally used.

We can draw the factor graph for a ring oscillator by simply replacing the inverter with a soft-inverter soft-gate as shown in figure 4-2. In the last chapter we saw an

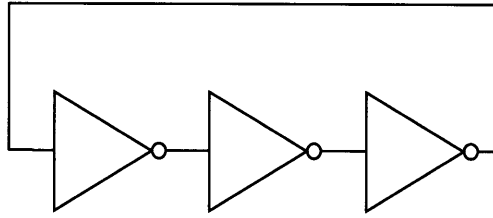


Figure 4-1: Schematic diagram for a ring (relaxation) oscillator

the example “loopy” factor which had just a variable node and a soft-inverter in a feedback loop. That graph eventually settled to a solution of $p_X(1) = .5, p_X(0) = .5$. This graph is different because it includes a delay element, represented by a delay factor node. The delay acts like a pipe or first-in-first-out (FIFO) buffer. A message that enters on end of the delay, exits at the other end some time later. The switching speed is set by the delay element, because a message that enters the delay cannot force the ring oscillator to switch until it comes out the other end. No matter if the delay can only contain one message at a time or if can store more, this factor graph ring oscillator will oscillate.

As we approach the limit where the delay can contain a very large number of messages, the system begins to approximate a continuous-time system with many samples per each cycle of the generated waveform. As we approach continuous-time operation, we can also add a low-pass filter to the loop in order to smooth the transitions and model the bandwidth limit of the inverter devices.

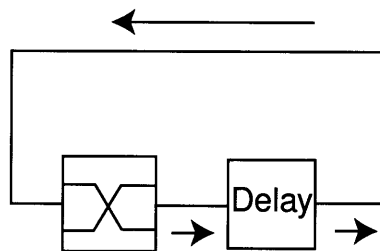


Figure 4-2: Factor graph for a ring (relaxation) oscillator

4.1.1 Trellis Decoding for Ring Oscillator Synchronization

Our goal is to synchronize to a ring oscillator. Another way to say this is that we would like to estimate the current state of a ring oscillator that is transmitting its state to us through a noisy channel. This sounds a lot like an error correction decoding task. Ordinarily if we wanted to generate a maximum-likelihood estimate of the state of a transmit system, we would draw a *trellis* graph for it and run Viterbi's algorithm.

A factor graph representing the trellis for a ring oscillator is shown in figure 4-3. In the graph, time progresses to the right with (noisy) received values successively filling the dark circles along the bottom of the graph. The variable nodes s_t represent the best estimate of the transmit ring oscillator's state at each successive time-step. This estimate is represented by a probability distribution over the possible states $\{0, 1\}$ of the transmit oscillator.

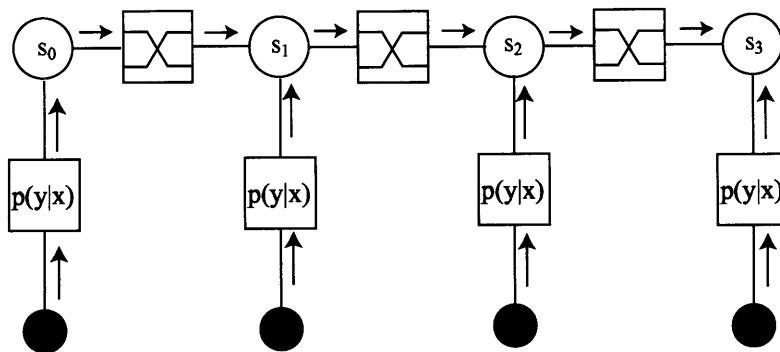


Figure 4-3: Factor graph for trellis for synchronization of a ring oscillator

Viterbi's algorithm on the trellis factor graph works as follows. Let us begin by supposing that we have prior information that makes us, say 60% certain that the transmitter oscillator is in state 0 at time 0. Before we receive any new information from the transmitter, we should already be 60% certain that the transmitter will be in state 1 at the next time-step, since the ring oscillator simply switches state at each time-step. This update is represented by the message being passed from state s_t through a soft-inverter to state s_{t+1} ,

$$\begin{aligned}
p_{inv}(1) &= p_s^{t-1}(0) \\
p_{inv}(0) &= p_s^{t-1}(1).
\end{aligned}
\tag{4.1}$$

The soft-inverter in this graph is precisely the same as a trellis section for ring oscillator receiver shown in figure 4-4 in which the probabilities of the two states are switched.

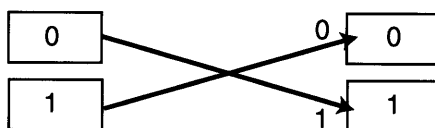


Figure 4-4: Trellis section for a ring oscillator

We also receive information from the transmitter via a noisy channel, however, and we would like to use this information to improve our current estimate. In the channel, we represent the transmitter's state with $\{1, -1\}$ instead of $\{0, 1\}$; We send a -1 when the transmitter's state is $x = 1$ and a 1 when the state is $x = 0$. In order to use the received information, we must first convert it to a valid probabilistic message that we can pass on the graph. If the channel is AWGN, then our model for the channel is

$$\begin{aligned}
p_{Y|X}(y|x=1) &= \frac{1}{\sqrt{2\pi}\sigma} \exp\left(\frac{-(y-1)^2}{2\sigma^2}\right) \\
p_{Y|X}(y|x=0) &= \frac{1}{\sqrt{2\pi}\sigma} \exp\left(\frac{-(y-(-1))^2}{2\sigma^2}\right).
\end{aligned}
\tag{4.2}$$

where x is transmitted and y is received. This expands to

$$p_{Y|X}(y|x) = \frac{1}{\sqrt{2\pi}\sigma} \exp\left(\frac{-(y-x)^2}{2\sigma^2}\right)$$

$$\begin{aligned}
p_{Y|X}(y|x) &= \frac{1}{\sqrt{2\pi}\sigma} \exp\left(\frac{-(y^2 - 2xy + x^2)}{2\sigma^2}\right) \\
p_{Y|X}(y|x) &= \frac{1}{\sqrt{2\pi}\sigma} \exp\left(\frac{-y^2}{2\sigma^2}\right) \exp\left(\frac{yx}{2\sigma^2}\right) \exp\left(\frac{x^2}{2\sigma^2}\right). \tag{4.3}
\end{aligned}$$

If we assume that σ is fixed, then for a given received value of y the $e^{-y^2/2\sigma^2}$ terms will normalize out. Equation (4.1.1) then becomes

$$p_{Y|X}(y|x) = \gamma \exp\left(\frac{yx}{2\sigma^2}\right) \exp\left(\frac{x^2}{2\sigma^2}\right) \tag{4.4}$$

where γ is a normalization constant. If we further assume that the channel is properly equalized so that $|x| = 1$ (as we have been doing) then the $e^{x^2/2\sigma^2}$ terms will also normalize out leaving

$$p_{Y|X}(y|x) = \gamma \exp(yx). \tag{4.5}$$

We can write the message from the channel model node as

$$\begin{aligned}
p_y(1) &= \exp(-1 \cdot y) \\
p_y(0) &= \exp(1 \cdot y). \tag{4.6}
\end{aligned}$$

Thus we see that for a properly equalized, binary, AWGN channel with known sigma, the channel model computation reduces essentially to an inner product of the received value with the possible transmitted symbols.

We need to combine the estimate from the received signal which has been modified by the channel model with the message from the soft-inverter in order to produce the current state estimate, s_t . As for any variable node with multiple incoming messages, the state nodes do this by performing an element by element product of the incoming messages and then normalizing. The resulting message output from the state node s_t

is therefore

$$\begin{aligned}
 p_s^t(1) &= p_s^{t-1}(0)p_{Y|X}(y|x=1) \\
 p_s^t(0) &= p_s^{t-1}(1)p_{Y|X}(y|x=0)
 \end{aligned}$$

4.1.2 Forward-only Message Passing on the Ring Oscillator Trellis

Notice that the messages we pass in the trellis factor graph in figure 4-4 are only sent to the right on the trellis factor graph - from past states to future states. This is because we are only interested in the current state of the transmitter, and there is no way to improve our estimate of the current state by adding any backward message passing. Furthermore if we have perfectly estimated the current state of the transmitter there is no reason to send messages backward to improve our estimates of past states of the transmitter. Knowing the current state of a deterministic transmitter gives us complete information about the history of the transmitter. We call this forward-only message passing.

We can “roll up” the forward-only message passing on the trellis factor graph. Examine figure 4-3 carefully. A given state node combines a message from the channel model with (soft-inverted) message from the last state. Exactly the same message calculations are performed by the factor graph on the right side of figure 4-5. So forward-only message passing on the trellis receiver graph can itself be written to closely resemble a ring oscillator. The only difference between this “receiver ring oscillator” and the transmit ring oscillator is that the receiver oscillator includes a channel model.

Note that the rolled up “factor graph” in figure figure 4-5, like many of the rolled up factor graphs in this document, abuses the factor graph notation because messages only travel in one direction on them. Also there should properly be a variable node in between any two connected factor nodes. We have left out variable nodes with only two incident edges which trivially pass messages without performing any computation.

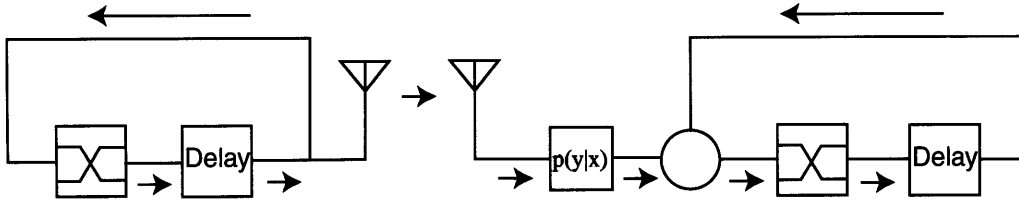


Figure 4-5: Factor graph for transmit and receive ring oscillators

The log-likelihood for a binary random variable is defined as

$$L_z \equiv \ln \left(\frac{p_z(0)}{p_z(1)} \right). \quad (4.7)$$

The message from the channel model written as a log-likelihood is

$$\begin{aligned} L_y &= \log \left(\frac{\exp(-(y-1)^2/2\sigma^2)}{\exp(-(y+1)^2/2\sigma^2)} \right) \\ L_y &= 2y/\sigma^2. \end{aligned} \quad (4.8)$$

The state nodes in the ring oscillator trellis factor graph perform a product of the incoming messages. We can write this operation in terms of log-likelihoods as

$$\begin{aligned} L_z \equiv \ln \left(\frac{p_z(0)}{p_z(1)} \right) &= \ln \left(\frac{p_x(0)p_y(0)}{p_x(1)p_y(1)} \right) \\ &= \ln \left(\frac{p_x(0)}{p_x(1)} \right) + \ln \left(\frac{p_y(0)}{p_y(1)} \right) \\ &= L_x + L_y. \end{aligned} \quad (4.9)$$

If we consider the voltages in a ring oscillator circuit to represent log-likelihoods, then the maximum-likelihood estimate of the phase of the transmit ring oscillator in AWGN can be achieved by multiplying the received value by a gain proportional to σ and then summing this voltage into the state of the receive ring oscillator. This actually works in continuous-time circuits where it is called *injection locking*. We will

discuss the continuous-time case in greater detail later.

A maximum-likelihood estimate is defined as the best estimate a receiver can make when its model captures all of the information about the transmitter system. In this system, the receive ring oscillator is a perfect model of the transmitter since it is in fact an identical copy of it. Furthermore we have also assumed a perfect model of the channel. Therefore we should not be surprised that properly performing injection locking of a ring oscillator produces a maximum-likelihood estimate of the transmit oscillator's phase. In real integrated injection locked systems, σ tends to be negligible compared to the signal, so the gain on the received signal should be set as large as possible before summing it into the receiver's state.

4.2 Synchronization to a Linear Feedback Shift Register (LFSR)

4.2.1 LFSRs Generate PN-Sequences

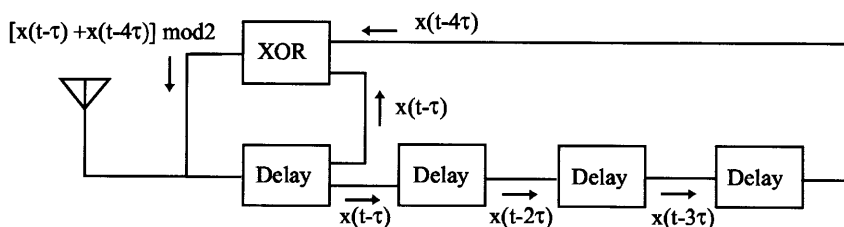


Figure 4-6: 4-bin, 2-tap LFSR

A Linear Feedback Shift Register (LFSR) is a finite state machine that generates a repeating sequence of zeros and ones known as a PN-sequence. The update function of this 4-bin 2-tap LFSR can be most compactly expressed as a iterated map or difference equation with binary variables,

$$x_t = x_{t-\tau} \oplus x_{t-4\tau}. \quad (4.10)$$

The factor graph (block diagram) for a 4-bin, 2-tap LFSR is shown in figure 4-6. All functional blocks in the diagram accept binary input messages and send binary-valued output messages. At each time-step of the LFSR algorithm, messages are passed along edges of the graph in the direction of the associated arrows. Delay elements delay a message by one time-step τ , so that the output message from a delay element is just the input message from the last time-step $t - \tau$. At each time-step, each delay element passes a message to the delay element to its right. One can think of these delay elements as consisting a shift memory with “bins” which each can store a bit. On each time-step, the shift memory shifts its contents one bin to the right.

Copies of the messages $x(t - \tau)$ and $x(t - 4\tau)$ output from the first and fourth delay elements are also sent to an XOR function where they are summed modulo 2 and the result is sent back to the first delay element, all in one time-step. These copies of the messages $x(t - \tau)$ and $x(t - 4\tau)$ are called the “taps” of the LFSR. The number of bins and placement of these taps determines the exact form of the pseudo-random number (PN) sequence [53].

We initialize the LFSR with messages with any binary values other than all zeros. The LFSR then cycles through a deterministic sequence of states as shown in figure 4-7. We can read off the PN sequence from the messages going by on any edge in the graph as the LFSR algorithm cycles through its repeating sequence of states, but we will adopt the convention that the transmitted bits are read from the output of the first delay element, the left most bit in each state shown in 4-7. We observe the PN sequence 101011001000111... which then repeats.

This particular 4-bin 2-tap LFSR produces a sequence that is $2^4 - 1 = 15$ bits long, which is the maximum possible for an LFSR with 4 delay elements. The placement of the taps on a particular set of delay elements determines the PN sequence and whether it will be *maximal length*. A particular LFSR can be tested to see if it will produce a maximal length sequence by taking the z-transform of its difference equation. The z-transform will result in a quotient of polynomials. If these polynomials have no factors in common (are mutually prime) then an LFSR with n bins will produce a maximal length sequence of length $2^n - 1$ bits [53].

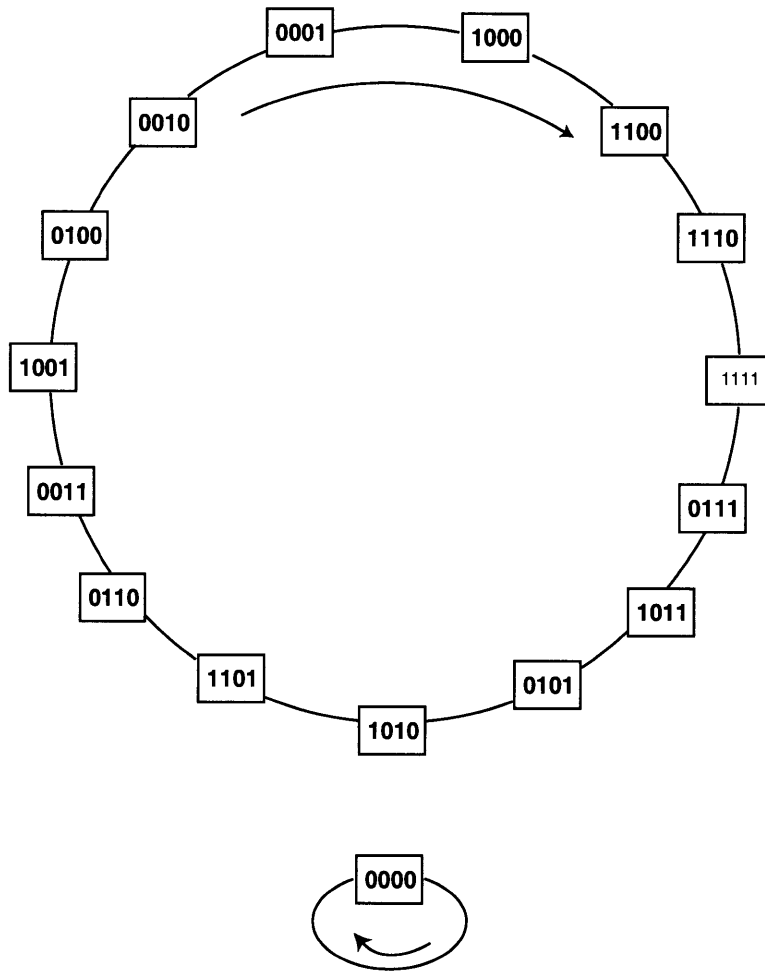


Figure 4-7: State cycle of a 4-bit, 2-tap LFSR

4.2.2 Applications of LFSR Synchronization

Why should we care about LFSR synchronization? In fact, LFSR synchronization is a rather important function in many applications. For example, a Global Positioning System (GPS) receiver spends significant resources to achieve highly accurate LFSR synchronization in a very low SNR environment. LFSR synchronization (known as PN-sequence acquisition) is also an important problem in direct-sequence code-division multiple access (DS/CDMA) communication such as is currently used in IS-95 and 3G cell phone networks and wireless LAN systems.

The most ubiquitous circuit primitive currently used for synchronization is known

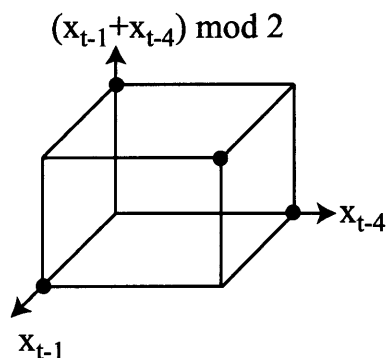


Figure 4-8: Mod 2 sum

as the Phase Lock Loop (PLL). PLLs are used in wireless receivers and VLSI computer chips for synchronizing to periodic carrier and clock signals. PLLs only work, however, on signals which simply oscillate between extreme values, a pattern that we might depict in discrete time with the regular expression $(01)^*$. It is interesting to think about generalizations of the PLL which could synchronize to more complex periodic patterns such as those produced by an LFSR. Such a circuit could be useful for a variety of applications such as multi-region clock distribution in VLSI chips or more agile radio modulation. A revolutionary idea would be “CDMA-lite” which would allow processor cores to act like users in a cell phone network - employing a low complexity multiuser communication system to talk to each other over shared high-speed buses.

LFSR Synchronization in DS/CDMA Spread Spectrum Communication

Multiuser or *Multiple Access* communication refers to communications systems where many users share the same channel. In multiple access systems, receivers must be able to distinguish messages coming from different users. FM radio solves this problem by using sinusoidal carriers with different frequencies to distinguish between different users (commercial radio stations). Sinusoids of different frequencies constitute an orthogonal bases which means that mathematically, the signals from different radio stations are linearly independent and therefore separable.

Code Division multiple-access refers to the practice of distinguishing different users with different bit sequences or codes. Direct-Sequence Code-Division Multiple Access (DS/CDMA) wireless systems often use codes generated by LFSRs to distinguish information transmitted by different users. A DS/CDMA transmitter and receiver are shown in figures 4-9 and 4-10 respectively. The message signal is multiplied by a PN-sequence generated by an LFSR. Since the different LFSR sequences may be orthogonal but are at least uncorrelated, they too may serve as carriers which are separable. Using a PN-sequence to directly *modulate* the message signal is called *Direct Sequence Code Division Multiple Access*. Since a PN-sequence has a white frequency spectrum, modulating the message signal by the PN-sequence has the effect of spreading the message signal over a wide frequency range while reducing the amount of power at any given frequency and is one method of producing a *Spread-Spectrum* signal.

There are other methods for spreading the spectrum of a message signal. A popular alternative to CDMA is Frequency Domain Multiple Access (FDMA) in which we periodically switch the frequency of a sinusoidal carrier. DS/CDMA has a number of particular advantages over other techniques such as nice spectrum sharing properties and resilience against jamming and multi-path interference.

LFSR synchronization in a DS/CDMA receiver is known as PN-sequence acquisition. In order to listen to a given user's message, the receiver must acquire that user's LFSR so that it can remove it and recover the transmitted signal. The performance of an acquisition system is measured in terms of its time to acquire and the repeatability of this acquisition time. False positives are also a consideration. In a *noncoherent* DS/CDMA system, acquisition is performed first, and then a *tracking loop* takes over to maintain the receiver's LFSR in close alignment with the transmitter's LFSR.

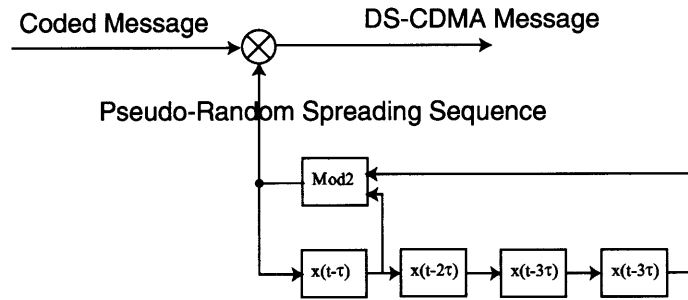


Figure 4-9: DS/CDMA *modulation* with PN-sequence generated by an LFSR

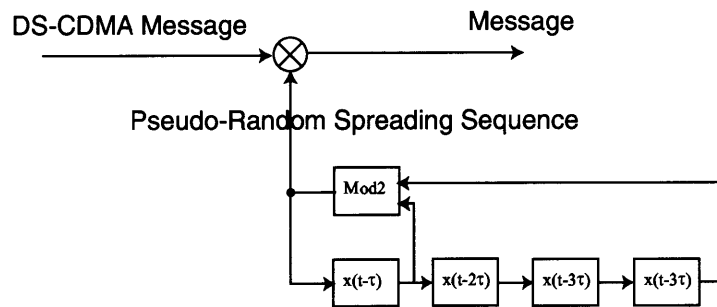


Figure 4-10: DS/CDMA *demodulation* with PN-sequence generated by an LFSR

4.3 Maximum Likelihood LFSR Acquisition

4.3.1 Trellis for Maximum-Likelihood LFSR Synchronization

For maximum-likelihood decoding of an LFSR transmitting via a noisy channel, we should again design a trellis decoder as we did for the ring oscillator. The trellis section for a 4-bin, 2-tap LFSR is shown in figure 4-11. The trellis is a graph consisting of state nodes and edge transitions. In the figure, the possible states of the LFSR are listed vertically, with edges indicating allowed transitions to states at the next time-step. From figure 4-11, we see that there are $2^n - 1$ states in one trellis section of an LFSR with n states. the height of the trellis grows exponentially in the size of the LFSR.

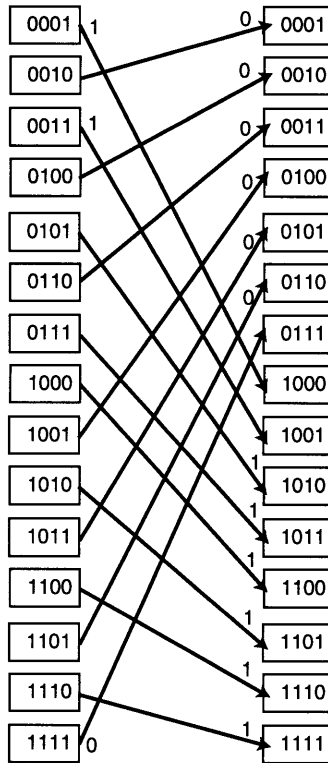


Figure 4-11: Trellis section for a 4-bin, 2-tap LFSR

4.3.2 Converting a the Trellis to a Factor Graph

We can draw the LFSR trellis as a factor graph. We form a factor graph from a trellis by grouping trellis sections into state-constraint-state triplets. For example the trellis in figure 4-11, would become the factor graph in figure 4-12. Each circular node s_i refers to a probability distribution over a single (vertical) set of trellis states. Each dark square is a constraint function which represents the transition edges in the trellis section. Note that this is a generalization of the factor graph for the ring oscillator trellis, in which the constraint function was a soft-inverter.

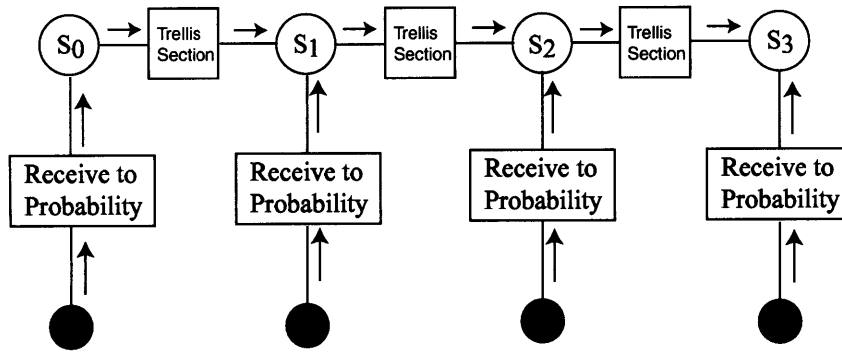


Figure 4-12: Factor graph for a trellis

4.3.3 The Sum Product (Forward-Backward) Algorithm on the LFSR Trellis

The forward-backward algorithm has long been the default algorithm for maximum-likelihood error correction decoding with a trellis. We will run the algorithm on the factor graph in figure 4-12 which represents the LFSR trellis. The forward-backward algorithm on a trellis factor graph proceeds as follows. First there is a “forward” part of the algorithm which passes messages to the right on the trellis factor graph. This part of the algorithm calculates the maximum-likelihood estimate for the right-most state:

1. Initialize s_0 with a uniform distribution - equal probability for every possible LFSR state.
2. Permute this probability distribution according to the allowed trellis transitions.
3. Receive a noisy symbols $\{y_0, y_1, y_2, y_3\}$ from the transmit LFSR via an AWGN channel.
4. Convert the received symbols to a probabilistic message by taking an inner product of the received symbol vector with each possible LFSR state.
5. Calculate the new state s_1 by multiplying the messages from steps 2 and 4.
6. Normalize s_1 .

7. Repeat: At each time-step, move to the right on the trellis, updating the state probability with information from each successively received symbol.

Then there is a backward part of the algorithm which passes messages to the left on the trellis factor graph. This part of the algorithm improves the state estimates of all of the states to the left of the right-most state, so that the end result is that every state in the trellis factor graph contains a maximum-likelihood estimate:

1. Initialize with the most recent (right-most) probability distribution over the trellis states, s_{tmax} .
2. Pass this message to the left through the trellis section.
3. Combine the left-going message from the trellis section with information from the most recently received (right-most) symbol from the channel.
4. Normalize the state.
5. Repeat: At each time-step, move to the left on the trellis.

It should be clear by now that the forward-backward algorithm is just the sum-product algorithm operating on the factor graph for a trellis. Since this graph is a tree, the sum-product algorithm will be exact and will produce maximum-likelihood estimates.

As in the ring oscillator example, there is no need for us to perform the backward step of the algorithm for this synchronization task. If we have a maximum-likelihood estimate in the right-most state, that gives us a maximum-likelihood estimate of the current state of the transmitter. The transmit LFSR is deterministic, so the trellis for any LFSR has only one edge emanating from any given state and only one way to transition between states. Therefore if we are given the most likely state in the right-most trellis section, this in turn gives us complete information about the history of the (deterministic) transmitter. The forward part of the algorithm suffices to recover the most likely history of the transmit LFSR.

In effect, the trellis synchronizer correlates every possible state with the received signal at every time-step. This computation is exponentially complex in the number of bins of the transmit LFSR. In practice, this parallel correlation operation is serialized and combined with decision theory to conserve resources. But reduced computational complexity comes at the expense of longer and unpredictable acquisition times [32].

4.3.4 The Max Product (Viterbi's) Algorithm

Many electrical engineers will have a passing familiarity with Viterbi's algorithm. Viterbi's algorithm is nearly identical to the forward-backward algorithm, but instead of storing a "soft" probability distribution at each time-step, Viterbi's algorithm picks the most likely state at each time-step and then assumes that it is 100% likely. So Viterbi's algorithm doesn't have to store a probability distribution over all the trellis states, it only has to store the most likely trellis state. Using this *max* operation instead of a *sum* operation is a different (less memory intensive) way of summarizing the information about which path through the trellis is most likely so far. The Viterbi algorithm is therefore also known as the max product algorithm.

Since multiplication is distributive over the *max* function just as it is distributive over the sum function, the operations still form a semi-ring as they do in the sum product (forward-backward) algorithm. In general we can use any *summary* function which forms a semi-ring with multiplication. The distributive property of a semi-ring assures us that we are still able to distribute products over the summary function, which is the pre-requisite for being able to express recursive concatenation of products and summary functions as local message passing on a graph.

4.4 Low-Complexity LFSR Acquisition

4.4.1 The LFSR Shift Graph

Though the trellis factor graph is optimum in the sense that it performs a maximum-likelihood estimate, it is not the only graph we can draw for synchronizing the LFSR.

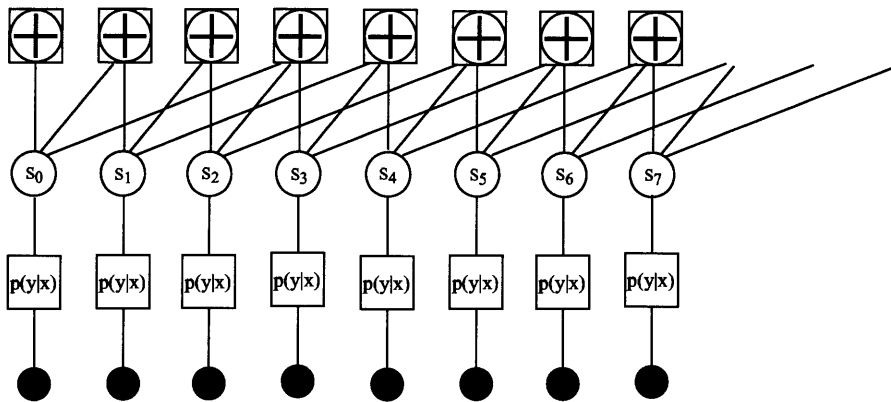


Figure 4-13: Shift graph for a linear feedback shift register

In fact another graph directly suggest itself. We could simply apply the LFSR constraints to the received time-series as shown in figure 4-13. I call this a shift graph following Lind and Marcus [27]. This graph has cycles and local evidence, so if we naively run the sum product algorithm with message passing in every direction, it is not guaranteed to produce accurate results or even to converge.

4.4.2 “Rolling Up the Shift Graph: The Noise Lock Loop

As we have discussed with the trellis factor graph, we are only interested in the most recent (right-most) estimate of the transmitter’s state. Therefore we need only perform forward message passing on the LFSR shift graph shown in figure 4-14, just as we have on the trellis. Figure 4-15 shows a single section of the shift graph. This section is used identically at each time-step to estimate the current state of the transmit LFSR. Once a state is estimated, it can be used to estimate future states, so messages on the diagonal edges in figure 4-14 are just copies of the state from which they originate. Rather than implement the entire shift graph as a system, we can design a less complex system (shown figure 4-16) to implement this recursive estimation. We call this system a *Noise Lock Loop* (NLL) [52]. The NLL is redrawn in figure 4-17 to resemble the factor graph we drew for the transmitter LFSR.

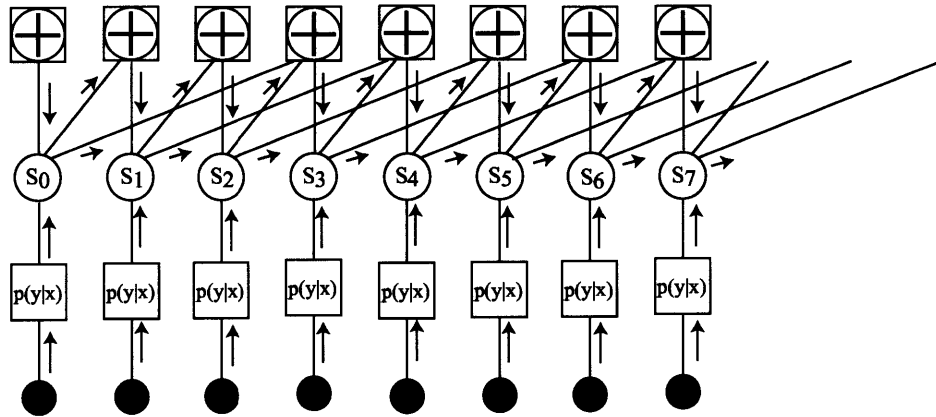


Figure 4-14: Forward-only message passing on shift graph for a linear feedback shift register

4.4.3 Performance of the Noise Lock Loop (NLL)

The NLL combines a low-complexity model of the transmit LFSR with a model of the channel. It therefore performs synchronization of a noisy LFSR better than the channel model alone. Acquisition is defined as the estimator guessing the true state for the transmit LFSR with greater than 95% confidence. Multiple trials of each experiment were simulated and the time until acquisition were recorded. As can be seen from figure 4-18, the NLL exhibits a tight unimodal distribution of synchronization times. This property makes the NLL interesting as a novel PN-sequence acquisition system. State-of-the-art systems lack a well-behaved distribution of acquisition times.

In zero noise the NLL synchronizes perfectly on every trial. The noise lock loop does not perform as well as the trellis if there is a lot of noise in the channel. With more noise, the NLL only synchronizes on some percentage of trials. If the noise amplitude exceeds the signal amplitude ($\sigma > 1$, $\text{SNR} > 3$ dB) then the NLL rarely manages to synchronize.

Unlike the NLL, the trellis always synchronizes eventually. For the trellis, more noise in the channel only leads to longer synchronization times. We might wish that we could improve the performance of the NLL so that it behaves more like the trellis.

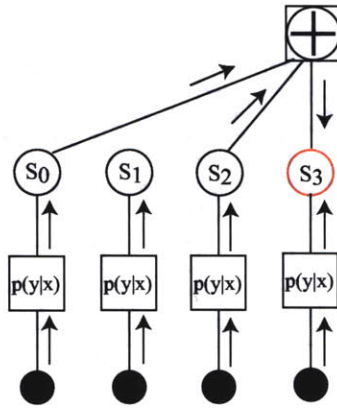


Figure 4-15: Section of the shift graph for a linear feedback shift register

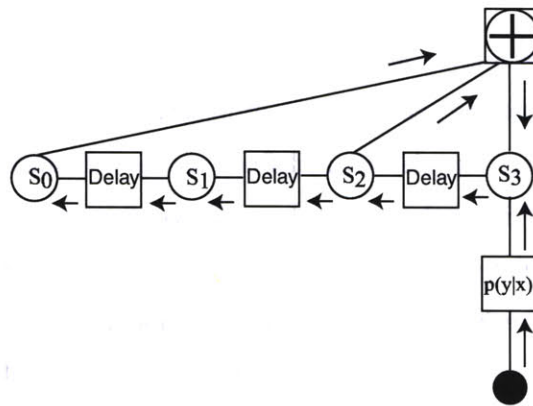


Figure 4-16: System to recursively implement section of the shift graph

In fact, we can use joint marginals to improve the performance of the NLL at the cost of increased computational complexity. At the most computationally complex extreme, we recover the exact trellis algorithm.

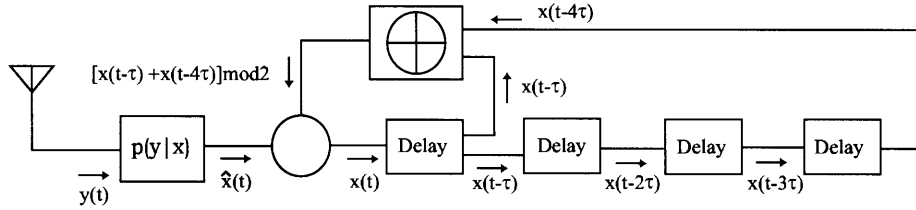


Figure 4-17: The Noise Lock Loop (NLL)

4.5 Joint Marginals Generalize Between the NLL and the trellis

With joint marginals we can turn a knob between the trellis and the NLL. The messages quickly become complex for a long LFSR, so we will examine only a 3-bin 2-tap LFSR. The shift for such an LFSR is shown in figure 4-14. We know that the trellis for this LFSR has 3-bit states, $\{(000), (001), \dots, (111)\}$. Since the trellis employs 3-bit states and performs maximum-likelihood estimation, joint messages over three time-steps of the LFSR shift graph will also suffice for maximum-likelihood estimation.

The joint 3 time-step messages are large however, so let us first calculate the joint messages over 2 time-steps as shown in figure 4-19. This will not result in a maximum-likelihood estimate, but will yield improved performance over the original NLL. The 2 time-step joint message from 2 soft-xor gates is given by

$$p_{(z_0, z_1)}(z_0, z_1) = \sum_{x_0, x_1} \sum_{y_0, y_1} p_{(X_0, X_1)}(x_0, x_1) p_{(Y_0, Y_1)}(y_0, y_1) f(x_0, y_0, z_0) f(x_1, y_1, z_1). \quad (4.11)$$

For $(z_0, z_1) = (0, 0)$, the constraints $f(x_0, y_0, z_0) = \delta(x_0 \oplus y_0 \oplus z_0 = 0)$, $f(x_1, y_1, z_1) =$

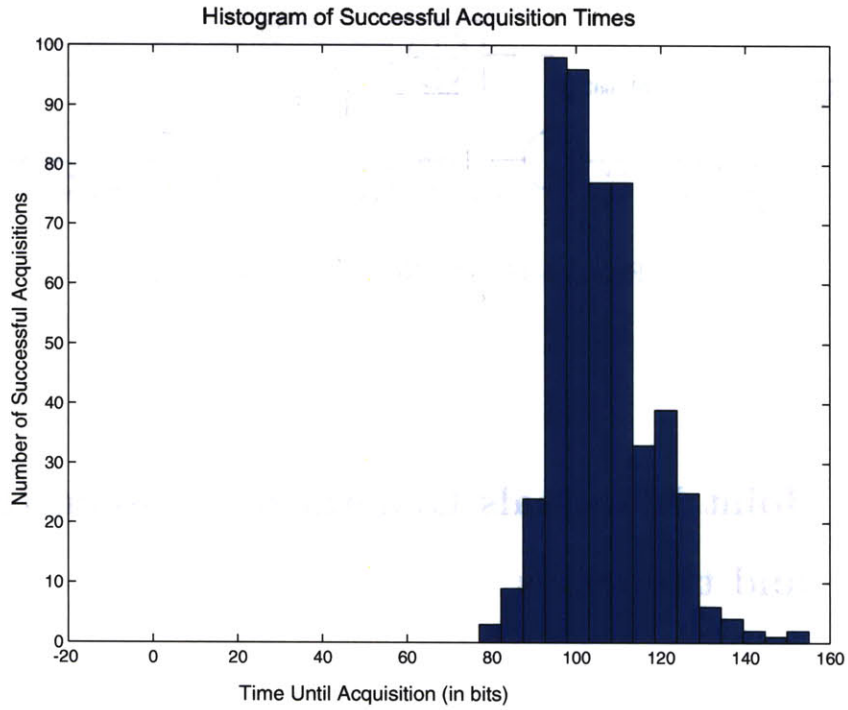


Figure 4-18: The Noise Lock Loop (NLL)

$\delta(x_1 \oplus y_1 \oplus z_1 = 0)$ are both equal to one for the following terms

x_0	y_0	x_1	y_1
0	0	0	0
0	0	1	1
1	1	0	0
1	1	1	1

(4.12)

So that

$$\begin{aligned}
 p_{(Z_0, Z_1)}(0, 0) &= p_{(X_0, X_1)}(0, 0)p_{(Y_0, Y_1)}(0, 0) \\
 &+ p_{(X_0, X_1)}(0, 1)p_{(Y_0, Y_1)}(0, 1) \\
 &+ p_{(X_0, X_1)}(1, 0)p_{(Y_0, Y_1)}(1, 0) \\
 &+ p_{(X_0, X_1)}(1, 1)p_{(Y_0, Y_1)}(1, 1).
 \end{aligned}
 \tag{4.13}$$

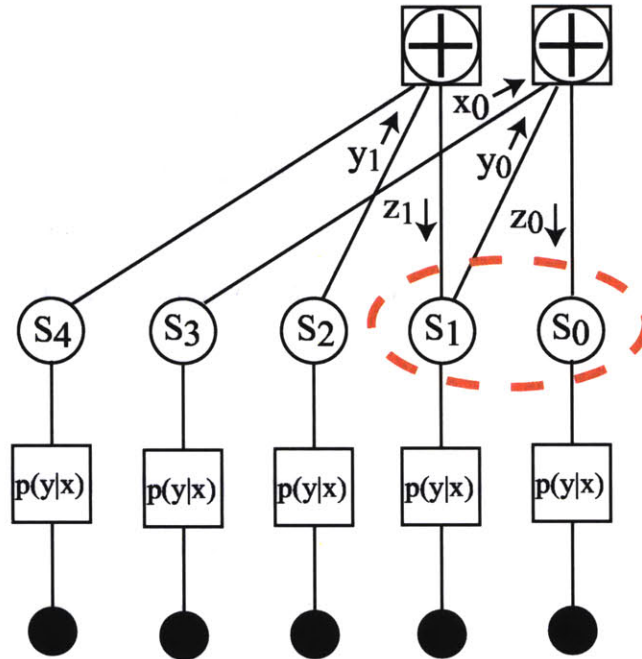


Figure 4-19: 2 time-step joint message on the LFSR shift graph

The other components of $p_{(z_0, z_1)}(z_0, z_1)$ can be similarly calculated. For $(z_0, z_1) = (0, 1)$, the constraints are both equal to one for the following terms

x_0	y_0	x_1	y_1
0	0	1	0
0	0	0	1
1	1	1	0
1	1	0	1

(4.14)

So that

$$\begin{aligned}
 p_{(z_0, z_1)}(0, 1) &= p_{(x_0, x_1)}(0, 1)p_{(y_0, y_1)}(0, 0) \\
 &+ p_{(x_0, x_1)}(0, 0)p_{(y_0, y_1)}(0, 1) \\
 &+ p_{(x_0, x_1)}(1, 1)p_{(y_0, y_1)}(1, 0) \\
 &+ p_{(x_0, x_1)}(1, 1)p_{(y_0, y_1)}(0, 1).
 \end{aligned}
 \tag{4.15}$$

Similarly,

$$\begin{aligned}
 p_{(z_0, z_1)}(1, 0) &= p_{(x_0, x_1)}(0, 1)p_{(y_0, y_1)}(0, 0) \\
 &+ p_{(x_0, x_1)}(0, 1)p_{(y_0, y_1)}(1, 1) \\
 &+ p_{(x_0, x_1)}(1, 0)p_{(y_0, y_1)}(0, 0) \\
 &+ p_{(x_0, x_1)}(1, 0)p_{(y_0, y_1)}(1, 1).
 \end{aligned} \tag{4.16}$$

and

$$\begin{aligned}
 p_{(z_0, z_1)}(1, 1) &= p_{(x_0, x_1)}(0, 1)p_{(y_0, y_1)}(0, 1) \\
 &+ p_{(x_0, x_1)}(0, 1)p_{(y_0, y_1)}(1, 0) \\
 &+ p_{(x_0, x_1)}(1, 0)p_{(y_0, y_1)}(0, 1) \\
 &+ p_{(x_0, x_1)}(1, 0)p_{(y_0, y_1)}(1, 0).
 \end{aligned} \tag{4.17}$$

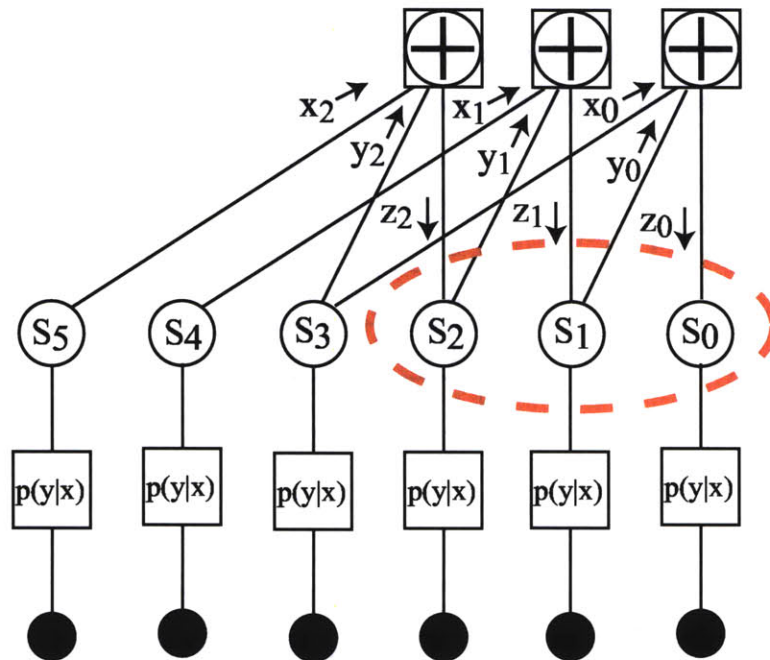


Figure 4-20: 3 time-step joint message on the LFSR shift graph (recovers the trellis)

Now let us calculate the 3 time-step joint message.

$$p_{(Z_0, Z_1, Z_2)}(z_0, z_1, z_2) = \sum_{x_0, x_1, x_2} \sum_{y_0, y_1, y_2} p_{(X_0, X_1, X_2)}(x_0, x_1, x_2) p_{(Y_0, Y_1, Y_2)}(y_0, y_1, y_2) \cdot f(x_0, y_0, z_0) f(x_1, y_1, z_1) f(x_2, y_2, z_2). \quad (4.18)$$

For $(z_0, z_1, z_2) = (0, 0, 0)$, the constraints $f(x_0, y_0, z_0) = \delta(x_0 \oplus y_0 \oplus z_0 = 0)$, $f(x_1, y_1, z_1) = \delta(x_1 \oplus y_1 \oplus z_1 = 0)$, and $f(x_2, y_2, z_2) = \delta(x_2 \oplus y_2 \oplus z_2 = 0)$ are all equal to one for the following terms

x_0	x_1	x_2	y_0	y_1	y_2
0	0	0	0	0	0
0	0	1	0	0	1
0	1	0	0	1	0
0	1	1	0	1	1
1	0	0	1	0	0
1	0	1	1	0	1
1	1	0	1	1	0
1	1	1	1	1	1

(4.19)

So that

$$\begin{aligned}
p_{(Z_0, Z_1, Z_2)}(0, 0, 0) &= p_{(X_0, X_1, X_2)}(0, 0, 0) p_{(Y_0, Y_1, Y_2)}(0, 0, 0) \\
&+ p_{(X_0, X_1, X_2)}(0, 0, 1) p_{(Y_0, Y_1, Y_2)}(0, 0, 1) \\
&+ p_{(X_0, X_1, X_2)}(0, 1, 0) p_{(Y_0, Y_1, Y_2)}(0, 1, 0) \\
&+ p_{(X_0, X_1, X_2)}(0, 1, 1) p_{(Y_0, Y_1, Y_2)}(0, 1, 1) \\
&+ p_{(X_0, X_1, X_2)}(1, 0, 0) p_{(Y_0, Y_1, Y_2)}(1, 0, 0) \\
&+ p_{(X_0, X_1, X_2)}(1, 0, 1) p_{(Y_0, Y_1, Y_2)}(1, 0, 1) \\
&+ p_{(X_0, X_1, X_2)}(1, 1, 0) p_{(Y_0, Y_1, Y_2)}(1, 1, 0) \\
&+ p_{(X_0, X_1, X_2)}(1, 1, 1) p_{(Y_0, Y_1, Y_2)}(1, 1, 1). \quad (4.20)
\end{aligned}$$

The other components of $p_{(z_0, z_1, z_2)}(z_0, z_1, z_2)$ can be similarly calculated, but in the interest of space will be left to the reader.

If we want to implement LFSR synchronization with these joint messages, on each iteration of the algorithm the x message is the z message from 3 time-steps before, $p_{(x_0, x_1, x_2)}^t(x_0, x_1, x_2) = p_{(z_0, z_1, z_2)}^{t-3}(z_0, z_1, z_2)$. Meanwhile the y message is the z message from the last time-step, $p_{(x_0, x_1, x_2)}^t(x_0, x_1, x_2) = p_{(z_0, z_1, z_2)}^{t-1}(z_0, z_1, z_2)$.

4.6 Scheduling

To run the sum product algorithm in discrete-time on any graph, we must choose an order in which to update the messages. We will assume that there is at most one message transmitted in each direction on a given edge during a single time-step. That message completely replaces any message that was being passed on that edge in that direction at previous time-steps. As we have seen in earlier chapters, a new outgoing message on one edge of a given node is calculated from local information, from incoming messages on the other edges of the node. We define a message as pending if it has been re-calculated due to new incoming messages.

A schedule could be chosen to allow all messages to be re-sent on all edges at each time-step, whether they are pending (have changed) or not. This is called a flooding schedule. However, we can accomplish exactly the same thing by only sending every pending message in the graph on every time-step. This is the most aggressive possible schedule for message passing. At the other extreme is a serial schedule, in which a single pending message in the graph is chosen at random to be sent at each time-step. In a cycle-free graph, with a schedule in which only pending messages are transmitted, the sum product algorithm will eventually halt in a state with no messages pending. If a graph has cycles, messages will continue to circulate around cycles in the graph even if their values are no longer changing.

4.7 Routing

So far we have assumed that every pending message should eventually be sent. Scheduling only answers the question of when. We are beginning to understand however, that sometimes we do not want to send every pending message on every time-step. We call this novel concept “routing” and take it mean the choosing to send some subset of all possible messages on the graph. At best, routing can significantly reduce the computational complexity of the sum product algorithm. At least, it can greatly reduce the complexity of the implementation hardware.

For example by choosing to only pass messages forward (rolling-up) the noise lock loop, we are able to re-use the same few soft-gates for each received data value, rather than storing a long analog time-series and parallel processing with a large number of soft-gates required by the complete shift graph. In essence, routing has enabled us to build pipe-lined signal processing architectures for the sum-product algorithm.

Another use of routing would be as follows. Suppose we want the quality of the complete trellis for LFSR synchronization, but not the computational complexity. We could try running the sum product algorithm on a (loopy) graph composed of a 3 time-step section of the LFSR shift graph in the example above. The marginals would be calculated for 3 time-steps, say s_0, s_1, s_2 . With any luck, after several iterations of the message-passing schedule on this section of the shift graph, these marginals would approximate the joint marginal $p_{(s_0, s_1, s_2)}(s_0, s_1, s_2)$. We can then move forward on the shift graph by one time-step just as we do above. This does indeed seem to improve performance of the NLL, but further experimentation is required.

If successful, this idea could also potentially be applied to extended Kalman filters and other applications of probabilistic message passing on graphs. If the update function of the nonlinear system is a function of several variables, it may indeed make sense to allow messages to share information within the system so that estimates of each of the variables can act on one another before the entire system shifts forward in time.

The path to further studies of routing seems clear. We will study other periodic

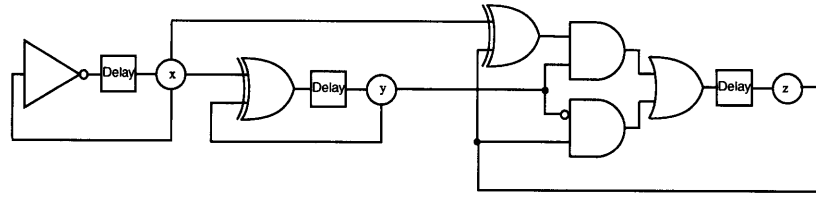


Figure 4-21: Block diagram for a binary counter

finite-state machines (FSM) such as a binary counter like that shown in figure 4-21. First we draw the complete “un-rolled” shift graph for the FSM as shown in figure 4-22. Then we study how choosing different routing schemes on this graph, such as forward-only and global forward-only/local forward-backward affect the performance of detection. We can actually study how decoding certainty spreads through the graph, by visualizing the entropy at every nodes as the sum product algorithm runs. To calculate the entropy at a node in the graph we must average over multiple detection trials. By gathering experience with different routing schemes on shift graphs for several different periodic FSM, we should be able to gain more intuition about what constitutes a useful routing scheme. The simulation tools to perform these experiments are currently under construction.

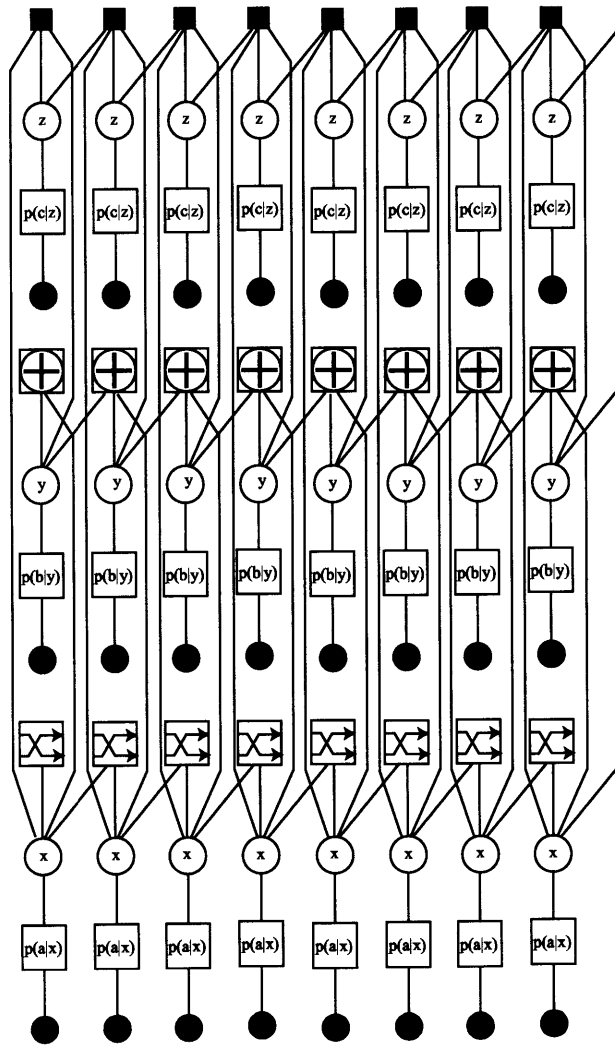


Figure 4-22: Shift graph for a binary counter

Chapter 5

Analog VLSI Circuits for Probabilistic Message Passing

5.1 Introduction: The Need for Multipliers

In order to build circuit implementations of the sum-product algorithm, we will need circuits that compute products of parameters of probability distributions and circuits that sum over these parameters. Summing operations are trivial with currents, because of Kirchoff's Current Law (KCL); one simply ties wires together to sum currents. Summing voltages is a bit more difficult, but one can use a summing amplifier. Multiplication poses more choices for the designer. In this document we will investigate many of the most important ways to implement a multiply operation with low-complexity analog transistor circuits.

An analog multiplier is a circuit which produces a scaled product Z of two inputs,

$$Z = kXY, \tag{5.1}$$

where k is a scaling constant. The values of X , Y and Z can be represented by the magnitude of a current or voltage. These values can also be represented by voltage or current spikes or pulses; by the rate of repetition of a series of voltage spike (pulse rate modulation or PRM), by the width of one or more spikes (pulse width

modulation or PWM), by the delays between spikes (Phase or Delay Modulation), or by a combination of the number of spikes and the spaces between them (pulse code modulation). Beyond spikes, other bases can be used to represent the values of X, Y, and Z, for example, the frequencies of sinusoids or any other basis that allows the design of a compact circuit for performing a multiply. The disadvantage of these various modulation schemes is that they require time to convey a value. Time is precious in RF applications, so we will primarily review a variety of known circuits for performing an analog multiply operation directly on current or voltage levels.

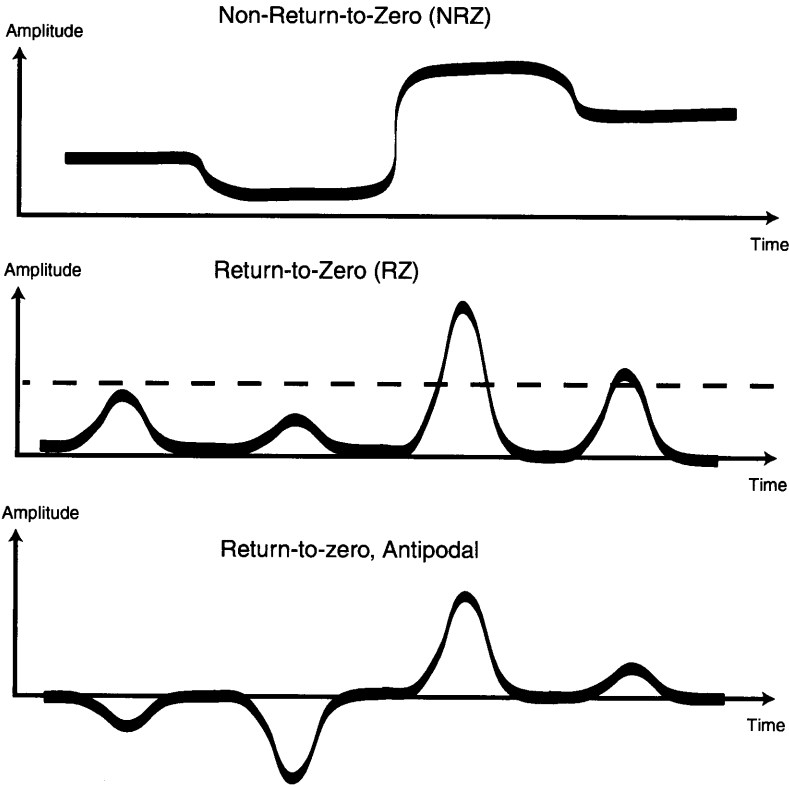


Figure 5-1: Signal consisting of successive analog samples represented by, respectively, NRZ analog levels with smooth transitions, RZ analog levels with a soliton-like waveform, and RZ antipodal soliton waveforms

We represent probabilities as successive analog samples. These could be clocked analog values with discrete transitions. In practice, we would prefer smooth transitions that don't generate high-frequency "glitch" noise and which tend to synchronize by entrainment. As shown in figure 5-1, the representation could be analog samples with smooth transitions, or it could be smooth unipodal or antipodal return-to-zero (RZ) analog bumps resembling solitons.

5.2 Multipliers Require Active Elements

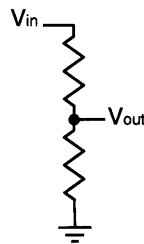


Figure 5-2: Resistor divider performs scalar multiplication, $V_{out} = V_{in}(R_1/R_1 + R_2)$.

In the algebraic sense, multiplication is a linear operation. To be a linear operator an operator L must satisfy the condition, $L(A) + L(B) = L(A + B)$. Multiplication of variables A and B by the scalar a satisfies this definition, $a(A) + a(B) = a(A + B)$. Scalar multiplication of a constant by a variable actually helps to define the most linear thing there is, a line, $y = a(x) + b$. A linear completely passive (un-powered) circuit can perform this kind of multiply. For example, a simple resistor divider like the one shown in figure 5-2 can multiply an input voltage by a fixed value between 0 and 1. If, however, we want to multiply two variables by each other such as $x * y$, or even a variable by itself $x * x = x^2$, then we require a quadratic operation. A quadratic operation is by definition, nonlinear.

A nonlinear operation could be as simple as the function $y = x^2$ defined over inputs $x = \{0, 1\}$ and yielding outputs $y = \{0, 1\}$. This is known as a single-quadrant multiply. It is a monotonic function and therefore performs a one-to-one map. Due to the nonlinearity however, a uniform distribution of input values will yield a non-

uniform distribution of output values compressed toward $y = 0$. Real valued voltages that were evenly spaced apart over V_{in} , are now closer together in V_{out} . Physical systems with finite energy which are measured over finite time, have finite resolution. Because of this compression and the resolution limit, implementation of a single-balanced multiply will erase some information about the input. Bennett's formulation of Maxwell's Demon teaches us that it takes energy to erase information [25]. So a single-quadrant multiply operation implemented by a physical system must dissipate some amount of the energy. This energy can come from the input signal though, and does not necessarily require an external power source.

Multipliers are often characterized as single quadrant ($x \geq 0$ and $y \geq 0$), double quadrant ($x \geq 0$ or $y \geq 0$) or four-quadrant (no restriction on the signs of x and y). A four-quadrant multiply maps inputs between $\{-1, 1\}$ to outputs between $\{-1, 1\}$. It performs a many-to-one mapping from input state space to output state space, meaning that different inputs can produce the same output, for example, $(-1)(-1) = 1$ and $(1)(1) = 1$. This many-to-one mapping erases an entire bit of information, the sign of the input. We can see this because we would require the sign of at least one input in order to reverse the operation. Therefore implementing a irreversible four-quadrant multiply in a physical system requires power. All quadratic multiplier circuit designs will use at least one active, powered circuit element.

We can approximate any nonlinear function with a Taylor series expansion. The Taylor series expansion of a nonlinear function will include quadratic or higher order terms. It will therefore require power to implement a nonlinear function in a physical system. There is one special exception to this rule. It is possible to carefully construct special multi-dimensional nonlinear functions which perform a one-to-one (unitary) mapping and therefore do not require power when physically implemented.

5.3 Active Elements Integrated in Silicon: Transistors

In practice, if we want to build integrated circuits in silicon, the active components available to us are diodes and transistors. A single transistor can in fact perform a rudimentary multiply, but we will use more than one in order to achieve better performance. Given layer-deposition 2-dimensional semiconductor fabrication, there are essentially two possible types of transistors, Bipolar Junction Transistors (BJTs) and Metal-Oxide Semiconductor Field-Effect Transistors (MOSFETs). High performance analog multipliers using BJTs have been available since Barry Gilbert proposed translinear circuits in the 1970's. High-performance MOSFET based multipliers are still the subject of active research.

We will eventually be interested in using analog multiply circuits on a chip that also contains digital circuits in order to integrate analog signal processing for radios together with digital logic in a single architecture. Large numbers of MOSFETs are much more economical to produce than BJTs, so digital circuits are generally manufactured in semiconductor manufacturing processes that can only produce MOSFETs. BiCMOS processes which offer both MOSFETs and BJT are also becoming available for integrating analog RF signal processing with digital circuits, but are not as economical as MOSFET-only processes. Circuits using MOSFETs (CMOS) will therefore be of greatest interest to us.

5.3.1 BJTs

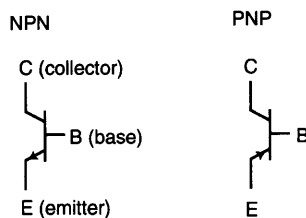


Figure 5-3: Bipolar Transistors

Bipolar Transistors (BJT) like the ones in figure 5-3 exhibit an exponential dependence of the collector current on the voltage difference between the base and emitter,

$$I_C = A_E J_S(T) e^{V_{BE}/nU_T} = I_S(T) e^{V_{BE}/nU_T}, \quad (5.2)$$

where A_E is the emitter area, J_S is the saturation current density, and I_S is the saturation current. The absolute temperature is T and U_T denotes the thermal voltage $\frac{kT}{q}$. The “emission coefficient” n is generally close to 1.

5.3.2 JFETs

A field effect transistor (FET) has a different arrangement of p-n junctions than a BJT and is easier to fabricate accurately and can therefore be made smaller and cheaper. In a junction field effect transistor (JFET), the base silicon directly contacts the channel silicon. Operating in the “saturated mode” ($V_{DS} \geq V_{GS} - V_{sat}$), JFETs can be modelled by

$$I_{d_{sat}} = \frac{G_0 V_p}{3} \left[1 - \frac{3(V_p + V_T - V_{GS})}{V_p} + 2 \left(\frac{V_p + V_T - V_{GS}}{V_p} \right)^{3/2} \right]. \quad (5.3)$$

The $2(\dots)^{3/2}$ term can be written as $2[1 - (V_{GS} - V_T)/V_p]^{3/2}$ and expanded in a three term binomial series

$$2 \left[1 - \left(\frac{V_{GS} - V_T}{V_p} \right) \right]^{3/2} = 2 \left[1 - \frac{3}{2} \left(\frac{V_{GS} - V_T}{V_p} \right) + \frac{3}{2} \frac{1}{2} \frac{1}{2} \left(\frac{V_{GS} - V_T}{V_p} \right)^2 \right] \quad (5.4)$$

so that equation 5.3 becomes

$$I_{d_{sat}} = \frac{G_0 V_p}{3} \left[1 - 3 + 3 \left(\frac{V_{GS} - V_T}{V_p} \right) + 2 - 3 \left(\frac{V_{GS} - V_T}{V_p} \right) + \frac{3}{4} \left(\frac{V_{GS} - V_T}{V_p} \right)^2 \right]. \quad (5.5)$$

Cancellation of terms gives

$$I_{d_{sat}} = \frac{G_0}{4V_p} (V_{GS} - V_T)^2. \quad (5.6)$$

If we let

$$\beta \equiv \frac{G_0}{4V_p} = \frac{\mu}{2a} \frac{W}{L} \epsilon_{Si}. \quad (5.7)$$

then we may write a simplified model of the JFET [6]

$$I_{d_{sat}} = \beta(V_{GS} - V_T)^2. \quad (5.8)$$

5.3.3 MOSFETs

Metal Oxide Semiconductor Field Effect Transistors (MOSFET) like the ones shown in figure 5-4 are an innovation over JFETs. MOSFETs incorporate a thin layer of silicon dioxide (SiO_2) known simply as an oxide layer separating the base from the channel. This essentially eliminates the flow of current from the base into the channel.

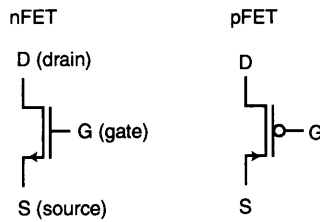


Figure 5-4: MOSFET transistors

MOSFETs exhibit a similar behavior to BJTs when they operate “below threshold” with the gate voltage less than the threshold voltage $V_{gs} \leq V_t$.

$$I_d = \frac{W}{L} J_0(T) e^{(V_G - nV_S)/nU_T} = I_0(T) e^{(V_G - nV_S)/nU_T}, \quad (5.9)$$

where W and L are the width and length of the transistor, J_0 is the specific current density, I_0 is the specific current, and the slope factor n is generally $\simeq 1$. At higher base voltages $V_{gs} \geq V_t$, MOSFETs are said to be operating “above threshold” and they exhibit different behavior. When $V_{ds} < V_{gs} - V_t$, the MOSFET operates in its “linear” region and is governed by

$$i_d = K \left[V_{gs} - V_t - \frac{V_{ds}}{2} \right] V_{ds}$$

$$= K[V_{gs}V_{ds} - V_tV_{ds} - \frac{V_{ds}^2}{2}], \quad (5.10)$$

where $K = \mu_0 C_{ox} \frac{W}{L}$. When $V_{ds} > V_{gs} - V_t$, the MOSFET operates in its “saturation” region and is governed by an equation resembling the JFET

$$\begin{aligned} i_d &= \frac{K}{2}[V_{gs} - V_t]^2 \\ &= \frac{K}{2}[V_{gs}^2 - 2V_{gs}V_t - V_t^2]. \end{aligned} \quad (5.11)$$

5.4 Single-Quadrant Multiplier Circuits

5.4.1 Multiply by Summing Logarithms

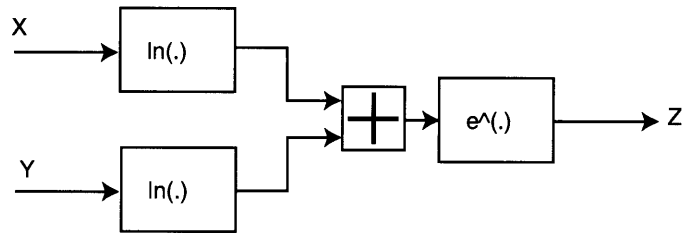


Figure 5-5: Logarithmic Summing Circuit

Besides translinear circuits, there are some other circuits for performing analog multiplication. A logarithmic summing circuit is shown in figure 5-5. In this circuit we take advantage of the fact that

$$Z = XY = e^{\ln XY} = e^{\ln X + \ln Y} \quad (5.12)$$

to implement a multiply.

One way to implement a logarithmic summing circuit with transistors is shown in figure 5-6. First we use the exponential relationship of bipolar transistors (or FETs below threshold) to take the natural logarithm of the input currents, X and Y. Then we sum the resulting output voltages from these transistors using a summing

amplifier. Finally, we use another transistor to take the exponential of this summed current to produce an output current, $Z = XY$.

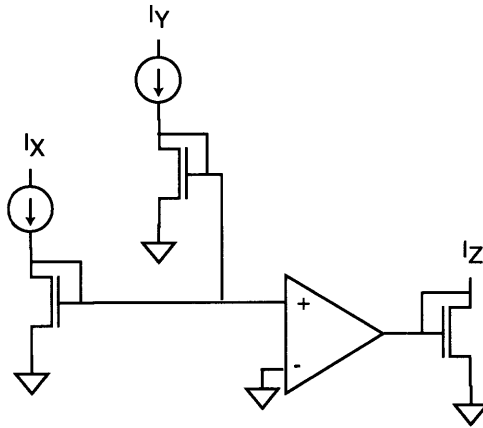


Figure 5-6: Logarithmic Summing Circuit

Alternatively, one could input voltages instead of currents to logarithmic operational amplifiers, then sum the resulting output currents from these log-amps using KCL by simply tying the output currents together, and finally inverting the logarithmic with an exponential amplifier.

Before we stated that addition was easy with KCL and that multiplication was more difficult. With the log-summing circuits, we seemingly get around this problem by reducing multiplication to summation. The catch is that we always end up using summing amps or log amps which yield circuit complexity on par with the complexity of other multiply circuits.

One drawback of any logarithmic summer circuit is that both inputs must be greater than zero. If they weren't, then the output from ideal logarithm elements would be $\ln(0) = -\infty$ which is not possible in practice. So this is a “single quadrant multiplier” for which the inputs $X, Y \geq 0$.

5.4.2 Multiply by Controlling Gain: The Differential Pair

The circuit shown in figure 5-7 is known as a differential pair. Like its component transistors, the differential pair accepts a voltage input outputs a current; it is a

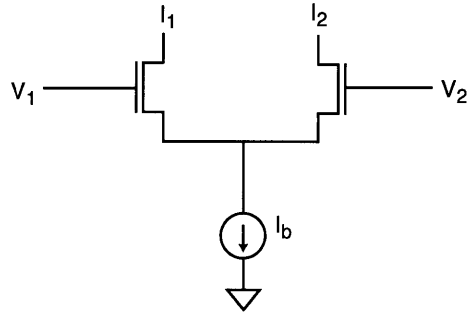


Figure 5-7: Differential pair

transconductor. The “diff-pair” is an essential gain element for building amplifiers. The amount of gain is controlled by the bias current. We can use this gain knob on the diff-pair as an input to perform a single-quadrant multiply of the differential voltage input. This is sometimes called a “programmable transconductor”. As we will see later, more programmable transconductors can be combined to make four-quadrant multipliers.

Let us analyze the diff-pair in more detail. We will use the expressions for I_{DS} given for a BJT or for a MOSFET operating below threshold, so that

$$I_1 = I_0 e^{V_{10}/V_T} \quad (5.13)$$

$$I_2 = I_0 e^{V_{20}/V_T} \quad (5.14)$$

where $V_{10} = V_1 - V_0$ and $V_{20} = V_2 - V_0$. The sum of the currents I_{DS} through each transistor in the diff-pair must equal the bias current I_b ,

$$I_1 + I_2 = I_0 e^{V_{10}/V_T} + I_0 e^{V_{20}/V_T} = I_b. \quad (5.15)$$

By bringing out $I_0 e^{V_{10}/V_T}$, this can be rewritten as

$$I_0 e^{V_{10}/V_T} \left(1 + e^{\frac{V_{20}-V_{10}}{V_T}} \right) = I_b. \quad (5.16)$$

Or by bringing out $I_0 e^{V_{20}/V_T}$ as

$$I_0 e^{V_{20}/V_T} \left(1 + e^{\frac{V_{10}-V_{20}}{V_T}} \right) = I_b. \quad (5.17)$$

Furthermore, since $V_{20} - V_{10} = (V_2 - V_0) - (V_1 - V_0) = V_2 - V_1 \equiv V_{21}$ and using equation 5.14, with a little algebra we can write

$$I_1 = \frac{I_b}{1 + e^{\frac{V_{21}}{V_T}}} = \frac{I_b}{2} \left[1 + \tanh \left(\frac{V_{21}}{2V_T} \right) \right] \quad (5.18)$$

and

$$I_2 = \frac{I_b}{1 + e^{-\frac{V_{21}}{V_T}}} = \frac{I_b}{2} \left[1 - \tanh \left(\frac{V_{21}}{2V_T} \right) \right]. \quad (5.19)$$

So the output of the differential amplifier is a function $\tanh \Delta V$ of the input voltage differential, $\Delta V = V_1 - V_2$ multiplied by I_b . When operating in the linear part of this \tanh function, the differential pair acts as a single-quadrant multiplier.

The differential pair has another important for the systems discussed in this dissertation. The \tanh function of the differential pair approximates the *erf* function (the integral of a Gaussian distribution) quite well. The differential pair therefore turns out to be an extremely efficient way to implement a model of a channel with additive white Gaussian noise (AWGN). Not only will we use this circuit to condition our received data, but we will also use it after each internal filter in circuit implementations of the NLL in order to convert the filter outputs back to well-posed probabilities. We call this the soft-limiter circuit.

5.5 General Theory of Multiplier Circuits

5.5.1 Nonlinearity Cancellation

Now that we have some hands-on knowledge of analog multiplier circuits, let us try to understand them better from a theoretical point of view. The essential idea behind an analog multiplier is shown in figure 5-8. The signals v_1 and v_2 are applied to a

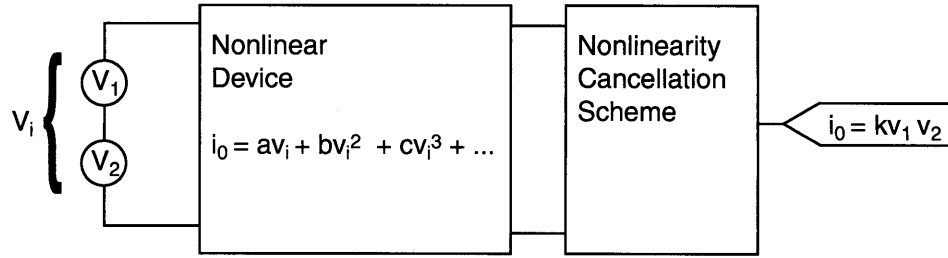


Figure 5-8: multiplier using a nonlinearity

nonlinear device which can be approximated by the first few terms of its Taylor series approximation. The Taylor series polynomial produces terms like v_1^2 , v_2^2 , v_1^3 , v_2^3 , $v_1^2 v_2$ and many more besides the desired term, $v_1 v_2$. It is then necessary to remove the unwanted terms by some form of nonlinearity cancellation circuit. For example, when we use a mixer to multiply two sinusoids, nonlinearity cancellation involves removing unwanted harmonic components by filtering the output.

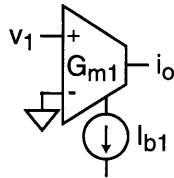


Figure 5-9: operational transconductance amplifier (OTA)

We can follow this idea of nonlinearity cancellation to construct a multiplier by combining programmable gain transconductors. The output of a transconductor such as a diff-pair represented here by the symbol in figure 5-9 is

$$i_o = G_{m1} v_1 \quad (5.20)$$

where G_{m1} is a function of I_{b1} . For a BJT based transconductor,

$$G_{m1} = I_{b1}/2V_t \quad (5.21)$$

where V_t is the thermal voltage kT/q .

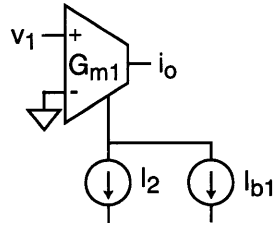


Figure 5-10: OTA with additional bias current i_2

Next we add a small current i_2 to the bias current as shown in figure 5-10.

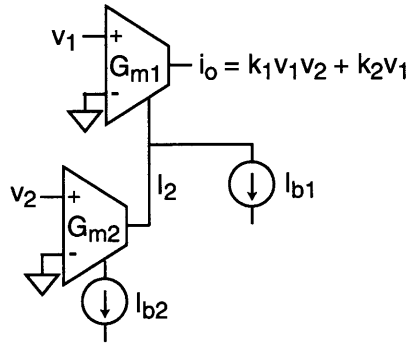


Figure 5-11: Controlling i_2 from v_2

We can control the current i_2 by a voltage v_2 via another transconductor so that,

$$i_2 = G_{m2}v_2 \quad (5.22)$$

as shown in figure 5-11. Then the output current becomes

$$i_o = G_{m1}v_1 = \frac{I_{b1} + G_{m2}v_2}{2V_t}v_1 \quad (5.23)$$

$$i_o = \frac{G_{m2}v_1v_2}{2V_t} + \frac{I_{b1}}{2V_t}v_1 \quad (5.24)$$

$$i_o = \frac{I_{b2}v_1v_2}{4V_t^2} + \frac{I_{b1}v_1}{2V_t} \quad (5.25)$$

$$i_o = k_1v_1v_2 + k_2v_1. \quad (5.26)$$

The output includes the desired term $k_1v_1v_2$ and an unwanted term k_2v_1 . We

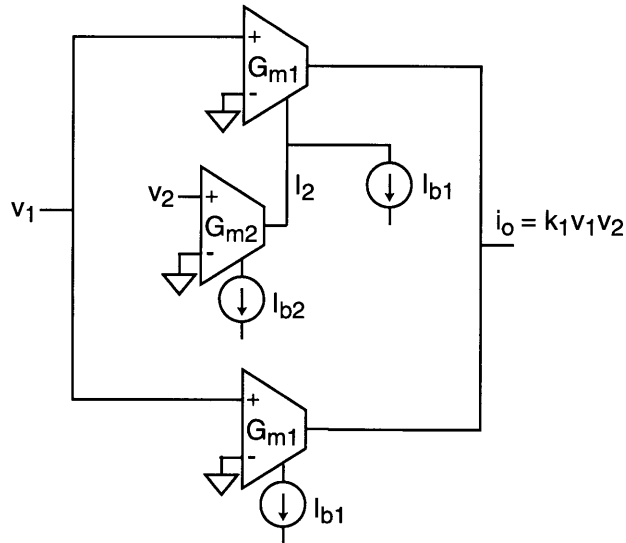


Figure 5-12: cancelling $k_2 v_1$ with a third transconductor

can cancel this unwanted term by adding a third transconductor that adds a current $-k_2 v_1$ to the output as shown in figure 5-12.

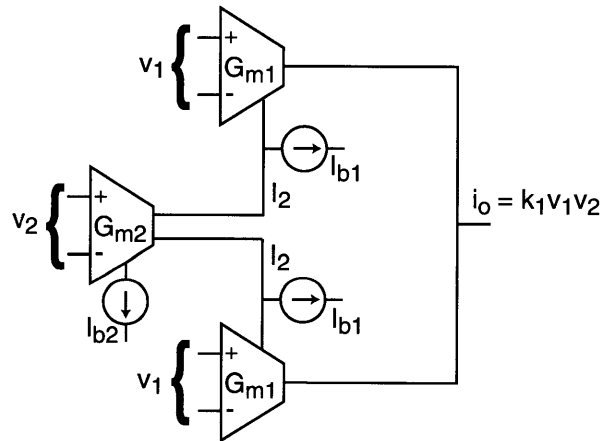


Figure 5-13: fully differential design

Finally, making the circuit completely symmetrical by making the third transconductor fully differential as seen in figure 5-13 improves the accuracy of the cancellation should there be any mismatch between the components. If the transconductors in this last circuit are BJT differential pairs, it is known as a Gilbert cell. Implementation

of this circuit with Operational Transconductance Amplifiers (OTA) have also been reported in the literature.

5.5.2 The Translinear Principle

Another way to understand the four-quadrant Gilbert multiplier is the way Barry Gilbert himself understood it in 1975 in terms of the translinear principle. The translinear principle can be used to generalize the analysis of the large-signal behavior of an important class of transistor circuits, of which multipliers are a special case. Using the equations for the behavior of transistors, we can use the translinear principle to analyze the differential pair in figure 5-7.

If V_1 and V_2 are connected together so that $V_1 = V_2$, then by Kirchhoff's voltage law,

$$(V_1 - V_3) = (V_2 - V_3) \quad (5.27)$$

Substituting

$$I_{C_i} = I_S(T)e^{V_{BE_i}/nU_T} \iff V_{BE_i} = nU_T \log(I_{C_i}/I_S(T)) \quad (5.28)$$

into 5.27 yields

$$I_{C_1}/I_S(T) = I_{C_2}/I_S(T). \quad (5.29)$$

Generalizing to the translinear loop in figure 5-14, we write

$$\sum_{CW} V_{BE_i} = \sum_{CCW} V_{BE_i} \quad (5.30)$$

and

$$\prod_{CW} I_{C_i}/I_{S_i} = \prod_{CCW} I_{C_i}/I_{S_i} \quad (5.31)$$

where CW denotes clockwise and CCW denotes counter-clockwise. With this for-

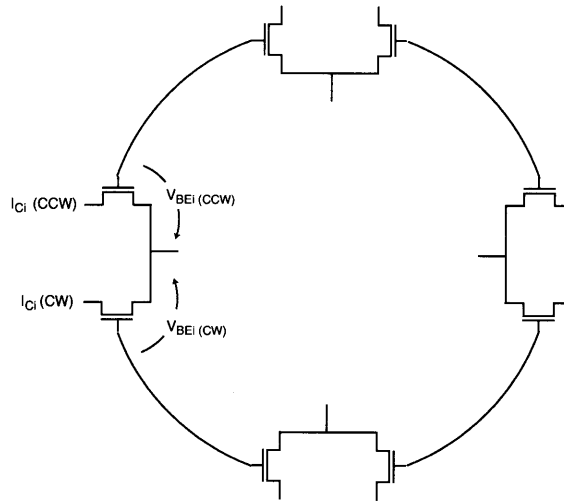


Figure 5-14: Translinear Loop Circuit

mula we can synthesize a large family of circuits which compute products of currents.

5.5.3 Comanding Current-Mirror Inputs

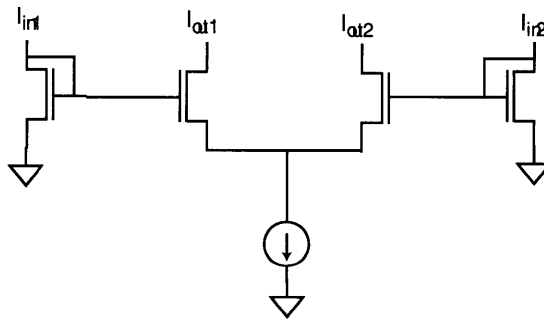


Figure 5-15: Current Controlled Current Divider

So far, our multiplier circuits multiply an input voltage V_X by an input current I_Y and produce an output current I_Z . It would be advantageous for system modularity however, if we could operate entirely on voltages or entirely on currents. We can multiply a current I_X by another current $I_Y = I_b$ using a circuit known as a current controlled current divider shown in figure 5-15. This circuit uses current mirrors to convert input currents to voltages which are suitable for input into the familiar

differential pair. The current mirrors form a *companding* circuit. They take the log of the input current and use this to control the transistors of the differential pair. Since the transistors in the differential pair take the exponential of their gate voltages, the currents through the transistors in the diff-pair exactly equal the input currents. Since the input voltages to the diff-pair transistors in the log domain, the dynamic range of the signal is small and the diff-pair tends to operate in the linear range of the tanh function. Since a current mirror is a translinear loop, this circuit also obeys the translinear principle, which makes it robust and allows it to be analyzed within the translinear framework.

5.6 Soft-Gates

Lustenberger has proposed a class of relatively low-complexity translinear circuits which implement the soft-gate functions precisely.

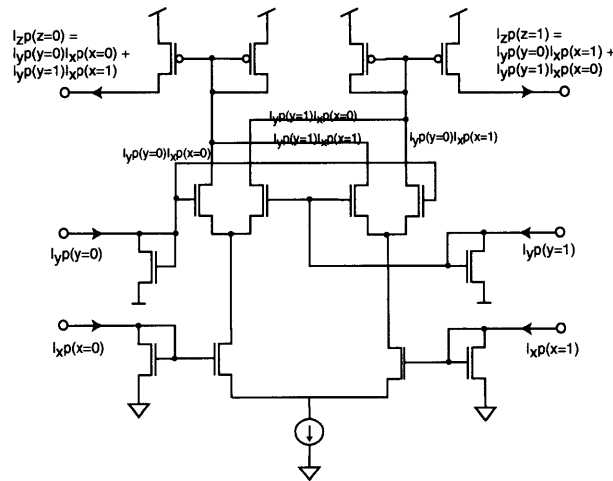


Figure 5-16: Gilbert Multiplier Implements Softxor Function

As can be seen in figure 5-16, a re-labelling of the Gilbert multiplier circuit is sufficient to implement the soft-xor function. A slight modification of the Gilbert multiplier implements the soft-equals function (variable node with more than 2 incident edges) as shown in figure 5-17.

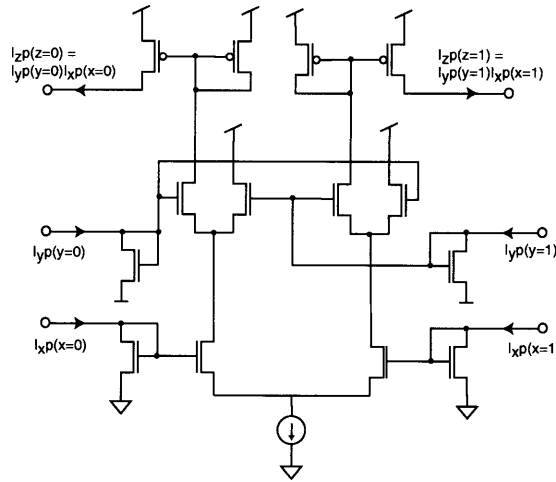


Figure 5-17: Modified Gilbert Multiplier Implements Softequals Function

5.7 Figures of Merit

A “mixer” is an analog multiplier circuit used in radio applications for modulation or demodulation. It is in this context that analog multipliers will likely be most familiar to RF designers. Typically one or both of the inputs to a mixer is a sinusoidal or modulated sinusoidal signal. By subtracting one trigonometric identity

$$\cos(u + v) = \cos(u) \cos(v) - \sin(u) \sin(v) \quad (5.32)$$

from another trigonometric identity

$$\cos(u - v) = \cos(u) \cos(v) + \sin(u) \sin(v), \quad (5.33)$$

we find that the product of two sinusoids of frequencies u and v

$$2 \sin(u) \sin(v) = \cos(u - v) - \cos(u + v) \quad (5.34)$$

consists of a sinusoid with the “sum” frequency $u + v$ and a sinusoid with the “difference” frequency $u - v$. When multiplying sinusoids, one typically filters out the sum frequency in order to leave the difference frequency. This is known as mixing-down

or *down-conversion* and is the essential building block in a heterodyne radio receiver.

We are using mixer-type circuits, but are using them to operate on completely different signals. Instead of sinusoidal signals, we have analog probability levels. The question is how well can mixer-type circuits perform this function?

The merit of a mixer is evaluated according to its “linearity”, port-to-port isolation, gain, noise figure, and dynamic range [54]. Attenuation or conversion loss and port-to-port isolation are generally measured in $\text{dBm} = \log(\text{signalpower}/1\text{mW})$ with a 50Ω load. Port-to-port isolation will effect our resolution to some degree, but it will be much less important for us than it is in sinusoidally based RF demodulation. This will be described in greater detail when we discuss the soft-MUX, but the basic idea is that leakage signals don’t tend to have as drastic impact on soft-decoding as it does on RF down-conversion. In any event, the best isolation is achieved by PIN diodes which are used as analog switches and offer approximately 70dBm of isolation. Typical “Gilbert cell” active mixers offer on the order of 30dB of isolation.

Linearity in this context means how accurately the actual mixer function adheres to an ideal mathematical multiplication. It is an open and interesting research question to fully characterize how linearity of the multipliers will affect the sum-product algorithm, but we know from preliminary simulations that the affect will not be catastrophic. Linearity should therefore be de-emphasized as a design constraint. In practice, this means we can push our circuits to operate outside of their linear range and therefore obtain a larger dynamic range from the same circuit for the same amount of power.

The sum-product algorithm is guaranteed to reach a maximum-likelihood estimate on a graph without cycles. By turning up the gain on a multiply in the sum-product algorithm it is actually possible to speed up the sum-product algorithm, while sacrificing the guarantee that the algorithm will converge to the maximum-likelihood estimate. Since we have already sacrificed this guarantee in graphs with cycles, we might even desire non-ideal multipliers to get quick and dirty estimates. If the actual multiplier gives a function which is steeper than a “linear” multiply in the middle range and then less steep at the edges, this may effectively schedule the annealing

process for the sum-product algorithm so that it goes faster in the beginning and then slows down as it refines its answers at the end. This may be a good thing to do in high SNR environments or in relatively easy searches where hasty early decisions are unlikely to freeze the answer irrevocably into a bad region of the search space.

Passive mixers have attenuation and depend on post-amplification for their gain. We are interested in active mixers which tend to have gain between 0 and 5. 8 would be a lot of gain for a mixer. For our purposes, we are free to scale our signals in any way we please so that we do not need gain from our mixer circuits, although we would prefer not to have attenuation. We simply take the ratio of dynamic range and the noise to obtain the resolution.

A typical mixer has 5-8 bits of resolution. This is pretty useful for decoding. In soft decoding we would like our resolution to be at least 2 bits and would prefer as much as 8 bits of resolution. By way of comparison, demodulation of sinusoids by digital signal processing uses 12 or 14 bits of resolution and CD quality audio utilizes 16 bits of resolution. The best analog-to-digital converters today offer 24 bits of resolution. Mixer circuits, like all analog circuits, tend to be specified with dynamic range and a noise figure in SNR and not in bits of resolution. The table below converts some common values of resolution (in bits) to SNR (power)

$$SNR = 20 \log \left(\frac{P_S}{P_N} \right) \quad (5.35)$$

where P_S is the signal power and P_N is the noise power.

resolution (bits)	power SNR (dB)
1 bit	3dB
2 bits	6dB
5 bits	15dB
8 bits	24dB
12 bits	36dB
14 bits	42dB
16 bits	48dB
24 bits	72dB

The following table converts resolution (in bits) to SNR (voltage),

$$SNR = 20 \log \left(\frac{V_S}{V_N} \right) \quad (5.36)$$

where V_S is the signal dynamic range in volts and V_N is the RMS noise voltage.

resolution (bits)	voltage SNR (dB)
1 bit	6dB
2 bits	12dB
5 bits	30dB
8 bits	48dB
12 bits	72dB
14 bits	84dB
16 bits	96dB
24 bits	144dB

5.7.1 Resolution and Power Consumption of Soft-Gates at 1GHz

Let us examine the performance of the simple circuit shown in figure 5-18.

In the TSMC .18 μ m process, the smallest possible dimension of any feature is $\lambda = .18\mu m$. We would like the circuit to perform a multiply operation on V_0 and V_1

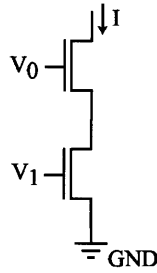


Figure 5-18: 2 transistor multiply single-quadrant multiply (component of a soft-gate)

once every nanosecond (1Gops) while consuming a maximum of 10uW of power. We only allow the circuit to consume 10uW of power, because then we will be able to use 100's of such circuits and still have very moderate power consumption for a portable wireless front-end. The question is how many bits of resolution can we expect from the circuit with these constraints? We define the resolution (in bits) as

$$R = \log_2 \left(\frac{\Delta I_{out}}{I_{noise}} \right) \quad (5.37)$$

where ΔI_{out} is the output current dynamic range and I_{noise} is the output-referred RMS current noise.

Devices in this process are designed to operate between GND=0V and VCC=1.8V. So the power supply rails are approximately 2V apart. 10uW of power gives us a maximum of 5uA of current at the output with 2V rails since $P = IV$. The minimum output current is very close to 0uA. So the output current dynamic range is 5uA.

Now we must find the output-referred current noise to complete the calculation of the resolution. The output referred current noise power is given by

$$I_{RMS}^2 = kT \frac{8}{3} g_m \Delta f \quad (5.38)$$

where Boltzman's constant $k = 1.38(10^{-23})$ and we assume a circuit at room temperature, $T = 300$ degrees Kelvin. MOSFETs with $W/L \approx 10$ in this process have

$$\beta = \mu C_{ox} \frac{W}{L} \approx 50 \quad (5.39)$$

We can therefore calculate the transconductance $g_m \approx 400\mu S$ from

$$\begin{aligned} g_m &= \beta \sqrt{\frac{2I}{\beta}} \\ &= \sqrt{2I\beta}. \end{aligned} \quad (5.40)$$

We are interested in a soft-gate that operates over a bandwidth of 1GHz so that $\Delta f = 10^9 \text{Hz}$. We can now calculate $I_{RMS}^2 \approx 10^{-15}$ and therefore the output-referred current noise is $I_{RMS} \approx 3.3(10^{-8})A$. The resolution is therefore approximately $R = \log_2(5\mu A / .033\mu A) = \log_2(150) \approx 7$ bits.

We might wonder what range of voltages we should use to drive this circuit at the input in order to achieve the above performance. For a transistor in this process, $C_{ox} \approx .02\mu A/V^2$. With $W/L = 2\mu m / .18\mu m \approx 10$, the gate capacitance is about $C_{gs} = (2/3)WLC_{ox} \approx 4fF$. Assuming a sinusoidal signal

$$\begin{aligned} V &= V_p \sin(2\pi f_c) \\ \frac{dV}{dt} &= V_p 2\pi f_c \cos(2\pi f_c) \\ \max \frac{dV}{dt} &= V_p 2\pi f_c |_{\cos(2\pi f_c)=1}, \end{aligned} \quad (5.41)$$

and substituting into the definition of capacitance $I = C \frac{dV}{dt}$, we find that

$$V_p = \frac{C}{I} 2\pi f_c \approx 200mV \quad (5.42)$$

where $I=5\mu A$, $C=4fF$, and $f_c = 1GHz$. So $v_{pp} = 400mV$.

Further simulation is needed to verify and extend these back-of-the-envelope calculations, but it seems promising that MOSFET soft-gates in non-heroic processes can operate on reasonably high-frequency signals.

Chapter 6

The Sum Product Algorithm in Continuous-Time

6.1 Differential Message Passing

Annealing is what happens when we try to cool a material so that it forms a perfect crystal without “discontinuities”. At the atomic level, a perfect crystal would be spatially invariant; Every part of the crystal would be a perfect copy of every other part of the crystal. This perfectly symmetrical state, although it is the lowest possible energy state of a crystal, is actually quite difficult to achieve, because different parts of the crystal often grow from unconnected “seeds”. Crystal will start to form independently at different places in a liquid that is beginning to freeze, and by time the entire material is frozen, there may be several different crystal orientations present. The frozen material tends to break more easily along the discontinuities between neighboring regions of differing orientation. To avoid this problem, Japanese Samurai swords were painstakingly *annealed* through a process of successive heating and cooling. On each heating stage, the metal crystal would be melted a bit, allowing regions of the crystal that might have been misaligned with one another to work out some of their “kinks.” Then the metal is cooled again and the process is repeated.

Annealing works because adjacent atoms in the material would prefer to be in alignment than randomly oriented to one another. This preference can be modelled

by an energy function over the possible alignments or states of the two atoms. In this way the total energy of a crystalline material is composed of a very large number of pairwise energy functions over pairs of atoms. As a crystal is annealed, the atoms are all acting on each other in continuous-time, trying to lower the energy of all of the pairs in which they participate.

Physicists model each atom in an annealing crystal as having a probability distribution over its possible states. The energy function, when normalized, is then really a joint probability distribution. Such a model should by now appear rather familiar. Physicists call such models a spin-glass, and research on spin-glasses was an important ancestor of probabilistic message passing algorithms.

When a crystal is annealed, the atoms in the material are in effect performing a constraint satisfaction computation. The converse is also true - constraint satisfaction problems in computer science bear a deep resemblance to spin-glass annealing. All the sum-product algorithm is really doing is performing pairwise interactions between adjacent states in an attempt to settle to a mutually compatible solution. Just like annealing, probabilistic message passing algorithms ought properly to be implemented as a continuous-time parallel process.

Unfortunately, because discrete-time serial computers are generally the only ones readily available to us, we adopt a discrete-time approximation to the continuous-time process. Such a discrete-time approximation should have the property that every message gets updated when there is enough new information available from other messages to justify recomputing the message. One definition of “enough” could be that a message is computed for an (outgoing) edge from a given node when all of the other (incoming) edges to that node have new messages coming in. This idea is the origin of the message passing schedule discussed in the last chapter. There is no proof, however, that this schedule is guaranteed to find the same answer as the continuous-time process would have. In fact, it will often diverge from the continuous-time solution, producing wrong answers which are merely an artifact of the scheduling. When this happens, we use damping.

6.1.1 Damping

Damping means that messages consist of a linear combination of the current calculated message and the last calculated message in the same direction on the same edge,

$$\mu_t = \alpha\mu_t + (1 - \alpha)\mu_{t-1}. \quad (6.1)$$

6.1.2 Von Neuman Stability Analysis of Finite Differences

Finite difference models of partial differential equations (PDE) have much in common with probabilistic message passing algorithms on a Markov Random Field. In each case we have a grid of states which update in time based on functions of their local neighbors. And in both cases, we approximate continuous-time updates with discrete-time updates. Of course there is an important difference; In a finite difference model of a PDE, the functions impose constraints on the derivative of the solution, while in probabilistic message passing, the constraints can be more general.

It is not yet understood under which conditions damping stabilizes discrete-time probabilistic message passing so that it converges to the continuous-time solution. There is, however, a suggestively similar procedure for stabilizing the discrete-time (and discrete-space) finite difference model of a PDE. A Von Neumann stability analysis is a well-understood way to analyze the stability of a finite difference model of a PDE.

Our finite difference model in one dimension will consist of a row of states, u indexed in space by j and in time by n . So at time n , a point in space on the solution of the PDE is a real number, u_j^n . To perform the stability analysis, we linearize the PDE (if it is not already) and observe the growth of sinusoidal modes

$$u_j^n = A(k)^n e^{ikjx} \quad (6.2)$$

in the system, where $A(k)$ gives an exponentially growing amplitude in time for

the sinusoidal spatial oscillation. We can substitute this into the finite difference equation as an ansatz. If $|A(k)| > 1$ for any k , then those modes will grow without bound and the model will be unstable.

Let us use as an example, a first order PDE in one dimension,

$$\frac{\partial u}{\partial t} = -\nu \frac{\partial u}{\partial x}. \quad (6.3)$$

Any function of the form $u = f(x - \nu t)$ can solve this equation exactly, as can be seen by substitution of this *ansatz* into the PDE. A naive finite difference model of this PDE would be first-order in time and second-order in space,

$$\frac{u_j^{n+1} - u_j^n}{\Delta t} = -\nu \left(\frac{u_{j+1}^n - u_{j-1}^n}{2\Delta x} \right). \quad (6.4)$$

Re-arranging terms this is written,

$$u_j^{n+1} = u_j^n - \frac{\nu \Delta t}{\Delta x} (u_{j+1}^n - u_{j-1}^n). \quad (6.5)$$

Choosing equation (6.1.2) as an ansatz and so substituting into the finite difference update we get

$$\begin{aligned} A^{n+1} e^{ikjx} &= A^n e^{ikjx} - \frac{\nu \Delta t}{2\Delta x} (A^n e^{ik(j+1)x} - A^n e^{ik(j-1)x}) \\ A &= 1 - \frac{\nu \Delta t}{2\Delta x} (e^{ikx} - e^{-ikx}) \\ &= 1 - i \frac{\nu \Delta t}{\Delta x} \sin kx \end{aligned} \quad (6.6)$$

The absolute magnitude of this is always greater than one, so the model will always diverge. This can be remedied by the LAX method which averages neighbors for the time derivative,

$$u_j^{n+1} = \frac{1}{2} (u_{j+1}^n + u_{j-1}^n) - \frac{\nu \Delta t}{2\Delta x} (u_{j+1}^n - u_{j-1}^n). \quad (6.7)$$

Performing the stability analysis again yields an amplitude,

$$A = \cos kx - \frac{\nu\Delta t}{\Delta x} \sin kx \quad (6.8)$$

For the model to be stable, we require the magnitude of this complex amplitude to always be less than 1 so that

$$|A|^2 = \cos^2 kx + \left(\frac{\nu\Delta t}{\Delta x}\right)^2 \sin^2 kx \leq 1 \quad (6.9)$$

which is true under the condition that

$$\frac{|\nu|\Delta t}{\Delta x} \leq 1. \quad (6.10)$$

This is the Courant-Friedrichs-Levy stability criterion, which essentially says that “the velocity at which information propagates in the numerical algorithm $\Delta x/\Delta t$, must be faster than the velocity of the solution ν ... Otherwise there will be a numerical “boom” as the real solution tries to out-run the rate at which the numerical solution can advance [15].”

Damping in probabilistic message passing solves the same problem that the LAX method solved in our finite difference model. If the true continuous-time annealing process is trying to out-run the flow of information by message passing updates, then the states need to change slower over more message updates. We can update messages more slowly by averaging a message update with previous messages on the same edge, ie. damping. It still remains for us to find an analogous bound to the Courant-Friedrichs-Levy stability criterion for sum product which would tell us how much and what kind of damping is enough to ensure stability and convergence of the discrete-time model to the continuous-time solution. It is likely for example, that for many inhomogeneous graphs, different amounts of damping could be tolerated at different places in the graph.

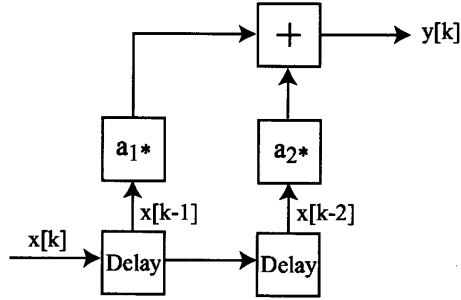


Figure 6-1: A two-tap FIR filter with tap weights a_1 and a_2

6.1.3 Filtering Probabilities and Likelihoods is Equivalent to Damping

The difference equation for the two-tap 1-pole FIR low-pass FIR filter illustrated in figure 6-1, above is given by

$$y[k] = a_1x[k-1] + a_2x[k-2]. \quad (6.11)$$

If we pass a probability $p(1)$ or $p(0)$ through such a filter, then we obtain

$$p_{y[k]}(1) = a_1p_{x[k-1]}(1) + a_2p_{x[k-2]}(1) \quad (6.12)$$

$$p_{y[k]}(0) = a_1p_{x[k-1]}(0) + a_2p_{x[k-2]}(0). \quad (6.13)$$

Summing these two equations we find

$$\begin{aligned} p_{y[k]}(1) + p_{y[k]}(0) &= a_1[p_{x[k-1]}(1) + p_{x[k-1]}(0)] + a_2[p_{x[k-2]}(1) + p_{x[k-2]}(0)] \\ p_{y[k]}(1) + p_{y[k]}(0) &= a_1 + a_2. \end{aligned} \quad (6.14)$$

Since we require $p_{y[k]}(1) + p_{y[k]}(0) = 1$ for proper normalization, $a_1 + a_2 = 1$ for probabilities to be preserved under filtering. This is not at all an onerous constraint on the filter. Forcing $1 - a_1 = a_2$ means that a 2-tap low-pass FIR filter is precisely

equivalent to our prior definition of damping.

In general, if we pass a probability $p(1)$ through a unitary FIR filter with N taps, where N is large, and where $\langle a_n \rangle = \frac{1}{N}$, we find that we obtain the expectation of $p(1)$,

$$\sum_{n=1}^N a_n p_{t-n\tau}(1) = \frac{1}{N} \sum_{n=1}^N p_{t-n\tau}(1) = \langle p(1) \rangle. \quad (6.15)$$

The same holds for likelihoods $l \equiv \frac{p(1)}{p(0)}$

$$\sum_{n=1}^N a_n \frac{p_{t-n\tau}(1)}{p_{t-n\tau}(0)} = \frac{1}{N} \sum_{n=1}^N \frac{p_{t-n\tau}(1)}{p_{t-n\tau}(0)} = \langle l \rangle. \quad (6.16)$$

6.1.4 Filtering Log-Likelihoods

However, filtering does not operate on log-likelihoods in the same way that it operates on probabilities. From the definition of a log-likelihood,

$$L = \log \left[\frac{p(1)}{p(0)} \right]. \quad (6.17)$$

We can see that

$$\begin{aligned} \sum_{n=1}^N a_n L_{t-n\tau} &= \sum_{n=1}^N a_n \log \left[\frac{p_{t-n\tau}(1)}{p_{t-n\tau}(0)} \right] \\ &= \log \left[\prod_{n=1}^N \left(\frac{p_{t-n\tau}(1)}{p_{t-n\tau}(0)} \right)^{a_n} \right]. \end{aligned} \quad (6.18)$$

For example, Simply substituting the log-likelihood into the difference equation for the two-tap FIR filter from above, we obtain

$$\begin{aligned} y[k] &= a_1 \log \left[\frac{p_{x[k-1]}(1)}{p_{x[k-1]}(0)} \right] + a_2 \log \left[\frac{p_{x[k-2]}(1)}{p_{x[k-2]}(0)} \right] \\ &= \log \left[\left(\frac{p_{x[k-1]}(1)}{p_{x[k-1]}(0)} \right)^{a_1} \left(\frac{p_{x[k-2]}(1)}{p_{x[k-2]}(0)} \right)^{a_2} \right] \end{aligned} \quad (6.19)$$

Let us suppose that the resulting $y[k]$ is a valid log-likelihood and see if that results in a contradiction. So let

$$\begin{aligned}
 L_y \equiv \log \left[\frac{p_{y[k]}(1)}{p_{y[k]}(0)} \right] &= \log \left[\left(\frac{p_{x[k-1]}(1)}{p_{x[k-1]}(0)} \right)^{a_1} \left(\frac{p_{x[k-2]}(1)}{p_{x[k-2]}(0)} \right)^{a_2} \right] \\
 \frac{p_{y[k]}(1)}{p_{y[k]}(0)} &= \left(\frac{p_{x[k-1]}(1)}{p_{x[k-1]}(0)} \right)^{a_1} \left(\frac{p_{x[k-2]}(1)}{p_{x[k-2]}(0)} \right)^{a_2} \tag{6.20}
 \end{aligned}$$

If $a_1 = a_2 = 1$, this is the likelihood form of a soft-equals gate. For arbitrary choices of a_1 and a_2 it is a weighted soft-equals gate. So the FIR filter acting on a log-likelihood representation does not perform the filtering operation that we had desired, but does something else entirely.

6.2 Analog Memory Circuits for Continuous-Time Implementation

Continuous-time (CT) analog memory will have a number of benefits for soft-gate systems. It will greatly reduce noisy glitches and can potentially run at much faster speeds compared to clocked analog memory. It should also be possible to invent active CT delay-line circuits such as soliton waveguide circuits or linear-phase filter circuits which are less susceptible to drift, parasitics, and leakage than passive charge storage such as S/H circuits. Perhaps the most important benefit, however, is that there is no sampler which must be synchronized to the transmitter's bit clock.

In the existing implementations of analog circuits computing the sum-product algorithm for error correction decoding, [28] et al. have presented the analog inputs simultaneously to all of the leaf nodes of the factor graph using Digital-to-Analog Converters (DAC). Demosthenous et al. have used a delay-line composed of sample and hold (S/H) circuits in a 2.8V CMOS current-mode analog Viterbi decoder to decode an 100Msps serial data stream [10]. I also implemented my own S/H delay line circuit shown in figure 6-2. Although the performance was acceptable, it was

difficult to compensate a string of sample-and-holds to have unity gain. The clocking also inserted significant glitch noise into the entire system.

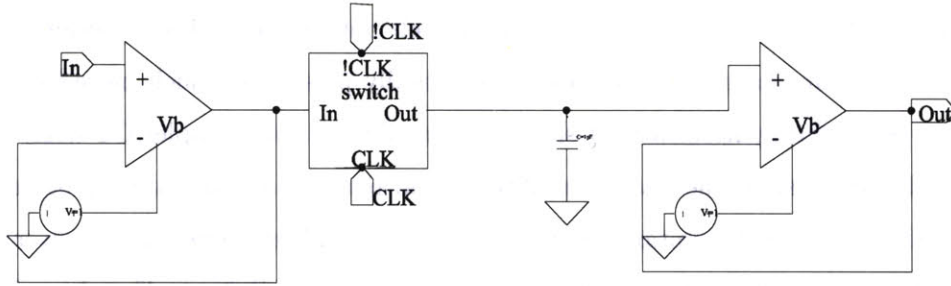


Figure 6-2: Schematic of sample-and-hold delay line circuit

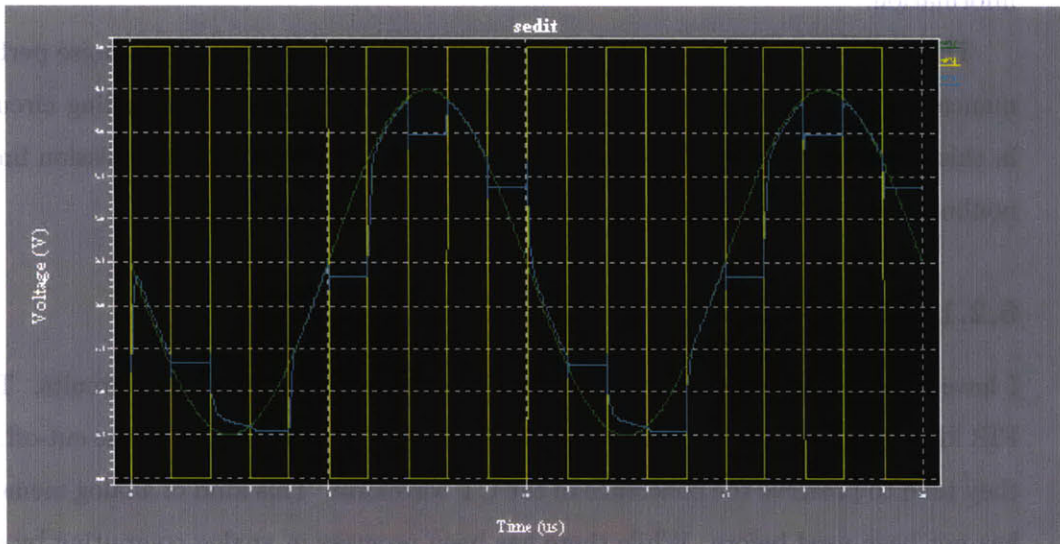


Figure 6-3: Sample-and-hold delay line circuit operating on sinusoidal signal

Although a worthwhile demonstration, S/H circuitry is relatively slow and noisy, and will not scale to RF. Another way to create analog memory is to sample the analog signal with an ADC and then use a DAC to convert it back to analog for presentation to the analog circuitry when it is needed [5]. While potentially useful in some applications, this Analog-to-Digital-to-Analog (A/D/A) approach is also only a competitive option in low frequency applications [41].

There are a number of possible ways to implement analog CT delay-lines. In this thesis I demonstrate a proof of principle by implementing analog CT delay with linear-phase FIR low-pass filters. Unfortunately, linear phase low-pass filters are likely to be too complex to be cost-effectively integrated. This is because by preserving linear phase, the FIR filters are actually preserving much more information than is absolutely necessary. It should be possible to build simpler CT delay circuits which still preserve the analog amplitudes and perform appropriate smoothing without the overhead of maintaining linear phase delay. A hint is offered by Carver Mead's much simpler CT delay-line circuits which delay (digital) "neural" pulses. What is needed are circuits which, like Mead's simple spike delay-lines, are less complex than linear-phase FIR filters, but which preserve the (for us) crucial analog amplitude information.

The engineering decisions for CT delay line circuits trade-off length, noise performance, bandwidth, and dispersion. Future work will be directed at finding circuits in this middle ground, perhaps drawing on integrated micro-strip transmission lines, nonlinear transmission lines, or soliton waveguide circuits [46].

6.2.1 Active Low-Pass Filters

I have implemented CT analog delay-lines with FIR Chebychev filter circuits. The FIR filters are designed to have linear phase delay over frequencies up to the cut-off, so they tend to preserve the coherence of the CT waveform. This kind of analog memory has not been used before. While there has been progress in analog computing by the invention of translinear circuits to implement sum-product computations, storing a baseband RF signal and presenting it to the decoder is a more open problem. We have analog logic, now we need analog memory.

The system was first simulated using the MATLAB filter design toolbox. Then the filter circuits schematic were designed using a filter design program from Filter Solutions. Once the filters were designed, the entire system was simulated using PSpice circuit simulator. Finally, it is a relatively straight-forward matter to convert the Spice net-list schematic representation into an actual printed circuit board or

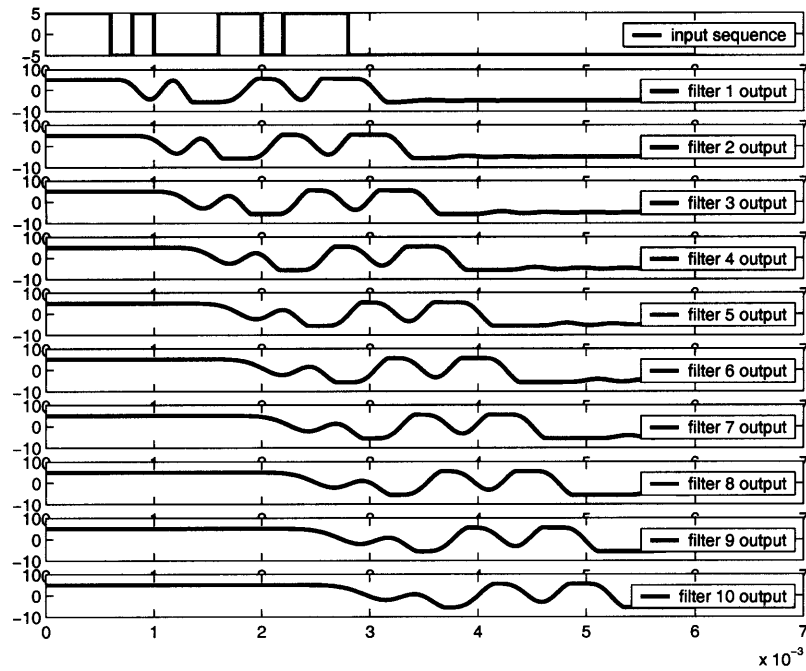


Figure 6-4: Spice simulations of serial delay line composed of 10 Chebyshev filters

integrated circuit (IC) layout. As can be seen in figures 6-5 and 6-5, the finished circuits show a close qualitative correspondence to simulations.

The delay element circuit in figure 6-6 was a fifth order Chebyshev type I low-pass filter with pass-band ripple of .01dB and pass-band frequency of 2kHz. This filter was implemented using a “positive SAB” circuit topology, with gain of 1. A characteristic resistance of 10k was chosen. The transfer function is given as,

$$\frac{4.079(10^{20})}{S^5 + 3.323(10^4)S^4 + 7.495(10^8)S^3 + 1.042(10^{13})S^2 + 9.251(10^{16})S + 4.079(10^{20})} \quad (6.21)$$

Ten of these circuits were connected in series as shown in figure 6-4.

The poles of this transfer function are visualized in the complex plane in figure 6-7. The filter has frequency, phase, and group delay shown in figures 6-8, 6-9, and 6-10 respectively. Ten of these filters were combined in series as shown in figure 6-6. In Spice simulation, a test signal was input to this delay line. The results of the simulation are shown in figure 6-4.

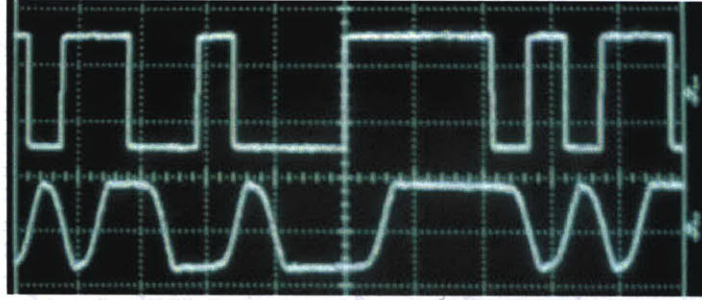


Figure 6-5: Oscilloscope traces of input to (top) and output from (bottom) a fifth order Chebyshev filter delay line

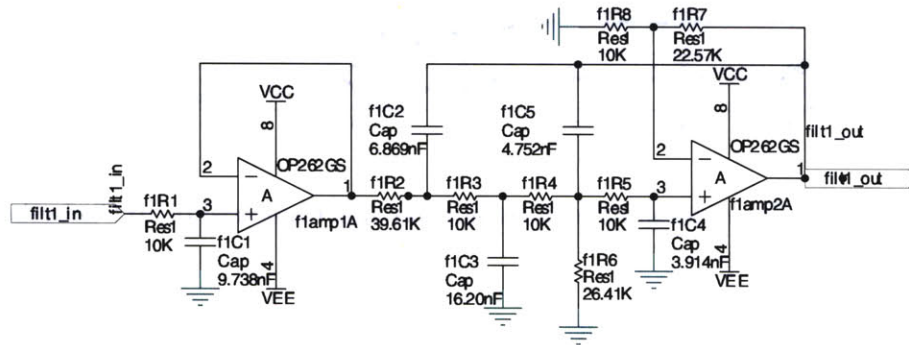


Figure 6-6: Schematic diagram of Chebyshev continuous-time delay circuit

6.3 Continuous-Time Dynamical Systems

6.3.1 Simple Harmonic Oscillators

The “simple harmonic oscillator” model in physics describes the dynamics of a particle trapped in a second order (quadratic) energy potential. A particle moving in such a potential will produce sinusoidal vibrations. The simple harmonic oscillator is an abundantly useful model for many phenomena in nature since a rugged energy surface can always be approximated as a quadratic potential near to its minimum by taking its second-order Taylor series approximation,

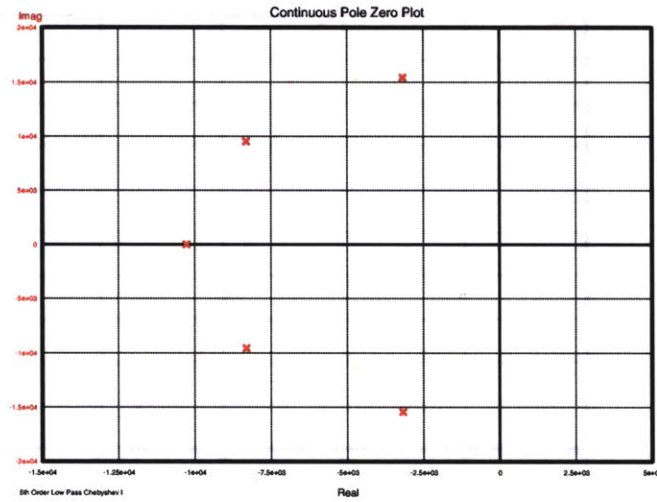


Figure 6-7: Poles of Chebychev delay filter

$$\begin{aligned}
 V(x) &= V|_{x=0} + \frac{1}{2} \frac{d^2V}{dx^2} x^2|_{x=0} + \mathcal{O}(x^3) \\
 V(x) &= V_0 + \frac{1}{2} V_2 x^2 + \mathcal{O}(x^3).
 \end{aligned}
 \tag{6.22}$$

The first order term of the series is not present, because the slope at a minima is zero. Taking the gradient of the potential to find the force, $F = ma$ becomes

$$\begin{aligned}
 m \frac{d^2x}{dt^2} &= -\frac{dV}{dx} = -V_2 x \\
 m\ddot{x} + V_2 x &= 0
 \end{aligned}
 \tag{6.23}$$

which is the equation of motion for a simple harmonic oscillator, a second order linear ordinary differential equation. If we can approximate a dynamical system as linear in this way, the solutions of the system will be a linear combination of rising or falling exponentials and complex sinusoids. Sinusoids are eigenfunctions of linear systems. So sine-wave oscillators are easy to make - they are the default behavior for any energy potential with a minima.

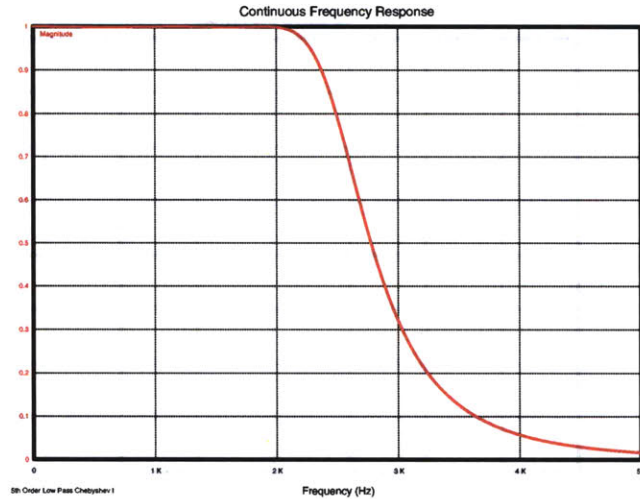


Figure 6-8: Frequency response of Chebychev delay filter

6.3.2 Ring Oscillator

One of the simplest nonlinear energy potentials is the bistable potential shown in figure 6-11. This potential consists of two adjacent quadratic troughs with a low barrier between them. The barrier between the two troughs is often referred to as the threshold. A particle in this kind of energy potential will occupy one of the two troughs and will require some amount of energy to switch over the threshold into the other trough. A system which can switch between two states with the application of a small amount of energy, is bi-stable. Such bistable switching systems are the basic building block of a digital computer.

In digital computers, we wire up such switches so that when one switch changes state it can send a signal to force another switch to change state. Digital computing consists of a cascade of these switching events. Of course such chains of switches will only work if there is no energy lost in any of the switching events or if we supply energy to the system to ensure that when a switch is triggered, there is energy available to cross the threshold. If we wanted to, we could connect a bistable switch to itself so that when it switches state it actually sends a signal to itself which forces it to switch again. This is called a ring oscillator. The default nonlinear oscillator is

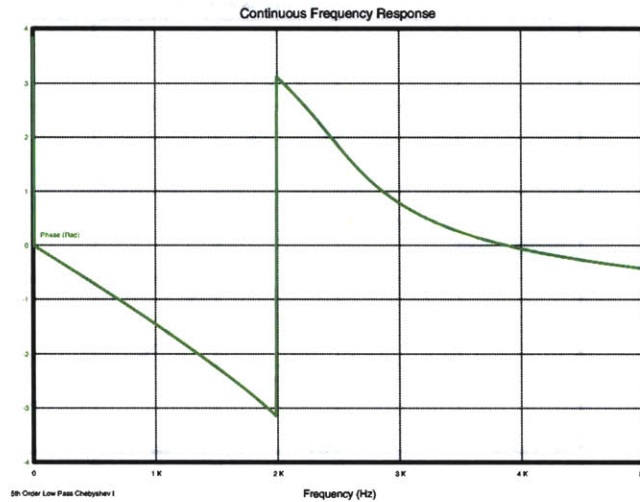


Figure 6-9: Phase response of Chebychev delay filter

a ring oscillator. Ring oscillators, like simple harmonic oscillators are ubiquitous in Nature as well as engineered systems. Any time the outcome of a decision reverses the assumptions by which the decision was made we have a ring oscillator. For example a person trying to work out a paradox constitutes a ring oscillator.

“The following sentence is true. The previous sentence is false.”

To build a ring oscillator with electronic circuits, we build an inverter and feed its output back to its input. If we make the inverting gain small compared to the switching speed of the ring oscillator, it will try to return to the trough it began in, before it even reaches the other trough. Without enough gain, the system will operate around the threshold point, never falling completely into one trough or the other. In this case, we can model the potential as a quadratic minima centered at the threshold, and the ring oscillator becomes a simple harmonic oscillator and will produce (very low amplitude) sinusoidal dynamics.

6.3.3 Continuous-Time LFSR Signal Generator

The system in figure 6-12 will generate an LFSR waveform with 8 samples per LFSR bit. We call this a pseudo-continuous-time LFSR because it does has more than one

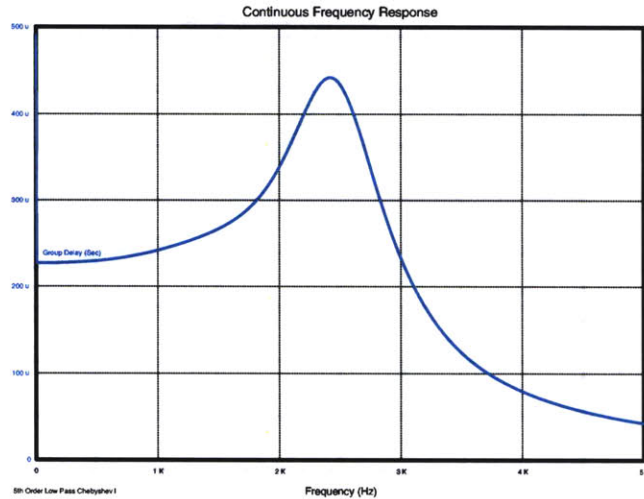


Figure 6-10: Group delay of Chebychev delay filter

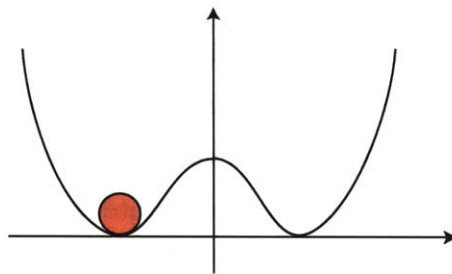


Figure 6-11: “W” shaped (nonlinear) energy potential with ball trapped in one minima

sample per LFSR bit. I have implemented this system using MN series bucket-brigade (BBD) chips intended for use in guitar delay pedals. The BBD chips were clocked at 8 times the desired LFSR bit-rate. The output of the free-running circuit is shown in figure 6-13. Unfortunately, for radio applications this is not a very attractive system because we would need to clock the memory nearly an order of magnitude faster than the signal processing sample rate. Furthermore in the continuum limit this system would have an infinite number of samples per LFSR bit, which requires infinite bandwidth and therefore infinite power. We need to put an upper bound on the bandwidth of the delay elements, if this system is to be physically realizable. We do this with a low-pass filter.

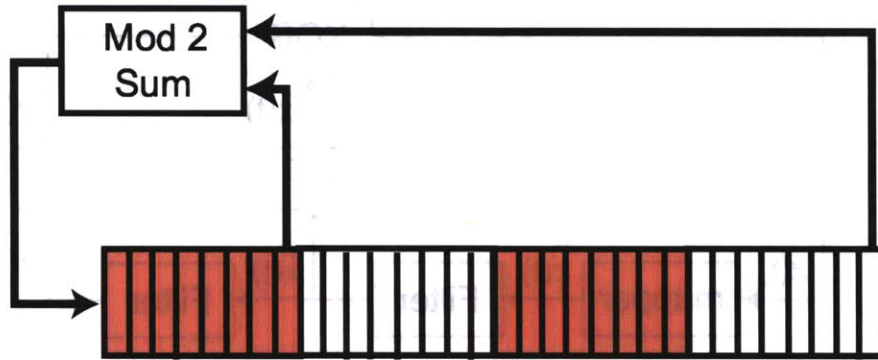


Figure 6-12: Continuous-time LFSR

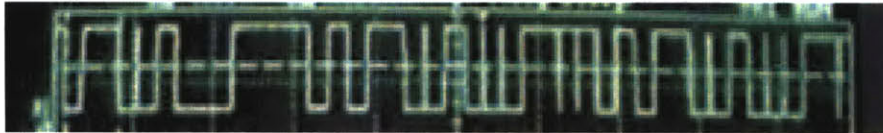


Figure 6-13: Output of continuous-time LFSR circuit

Figure 6-14 shows the construction of a CT LFSR using linear-phase low-pass filters as delay elements. The filters can be any IIR or FIR low-pass filters. The choice of filters greatly effects the signal generated by the system. In fact the system can be chaotic and non-periodic for some choice of filters.

These filters act like a AWGN channel, accepting inputs and producing outputs over the range $[+1, -1]$. The XOR gate on the other hand operates on bits and produces bits $\{0, 1\}$. We therefore need two new elements, the mapper and the limiter, to map values between these two representations. The mapper maps the logic bits $x(t) \in \{0, 1\}$ to antipodal signals $\tilde{x}(t) \in \{+1, -1\}$ such that

$$\tilde{x}(t) = 1 - 2x(t). \quad (6.24)$$

The hard limiter transforms a signal $\tilde{u}(t) \in \mathbf{R}$ back to a bit $u(t) \in \{0, 1\}$ such that

$$\begin{aligned} \tilde{u}(t) > 0 &\rightarrow 0 \\ \tilde{u}(t) \leq 0 &\rightarrow 1. \end{aligned} \quad (6.25)$$

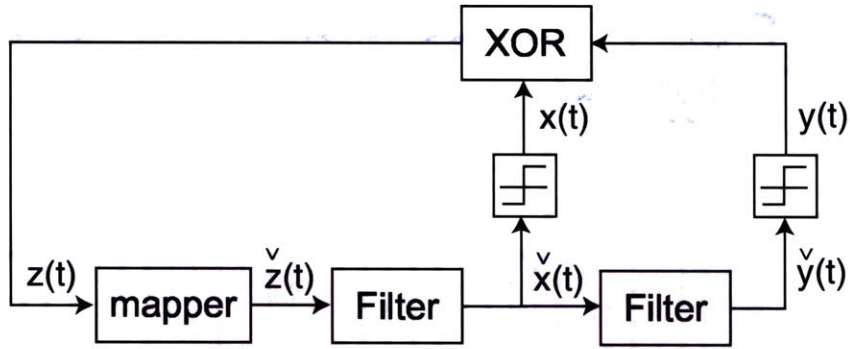


Figure 6-14: Continuous-time LFSR circuit with mapper and limiter

When we design receiver system it will require soft version of these elements, a soft-mapper and soft-limiter.

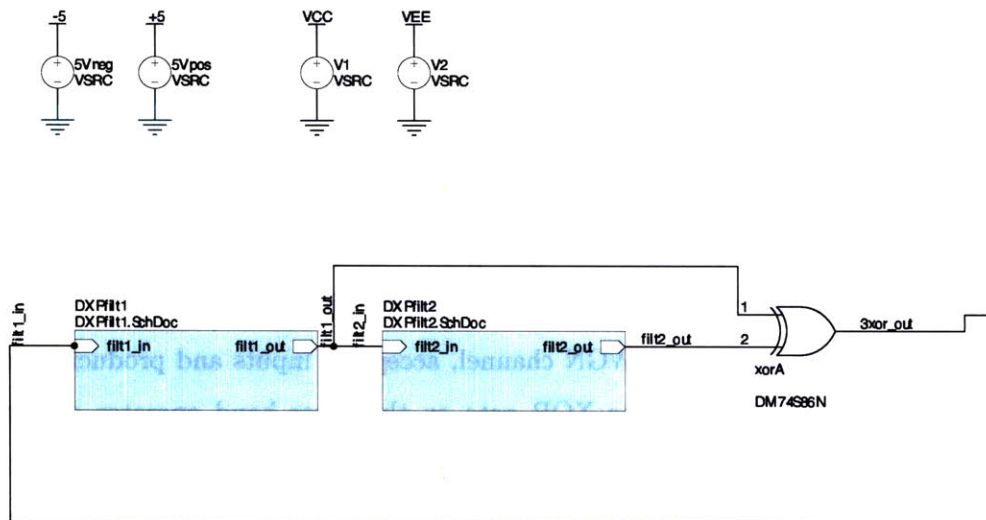


Figure 6-15: Block diagram of noise lock loop (NLL) transmit system

A circuit implementation of this system was modelled in spice as shown in figure 6-15. The model incorporates the continuous-time delay filters from section 6.2.1 and a standard 74 series TTL XOR logic gate. The first filter acts as a single bit delay, while the second filter block contains such delay circuits connected in series. The

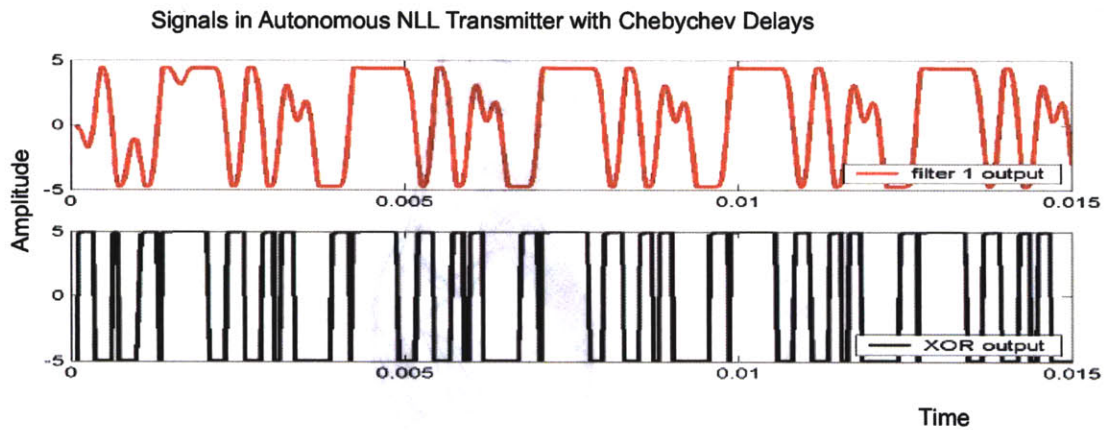


Figure 6-16: Output of filter 1 and XOR in NLL transmit system

circuit ought therefore to behave approximately like a 4-bin 2-tap LFSR with the taps on the first and last bins which produces the sequence $(111101011001000)^*$.

The LFSR-like waveform shown in figure 6-16 was produced by Spice simulation. It is not a perfect LFSR waveform like the one in figure 6-13 due to the low-pass cutoff and (minimal) phase distortion of the delay filters. The waveform is quite repeatable, however as can be seen in the lag-space plot of the waveform shown in 6-17 which was generated from approximately 30 simulated cycles of the waveform.

In figure 6-16, we see that we do not achieve a perfect LFSR signal. This problem gets worse when we try to implement CT LFSRs with more bins. As we try to design filters with longer delays it gets more difficult to determine the filter parameters and implement them with a sane number of devices. The feedback will cause even small errors in the filter to distort the signal so that it is not recognizable as an LFSR signal composed of discrete bits. However, it is not necessary to create perfect delay filters. We can actually use arbitrary low-pass filters as long as they impose a delay. Such a system may produce an unexpected waveform which may even be chaotic and not periodic. As long as the transmitter and receiver system have the same filters, however, the systems will synchronize.

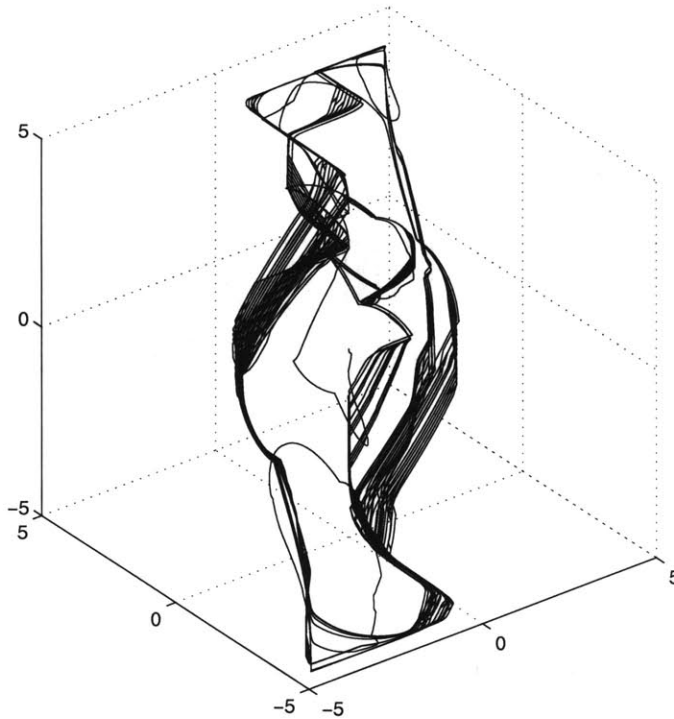


Figure 6-17: Phase space lag plot of output of filter1 in NLL transmit system

6.4 Continuous-Time Synchronization by Injection Locking as Statistical Estimation

6.4.1 Synchronization of Simple Harmonic Oscillator by Entrainment

Injection locking or real addition of the (noisy) transmitter state into the receiver is the mechanism for entrainment of all coupled oscillators. Let us examine injection locking of coupled simple harmonic oscillators (such as pendulums). The equation for an unforced mechanical pendulum is

$$m\ddot{x} + k \sin(x) = 0 \tag{6.26}$$

For small angles of deflection, we can approximate $\sin(x)$ by x leaving the equation for a simple harmonic oscillator (SHO)

$$m\ddot{x} + kx = 0. \tag{6.27}$$

Setting $m \equiv k \equiv 1$

$$\ddot{x} + x = 0 \tag{6.28}$$

We will parameterize this second order differential equation as two first order differential equations by defining

$$x_0 \equiv \dot{x} \tag{6.29}$$

$$x_1 \equiv \dot{x}_0. \tag{6.30}$$

$$\tag{6.31}$$

Equation (6.28) then becomes

$$\dot{x}_1 + x_0 = 0$$

$$x_0 = -x_1 \tag{6.32}$$

$$\tag{6.33}$$

It can now be written as a system of first order ordinary differential equations (ODE).

$$x_1 = \dot{x}_0$$

$$x_0 = -x_1. \tag{6.34}$$

$$\tag{6.35}$$

The factor graph for two coupled SHO is therefore given by figure 6-18. Drawing the factor graph for a SHO required a rather strange function node, the time derivative. But what does it mean to take the derivative of a probability? The definition of the

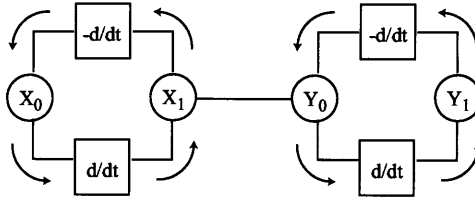


Figure 6-18: Factor graph for two coupled simple harmonic oscillators

time derivative is

$$\frac{df(x)}{dt} = \frac{\Delta f(t)}{\Delta t} = \frac{f(t + \Delta t) - f(t)}{(t + \Delta t) - t} = \frac{f(t + \Delta t) - f(t)}{\Delta t}. \quad (6.36)$$

In discrete time we define $\Delta t \equiv 1$ so that

$$\frac{df(x)}{dt} = [f(t + 1) - f(t)]. \quad (6.37)$$

So in discrete-time we see that a derivative is essentially a two-tap filter with taps of $a_1 = 1$ and $a_2 = -1$. Unlike the two-tap filter we required for damping, $a_1 + a_2 = 0$. This may be obvious to many readers, however we write it explicitly because it helps us to see a trend: any oscillator can be written as a cyclical factor graph with one or more filter functions. And in fact, this teaches us enough to characterize entrainment as a statistical estimator.

The optimum (maximum-likelihood) estimator of the state of a SHO in AWGN is a Kalman filter. The derivative introduces memory into the system in the same way that the delay line did in the LFSR and the Kalman filter acts like the trellis decoder over the (real-valued) states of these memory elements. This real-valued state is usually parameterized in the Kalman filter in terms of a mean μ and the variance σ of the noise around this mean. The Kalman filter can then use the known dynamics of the SHO and the last three state estimates to calculate an estimate of the next state. If we roll up this Kalman filter, we find that it is identical to the SHO factor graph where the variable (soft-equals) node calculates the Kalman gain matrix.

6.4.2 Noise Lock Loop Tracking by Injection Locking

A digital software radio must estimate the phase of the transmitter's bit clock in order to properly sample the code bits. This synchronization function is known as tracking. In a software radio tracking is a separate function performed by a system such as a PLL, DLL or Tau-Dither Loop. The DT NLL performs acquisition, but it needs to be clocked synchronously with the transmitter's LFSR in order to do this. We might hope that if implemented with CT circuits, it might also be able to perform tracking without an external tracking loop. The NLL would then not only estimate the state of the transmit LFSR, but also entrain to its bit clock. This would be useful, because then we would get tracking essentially for free by implementing the DT algorithm with CT circuits. It might also lead to more robust hand-off between acquisition and tracking which are separate functions in digital software radios.

Synchronization of coupled continuous-time oscillators occurs by entrainment. Entrainment requires that the coupled oscillators (or at least the "receive" oscillator) be dissipative. Dissipation means that the volume of the phase space of the entire coupled system must shrink over time. With coupled linear oscillators, the dissipation could be friction - energy lost to heat. With coupled nonlinear oscillators, the dissipation can be provided by the nonlinearity itself. In either case, coupling the oscillators involves summing a small amount of the state of one of the independent variables from the "transmit" oscillator into the equivalent state in the receive oscillator.

In electronic systems, coupling two oscillators by adding some of the output of one oscillator to the input of another oscillator is called injection locking. This is just real addition of the (attenuated) transmitter's signal to the receiver's signal. Injection locking has been used in electronics to produce extremely stable high-frequency sinusoidal oscillators by injecting the output of a digital clock into a sinusoidal ring oscillator. When driven by a square wave, the ring oscillator still produces a sinusoid, but with decreased phase jitter [4].

The CT NLL receiver system is shown in figure 6-19. The soft-xor and channel model $p(y|x)$ have been explained previously. The soft-mapper is a probabilistic

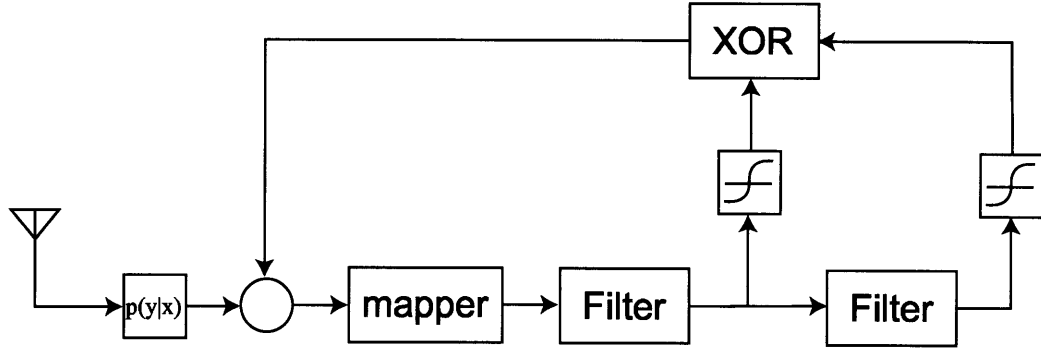


Figure 6-19: Block diagram of noise lock loop (NLL) receiver system

generalization of the mapper in the CT LFSR which mapped $x \in \{0, 1\} \rightarrow \tilde{x} \in \{1, -1\}$. The output of the soft-mapper is the expectation

$$\begin{aligned}
 m(t) &= E[\tilde{x}(t)] \\
 &= p(\tilde{x}(t) = 1) - p(\tilde{x}(t) = -1) \\
 &= p(x(t) = 0) - p(x(t) = 1).
 \end{aligned} \tag{6.38}$$

In other words, the soft-mapper presents a mean as the input to the first delay filter. The filters, filt1 and filt2, in the receiver CT NLL are identical to those in the CT LFSR transmitter. Let m_{filt1} and m_{filt2} be the outputs of a filt1 and filt2 in the receiver. m_{filt1} and m_{filt2} will be the expectation of the output of the corresponding filter in the transmitter $E[\tilde{x}(t)]$ and $E[\tilde{y}(t)]$, respectively.

$$\tilde{x}(t) = \tilde{z}(t) * h_{filter}(t) \tag{6.39}$$

$$\tilde{y}(t) = \tilde{x}(t) * h_{filter}(t) \tag{6.40}$$

$$\tag{6.41}$$

$$\begin{aligned}
E[\tilde{x}(t)] &= E\left[\int h_{filt1}(\tau)\tilde{z}(t-\tau)d\tau\right] \\
&= \int h_{filt1}(\tau)E[\tilde{z}(t-\tau)]d\tau \\
&= (h_{filt1} * m)(t) \\
&= m_{filt1}(t)
\end{aligned} \tag{6.42}$$

and similarly,

$$\begin{aligned}
E[\tilde{y}(t)] &= (h_{filt2} * m)(t) \\
&= m_{filt2}(t)
\end{aligned} \tag{6.43}$$

So the outputs of the filters in the receiver are the expectations of the outputs of the corresponding filters in the transmitter.

The soft-limiters in the receiver compute the messages $p_X(x)$ and $p_Y(y)$ given expectations m_{filt1} and m_{filt2} , respectively [24]. The design of the soft-limiter is dependent on the probability density function of the filter outputs. Recalling the central limit theorem, we can approximate any sufficiently high-order filter as a channel that adds Gaussian noise to the signal \tilde{x} or \tilde{y} passing through it. Therefore we will assume the outputs of the filters to be Gaussian distributed with (mean, variance), (m_{filt1}, σ_1^2) and (m_{filt2}, σ_2^2) , respectively. The soft-limiter must in this case compute an erf function, for example

$$p_X(x(t) = 0) = \frac{1}{2} \left(1 + \operatorname{erf} \left(\frac{m_{filt1}(t)}{\sqrt{2}\sigma_1} \right) \right) \tag{6.44}$$

$$p_Y(y(t) = 0) = \frac{1}{2} \left(1 + \operatorname{erf} \left(\frac{m_{filt2}(t)}{\sqrt{2}\sigma_2} \right) \right). \tag{6.45}$$

In the circuit implementation, we approximate the sigmoidal shape of the erf function with a tanh function which can be easily implemented by a differential pair.

After much experimentation with MATLAB simulations, the NLL shown in figure

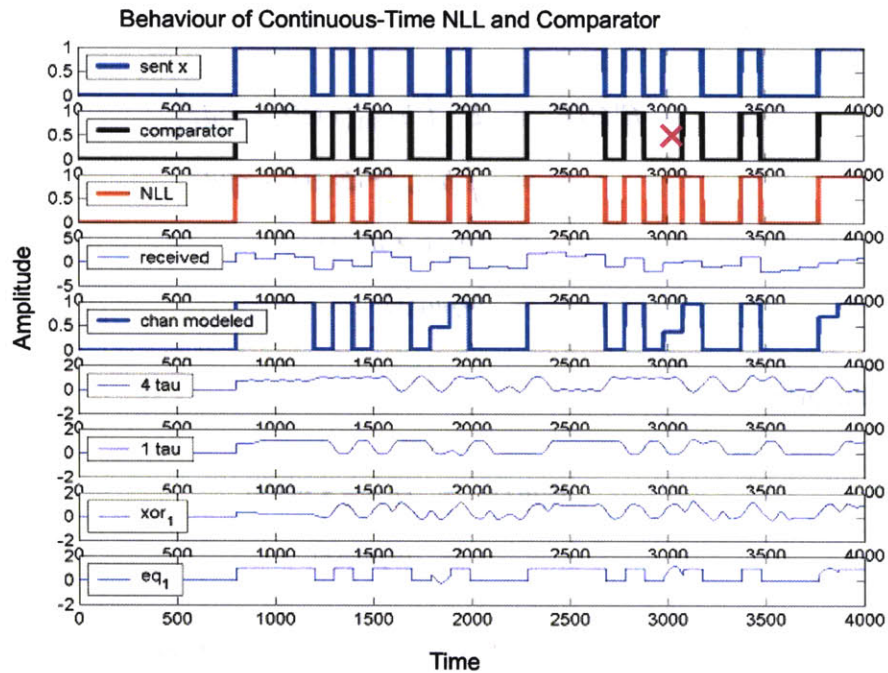


Figure 6-20: Performance of NLL and comparator to perform continuous-time estimation of transmit LFSR in AWGN. The comparator (second line) makes an error where the NLL (third line) does not. The top line shows the transmitted bits. The fourth line shows the received bits with AWGN. The fifth line shows the received bits after processing by the channel model. The other lines below show aspects of the internal dynamics of the NLL.

6-21 was able to perform both acquisition and tracking as shown by the third trace in figure 6-20. The CT NLL is bench-marked against a comparator. In the second line of figure 6-20 there is a red “x” that indicates where the comparator makes an incorrect estimate of the transmitter’s state. The CT NLL however properly guesses this same bit using the same received information. It is also obvious that this continuous-time NLL is properly tracking the transmitter, but it is not clear whether the dissipation necessary for entrainment is being provided by the soft-gates or by the smoothing in the FIR filters.

As we showed in equation (eq:log-likelihood-soft-equals), injection locking by summing a voltage into the receiver’s state is the probabilistically correct way to achieve maximum-likelihood synchronization in discrete-time. But is injection locking also

optimum in continuous-time? What is the connection between DT and CT estimation? The simulation shown in figure 6-20 assumes AWGN synchronous with and on the time scale of the bits. In the language we have been using, this is essentially “discrete-time noise.” Can injection locking also synchronize in the presence of continuous-time noise?

It is not obvious that injection locking would act as a good estimator in continuous-time, because there is a kind of contradiction in the system. In order to allow entrainment, the CT delay-lines (analog memory) in some sense need to accurately reproduce the waveform as it occurs within a single bit period, but in order to perform DT statistical estimation, the analog memory needs to average this waveform information away, retaining only the amplitude of the bit. The CT synchronization operates at a much finer time-scale than the DT statistical estimation, and these two time scales must be reconciled. The time scale is an outcome of the fact that we attempt to stay on a bit for some time and then transition quickly. Acquisition happens at the bit time-scale while tracking happens at the tracking time-scale.

If we use arbitrary low-pass filters with arbitrary phase-distortion in the transmitter system, the waveform produced will not have sharp bits and transitions. If we properly design the system for spread spectrum, then the waveform will behave across a wide range of time-scales. The distinction between bit and transition time scales then becomes less important. The synchronization error in such a fully continuous-time transmit-receive system can be quantified as the mean squared error between the transmitter and receiver signals.

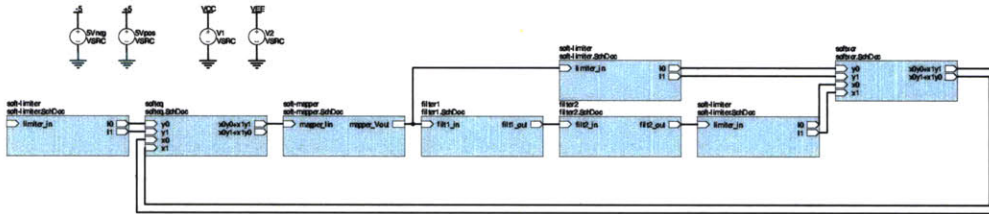


Figure 6-21: Block diagram of Spice model of noise lock loop (NLL) receiver system

Chapter 7

Systems

“Most verification of VLSI designs, synchronous and asynchronous, assumes discrete models discrete models for signal values and transition times. These discrete models lend themselves well to event-driven simulation, model checking, and theorem proving. However, many important circuit phenomenon cannot be modelled with discrete time and values, and failure to account for these phenomena can lead to faulty designs. These problems are especially apparent in the design of asynchronous circuits where computation is driven by internal events and not regulated by an external clock. This has led to many heuristic guidelines for designing such circuits referring to such things as “monotonic transitions,” “isochronic forks,” and debates of “interleaving semantics” versus “true concurrency.” Underlying these issues is a more basic question, “can discrete models of circuit behavior be based on a physically sound model of circuit behavior?” [17]

7.1 Extending Digital Primitives with Soft-Gates

We have seen that we can abstract the truth table of any digital logic gate into a probabilistic soft-gate. We might therefore be curious what would happen if we attempt to combine these probabilistic logic primitives to create probabilistic versions

of digital building blocks such as logic arrays, registers, multiplexers, etc. One way to look at these systems would be as simulating an ensemble of digital building blocks operating in noisy conditions. Future work will examine whether this way of thinking might point towards a useful methodology for studying lock-up, race conditions, and other results of asynchrony and noise in high-speed digital systems by performing efficient statistical simulations of the continuous-time analog dynamics of the circuits. To begin this investigation, let us start with a soft multiplexer, the “soft-MUX” and a soft flip-flop, the “soft-flip-flop.” These circuits have interesting and useful properties in their own right.

7.1.1 Soft-Multiplexer (soft-MUX)

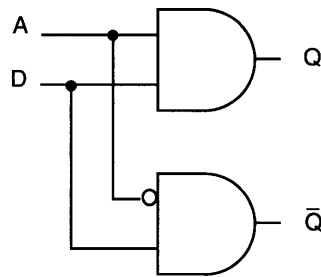


Figure 7-1: One bit multiplexer

A multiplexer is shown in figure 7-1. In digital logic, multiplexers provide routing functionality so that we can address digital signals to different outputs. By contrast, routing of analog signals is difficult. Transistors do not make very good analog switches. When they are on, they are not really on and often attenuate the signal. They also add noise to the signal. When they are off they are not really off and provide poor isolation by leaking.

The message from a soft-and gate with three connections x, y, z is

$$p_z(1) = p_x(1)p_y(1)$$

$$p_Z(0) = p_X(0)p_Y(0) + p_X(0)p_Y(1) + p_X(1)p_Y(0). \quad (7.1)$$

We might wonder what would happen if we build a multiplexer with soft-and gates instead of digital and gates. Could such a circuit be useful for routing analog signals? If we naively pursue such a circuit, we do get a circuit which passes the analog currents in an addressable manner. The addressed output produces a (normalized) copy of the input signal.

We find that the output from the other soft-and gate, however, has an output of $(p_Z(0) = 1, p_Z(1) = 0)$. This is not precisely what we want. We would like the gate that is off to output *nothing*, i.e. $(p_X(0) = .5, p_X(1) = .5)$. We can accomplish this with a modified soft-and gate that obeys the equation,

$$\begin{aligned} p_Z(1) &= p_X(1)p_Y(1) + p_X(0)p_Y(0) + p_X(0)p_Y(1) \\ p_Z(0) &= p_X(0)p_Y(0) + p_X(0)p_Y(1) + p_X(1)p_Y(0), \end{aligned} \quad (7.2)$$

Let x be the address signal and y be the data signal. Let us examine only one modified soft-and in the soft-multiplexer - say the one with the Q output in figure 7-1. If $x = 1$, then $p_X(0) = 0, p_X(1) = 1$ which means that the output of the soft-and gate mirrors the y input,

$$\begin{aligned} p_Z(1) &= p_Y(1) \\ p_Z(0) &= p_Y(0). \end{aligned} \quad (7.3)$$

But if $x = 0$, then $p_X(0) = 1, p_X(1) = 0$. This means that the other modified soft-and should be mirroring the data signal. The Q modified soft-and does the right thing.

$$\begin{aligned} p_Z(1) &= p_Y(0) + p_Y(1) = 1 \\ p_Z(0) &= p_Y(0) + p_Y(1) = 1. \end{aligned} \quad (7.4)$$

After normalization, this becomes $p_z(1) = .5, p_z(0) = .5$ which contains no information to effect further soft-gate computations downstream. The circuit in figure 7-2 implements the modified soft-and gate.

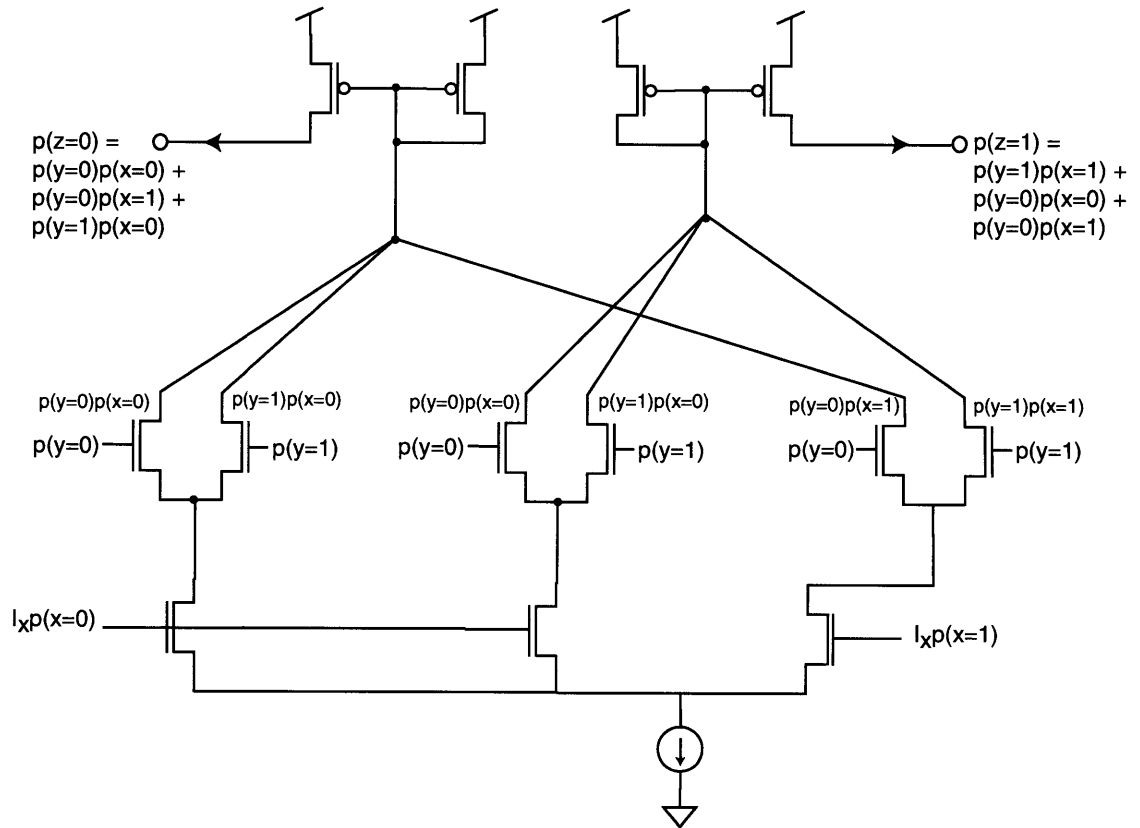


Figure 7-2: A modified soft-and gate for the soft-MUX

7.1.2 Soft Flip-Flop

In conventional digital logic circuits, memory is often implemented using “dynamic RAM” or shift registers which are composed of bistable circuits known as flip-flops. Figures 7-3, 7-4, and 7-5 show the schematic diagrams for several kinds of digital flip-flop. The simplest is known as an RS flip-flop. It is composed of two interconnected digital NAND gates. Its behavior for every possible input is enunciated in the truth table below.

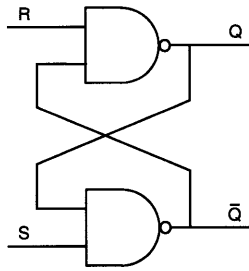


Figure 7-3: RS flip flop

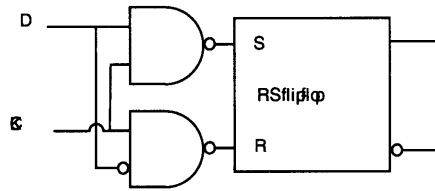


Figure 7-4: D flip-flop

R	S	Q	\bar{Q}
0	0	1	1
0	1	1	0
1	0	0	1
1	1	0/1	1/0

We define a “soft” RS-flip-flop as a conventional RS-flip-flop composed of two interconnected soft-NAND gates. The equation for a soft-NAND is

$$\begin{aligned}
 p_Z(1) &= p_X(0)p_Y(0) + p_X(0)p_Y(1) + p_X(1)p_Y(0) \\
 p_Z(0) &= p_X(1)p_Y(1).
 \end{aligned}
 \tag{7.5}$$

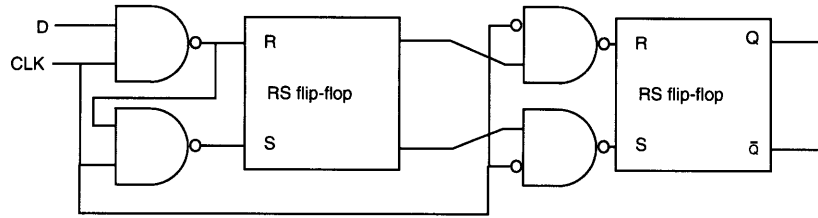


Figure 7-5: Edge-triggered D flip-flop

We might wonder if a flip-flop composed of soft-gates instead of digital logic gates might be useful as an analog memory element? Unfortunately this is not the case, as we might have realized upon further reflection. A bistable circuit like a flip-flop with a “W” shaped energy potential well is useful for storing digital information, precisely because it is digital information with two possible states. The bistable circuit remains in one state or the other until it receives enough energy to switch state across its threshold. By contrast an analog storage device would need many thresholds and a minima for every value that we would like to store. Since we would like to store at least 256 different levels for 8-bit accuracy in our analog circuits, such a circuit would be of much greater complexity than the soft-flip-flop. Such a circuit, if it were possible to construct one, would also not really be analog in the pure sense since it has discretized states. Instead it would really be a base-256 digital storage system.

The soft-RS-flip-flop actually does do something quite interesting, even if it may not be useful as an analog storage device. It acts as a digital flip-flop when the inputs are digital. The (un-normalized) behavior of the soft-RS-flip-flop with the internal feedback states initialized to (.5,.5) is summarized in the table below.

R	S	Q	\bar{Q}
.5	.5	$\bar{.6}$	$\bar{.6}$
0	0	1	1
0	1	1	0
1	0	0	1
1	1	.5	.5

If we normalize this we get

R	S	Q	\bar{Q}
.5	.5	.5	.5
0	0	1	1
0	1	1	0
1	0	0	1
1	1	.5	.5
.9	.1	.9	.1

The table above 7.1.2 is necessarily incomplete as the inputs (R, S) to the soft RS flip-flop can be any real valued numbers between $(0, 1)$. Figures 7-6, 7-7, and 7-8 below plots the behavior of the circuit in time given input values $(R, S) = (1, 1)$, $(1, 0)$, $(0, 1)$ and $(.5, .5)$ respectively. The internal feedback states are initialized to $(.5, .5)$ in each case.

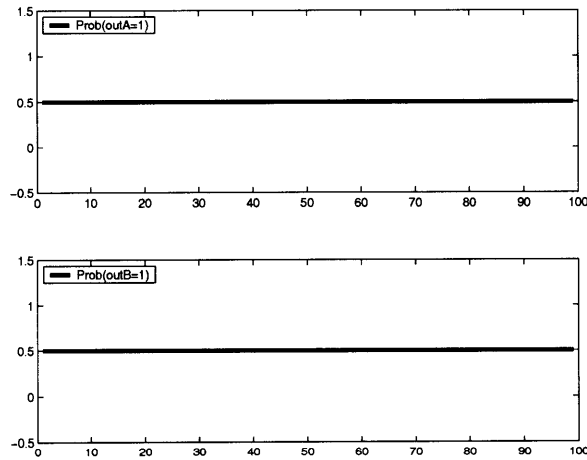


Figure 7-6: Time course of outputs Q and \bar{Q} with inputs $(R, S) = (1, 1)$ and initial internal states $= (.5, .5)$

We have been initializing the internal states to $(.5, .5)$, but this prevents us from seeing how the bi-stability of the soft RS flip-flop depends on the inputs. Figures 7-10, 7-11, and 7-12 below show the final output of the circuit for initial values of the internal state $(R, S) = (1, 1)$, $(1, 0)$, $(0, 1)$ and $(.5, .5)$. The x and y axes range over

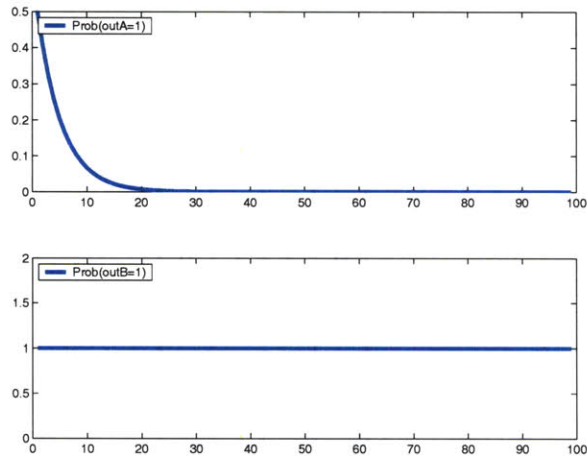


Figure 7-7: Time course of outputs Q and \bar{Q} with inputs $(R,S) = (1,0)$ and initial internal states $= (.5,.5)$

all possible values of the inputs (R,S) . It can be seen from these figures that, just as we would expect, the initial values of the internal state only matter when the the flip-flop is in its bi-stable "memory" state for which the inputs have no effect on the outputs. Because it is a soft flip-flop, there are values of the inputs (R,S) near this extreme where the inputs matter a bit, but the initialization of the internal states also matters. So it is possible to have the outputs be partially effected by the inputs and partially by the previous internal state.

The RS-flip-flop is a component in a D-flip-flop. A soft-D-flip-flop has very interesting behavior. By tuning the CLK input between 0 and 1, we can turn the bi-stability of the soft-D-flip-flop up and down. In effect the CLK line controls the height of the threshold peak in the middle of the "W" shaped energy potential. Even though soft-flip-flops do not act individually as static random-access memory (SRAM) for analog values, shift registers made of soft-slip-flops may still be promising as delay lines for analog signals.

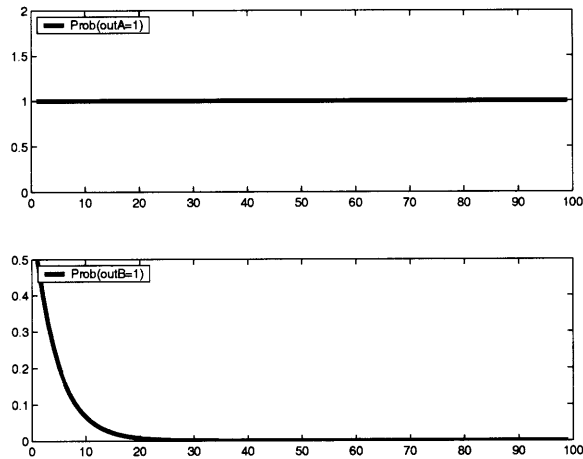


Figure 7-8: Time course of outputs Q and \bar{Q} with inputs $(R,S) = (0,1)$ and initial internal states $= (.5,.5)$

7.2 Application to Wireless Transceivers

7.2.1 Conventional Wireless Receiver

A conventional “digital” wireless front-end is illustrated in figure 7-15. The digital circuitry in a receiver can generally be divided into “fast” digital and “slow” digital. First the RF signal is demodulated using analog circuitry to produce the baseband signal. Then this information is over-sampled by the ADC in the front-end of a “fast” digital signal processor (DSP) chip. Statistical signal processing algorithms in this “fast” digital chip then infer the actual transmitted message from the encoded and corrupted baseband information. Baseband signal processing includes such operations as channel equalization, error correction, interference cancellation, and multiuser detection.

Once the transmitted message is extracted from the baseband signal, this lower bit-rate data stream can be passed to the “slow” digital part of the system which implements the interface between the received bits and the user as well as providing coordination and control of the receiver’s subsystems such as communication handshaking and protocols, the screen, keypad, speaker, microphone, etc. The “slow” digital performs less demanding tasks and therefore uses a lower complexity, less

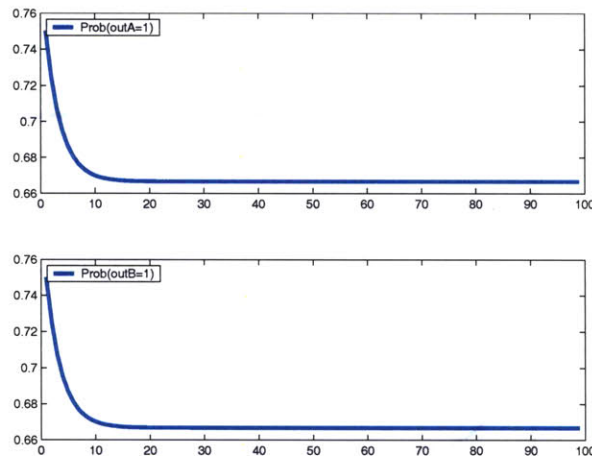


Figure 7-9: Time course of outputs Q and \bar{Q} with inputs $(R,S) = (.5,.5)$ and initial internal states $= (.5,.5)$

expensive, and lower power chip than the “fast” DSP. The “fast” digital signal processing system in a cell-phone handset is typically more than an order of magnitude more resource intensive than the “slow” digital.

A programmable array of analog CT statistical signal processing circuits could one day replace some or all of the “fast” digital in a conventional data wireless receiver, and could enable much higher processing speeds. Figure 7-16 shows a conceptual sketch of reconfigurable analog signal processing circuits, much like programmable logic blocks. The result would be a “software” radio implemented with programmable analog hardware.

The ability to perform decoding operations at demodulation frequencies (Gbits/second) could change the entire design of wireless receivers and protocols in significant ways. We could speculate, for example, that programmable CT analog VLSI used in this context could replace demodulation entirely. This could eliminate the necessity to use sinusoidal carriers at all since the power spectrum of the transmitted signal could be matched to an arbitrary channel by the proper encoding. Without sinusoidal carriers, a receiver would no longer be shackled to a front-end designed for a particular set of carrier signals. In turn, this would lead to a large increase in the inter-operability of diverse wireless systems - the so-called “tower of Babel problem”

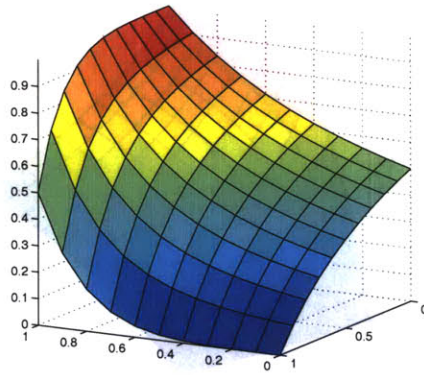


Figure 7-10: Map of final output Q for all possible inputs (R,S) and initial internal states = $(1,1)$

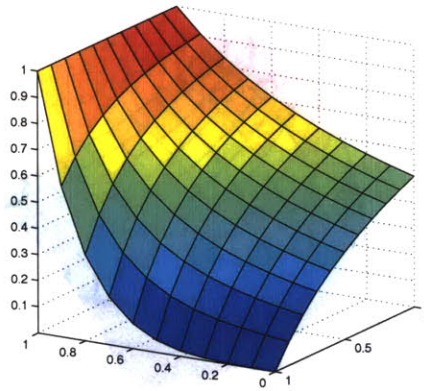


Figure 7-11: Map of final output Q for all possible inputs (R,S) and initial internal states = $(0,1)$

for wireless transceivers. A wireless transceiver could learn to “speak the right language” in order to communicate with a newly encountered transmitter. Solving the wireless “tower of Babel” problem would be significant, because it could allow a roaming device to bargain for connectivity with any networked wireless base station in its vicinity, making wireless access much more ubiquitous. The internet revolutionized the desktop by exploiting the ubiquity of personal computers and phone lines. According to many industry analysts, ubiquitous multi-protocol wireless could lead to a similar revolution for mobile devices and the telecommunications industry [23].

Less speculatively, high-speed analog circuits performing statistical estimation

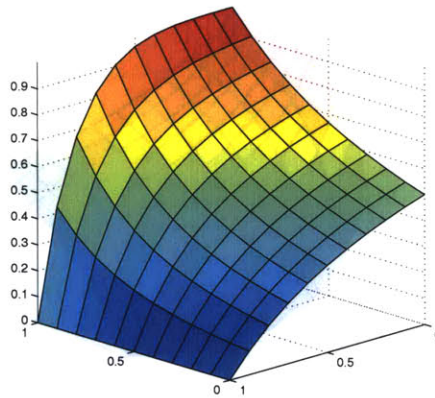


Figure 7-12: Map of final output Q for all possible inputs (R,S) and initial internal states = $(1,0)$

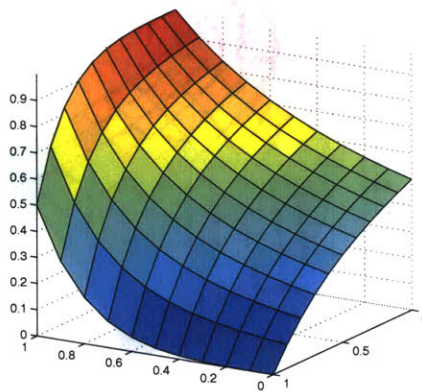


Figure 7-13: Map of final output Q for all possible inputs (R,S) and initial internal states = $(0,0)$

could perform signal processing on conventional carrier or intermediate frequency (IF) signals. The resulting estimates of interference and spectrum availability in the channel could be used to tune filter and amplifier parameters in the analog front-end of a conventional radio.

7.2.2 Application to Time-Domain (Pulse-based) Radios

The first radio was built by Guglielmo Marconi in 1894 when he was 21 years old. It was a spark gap radio. The transmitter produced a high-voltage spark. A spark,

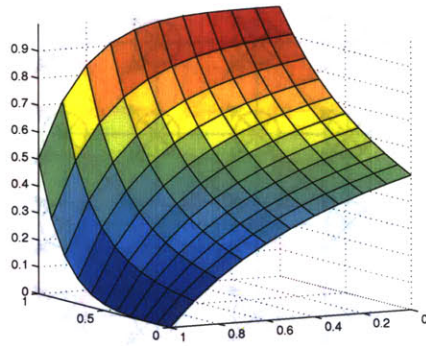


Figure 7-14: Map of final output Q for all possible inputs (R,S) and initial internal states = (.5,.5)

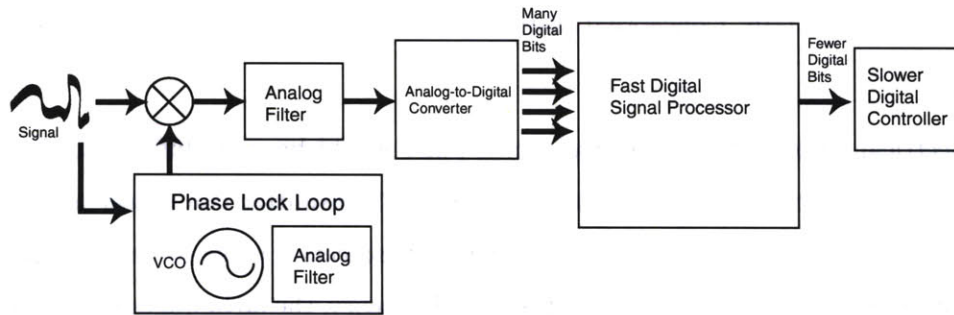


Figure 7-15: Conventional radio receiver signal chain

since it is a delta in time, has a very wide frequency range. Marconi's sparks had high enough frequency components to radiate from the antenna and be received at distances of thousands of miles. The very success of a high-powered spark to radiate great distances on a wide-frequency range also led to its demise. A pure spark based radio made it impossible for any other spark radio to operate within its transmission radius. By the mid-twentieth century, the spark gap radio had been largely abandoned in favor of radios based on sinusoidal oscillators which allowed multiple users to communicate simultaneously without interfering with one another.

But the demise of the pulse based radio was only temporary. In recent years, the emergence of inexpensive high speed signal processors with exquisite timing accuracy has led to a revival of the spark based radio idea. Often known as ultra-wideband, the idea is that a microprocessor can open and close a switch to produce a tiny

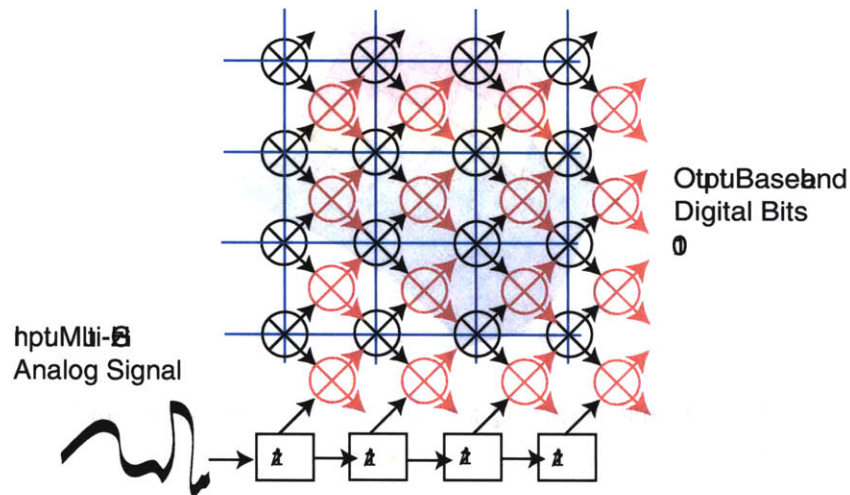


Figure 7-16: Conceptual sketch of CT softgate array in a radio receiver

electrical spike or pulse. A single such pulse would be very difficult to detect, but a receiver microprocessor synchronized to the transmitter can detect a sequence of such pulses by closing its switch only when it expects a pulse to be transmitted and correlating over a long sequence of pulses. In theory, the advantages of such a system would be extremely low hardware complexity, it would consist purely of a digital microprocessor and digitally controlled pulse generating or receiving switch. Multiple users could be accommodated by, for example, time interleaving of pulses intended for different users.

The reality has not been so elegant and these pulse-based radios have encountered exactly the same problem as the first spark radios - the pulses produce wide-band radio energy that have the dangerous (and possibly unpredictable) potential to interfere with other essential wireless services such as GPS. Solutions to this problem have so far primarily focused on filtering the shape of the pulses so that they fit within a required spectral envelope. Pulses in modern ultra-wideband systems are intended to last on the order of $.1ns$, enabling communication at frequencies up to 10GHz. At these frequencies, real-world indoor and outdoor channels disperse the pulses. Furthermore, a slight change in the relative positions of reflectors can have a large effect on the extremely short wavelength, high-frequency components that are present

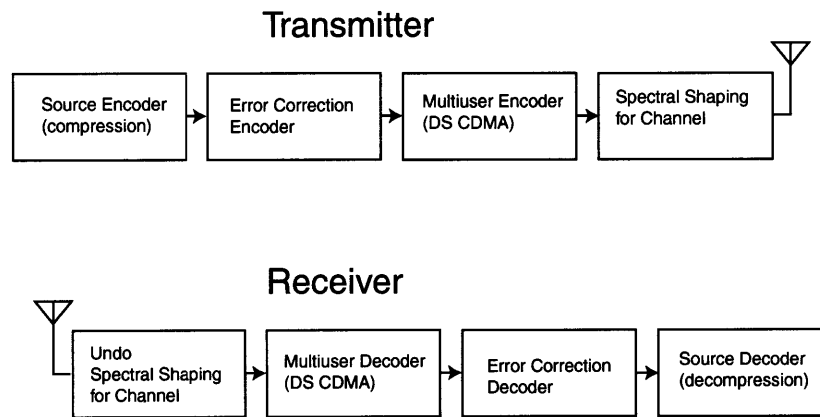


Figure 7-17: Time-domain (pulse) radio communications system

in the pulse. This sensitivity to the spatial relations of the channel reflectors, requires that the channels be modelled as time-varying. The receiver in such a system must be equipped with complex time-domain signal processing at very high frequencies to decode high data-rate transmissions. Unfortunately, there has not a practical scheme for performing such high-speed decoding operations with practical receiver hardware. Until now.

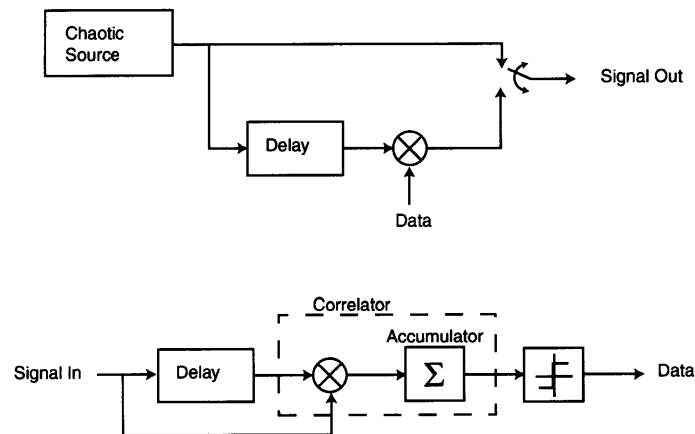


Figure 7-18: Chaotic communications system proposed by Mandal et al. [30]

The beginnings of an idea are present in the chaotic communication literature. Mandel et al. proposed a transmitter based on a controlled chaotic system and

a receiver with a correlator as shown in figure 7-18 [30]. They called this scheme modified differential chaos shift keying (M-DCSK).

M-DCSK is a novel scheme for spread spectrum communication using chaotic signals. It relies upon using a chaotic signal as the spreading sequence, instead of the more conventional PN-sequences. The advantage of such a system is that of simplicity and true randomness of the spreading sequence; the disadvantage is that it is very difficult to recreate and synchronize the spreading sequence at the receiver end. To avoid this problem, DCSK uses a transmitted reference system where for half a bit period, a reference chaotic waveform is transmitted; then another half bit period is transmitted, which is either the same as the reference waveform (if the bit is a '0') or it's inverted version (if the bit is a '1'). A transmitted reference system intrinsically has a higher error probability than a stored reference system such as CDMA; this is because in such a system, the reference itself is transmitted over a noisy channel and suffers from quality degradation. Nevertheless, previous experiments with DCSK have shown bit-error-rate (BER) performance approaching conventional systems especially at low values of SNR.

They recognize that synchronization is an important consideration in such a scheme.

“For this to work in practice, the clock at the receiver must be synchronized to the transmitted clock. In commercial spread spectrum systems, chip clock recovery is generally done in two stages: a coarse synchronization known as acquisition, which aligns the waveforms to within one chip period, and a fine synchronization known as tracking, which corrects remaining timing errors between the two waveforms. Tracking is generally done using a Delay Locked Loop (DLL). Since there was insufficient time to build a chip synchronization unit in this case, the receiver block uses

the same base clock as the transmitter. This is, however, not a major limitation, since the system being built is an experimental/ proof-of-concept one.”

There is actually a deep reason why synchronization and pulse shaping are salient issues in pulse-based radios. Pulse radios are essentially the Fourier transform of conventional sinusoidal radios. Therefore the purposes of this discussion, I call pulse-based radios, time-domain radios, and I call conventional sinusoidal-based radios, frequency-domain radios. Frequency-domain radios employ a delta in frequency, while pulse-based time-domain radios employ delta's in time. (DS/CDMA should also be properly considered time-domain radio, but it uses a pseudo-random bit stream to produce a wideband frequency spectrum instead of short pulses.) The frequency-time translation carries over to issues in hardware design. Every difficulty in controlling frequency in a frequency-domain radio rears its head as a difficulty with controlling timing in a time-domain radio. For example, local high-frequency oscillators with good phase-stability are difficult to build in frequency-domain radios. In time-domain radios, delay-lines with stable delay-times are challenging to build. Making good receiver filters to detect particular frequencies translates into requiring good receiver synchronization to pick out particular instants in time. Making good filters and designing modulation schemes using oscillators to shape the transmitted spectral envelope translates into controlling timing and designing sequences which accomplish this same end in the time domain. Since time-domain signal processing has traditionally been the domain of digital signal processors, time-domain radios have not been able to overcome these hurdles cost-effectively at high-frequencies. In fact, in the commercialization of ultra-wideband wireless systems, sinusoidal based radios seem poised to win yet again. The technology presented in this dissertation, however, seems uniquely suited to solve precisely the problem of high-speed low-power analog circuits for time-domain statistical signal processing.

Chapter 8

Biographies

8.1 Anantha P. Chandrakasan, MIT EECS, Cambridge, MA

Anantha P. Chandrakasan received B.S, M.S. and Ph.D. degrees in Electrical Engineering and Computer Sciences from the University of California, Berkeley, in 1989, 1990, and 1994 respectively. Since September 1994, he has been at the Massachusetts Institute of Technology, Cambridge, and is currently an Associate Professor of Electrical Engineering and Computer Science. He held the Analog Devices Career Development Chair from 1994 to 1997. He received the NSF Career Development award in 1995, the IBM Faculty Development award in 1995 and the National Semiconductor Faculty Development award in 1996 and 1997. He is a Co-founder and Chief Scientist at Engim, a company focused on high-performance wireless communications.

He has received several best paper awards including the 1993 IEEE Communications Society's Best Tutorial Paper Award, the IEEE Electron Devices Society's 1997 Paul Rappaport Award for the Best Paper in an EDS publication during 1997 and the 1999 Design Automation Conference Design Contest Award.

His research interests include the ultra low power implementation of custom and programmable digital signal processors, distributed wireless sensors, multimedia devices, emerging technologies, and CAD tools for VLSI. He is a co-author "Low Power Digital CMOS Design" by Kluwer Academic Publishers and "Digital Integrated Circuits" (second edition) by Prentice-Hall. He is also a co-editor of "Low Power CMOS Design" and "Design of High-Performance Microprocessor Circuits" from IEEE press.

He has served on the technical program committee of various conferences including ISSCC, VLSI Circuits Symposium, DAC, and ISLPED. He has served as a technical program co-chair for the 1997 International Symposium on Low-power Electronics and Design (ISLPED), VLSI Design '98, and the 1998 IEEE Workshop on Signal Processing Systems, and as a general co-chair of the 1998 ISLPED. He was an associate editor for the IEEE Journal of Solid-State Circuits from 1998 to 2001. He

served as an elected member of the Design and Implementation of Signal Processing Systems (DISPS) Technical Committee of the Signal Processing Society and serves on the SSCS AdCOM. He was the Signal Processing Sub-committee chair for ISSCC 1999 through 2001, the program vice-chair for ISSCC 2002, the technical program chair for ISSCC 2003.

8.2 Hans-Andrea Loeliger, ETH, Zurich, Switzerland

Hans-Andrea Loeliger has been full Professor of Signal Processing at the Signal Processing Laboratory of ETH Zurich since June 2000. He studied Electrical Engineering at ETH Zurich, and there he also received the Ph.D. degree in 1992. He then joined Linköping University, Sweden, as assistant professor (“forskarassistent”). In 1995, he returned to Switzerland and (together with Felix Tarky) founded the consulting company Endora Tech AG, Basel, with which he remained until his return to ETH.

His research focuses on error correcting codes and coded modulation, modelling and analysis of signals and systems, and robust nonlinear analog computation networks. His research interests include Information theory and its applications in communications and signal processing Error correcting codes and coded modulation schemes Digital signal processing in communications, acoustics, and other fields Graphical models (“factor graphs”) for coding and signal processing Signal processing with robust nonlinear analog networks (“analog decoder”).

8.3 Jonathan Yedidia, Mitsubishi Electronics Research Lab, Cambridge, MA

Jonathan Yedidia’s graduate work at Princeton (1985-1990) and post-doctoral work at Harvard’s Society of Fellows (1990-1993) focused on theoretical condensed-matter physics, particularly the statistical mechanics of systems with quenched disorder. From 1993 to 1997, he was a professional chess player and teacher. He then worked at the internet startup company Viaweb, where he helped develop the shopping search engine that has since become Yahoo’s shopping service. In 1998, Dr. Yedidia joined the Mitsubishi Electric Research Laboratory (MERL)Cambridge Research Laboratory. He is particularly interested in the development of new methods to analyze graphical models. His work has applications in the fields of artificial intelligence, digital communications, and statistical physics.

Most of Yedidia’s current research involves the application of statistical methods to “inference” problems. Some important fields which are dominated by the issue of inference are computer vision, speech recognition, natural language processing, error-correction, and diagnosis. Essentially, any time you are receiving a noisy signal, and need to infer what is really out there, you are dealing with an inference problem. A productive way to deal with an inference problem is to formalize it as a problem of

computing probabilities in a graphical model. Graphical models, which are referred to in various guises as “Markov random fields,” “Bayesian networks,” or “factor graphs,” provide a statistical framework to encapsulate our knowledge of a system and to infer from incomplete information.

Physicists who use the techniques of statistical mechanics to study the behavior of disordered magnetic spin systems are actually studying a mathematically equivalent problem to the inference problem studied by computer scientists, but with different terminology, goals, and perspectives. Yedidia’s own research has focused on the surprising relationships between methods that are used in the two communities, and on powerful new techniques and algorithms that exploit those relationships. A major current project involves analyzing and designing error-correcting codes using generalized belief propagation algorithms.

8.4 Neil Gershenfeld, MIT Media Lab, Cambridge, MA

Professor Neil Gershenfeld is the Director of MIT’s Center for Bits and Atoms, an interdisciplinary initiative that is broadly exploring how the content of information relates to its physical representation, from atomic nuclei to global networks. CBA’s intellectual community and research resources cut across traditional divisions of inquiry by disciplines and length scales in order to bring together the best features of the bits of new digital worlds with the atoms of the physical world. Dr. Gershenfeld has also led the Media Lab’s Things That Think industrial research consortium, which pioneered moving computation out of conventional computers and into the rest of the world, and works with the Media Lab Asia on coordinating the technical guidance for this ambitious international effort based in India that is investigating technology for global development. His own laboratory studies fundamental mechanisms for manipulating information (which led to the development of molecular logic used to implement the first complete quantum computation and to analog circuits that can efficiently perform optimal digital operations), the integration of these ideas into everyday objects such as furniture (seen in the Museum of Modern Art and used in automobile safety systems), and applications with partners ranging from developing a computerized cello for Yo-Yo Ma and stage for the Flying Karamazov Brothers to instrumentation used by rural Indian villagers and nomadic reindeer herders. Beyond his many technical publications and patents, he is the author of best-selling books including “When Things Start To Think” and the texts “The Nature of Mathematical Modelling” and “The Physics of Information Technology.” His work has been featured by the White House and Smithsonian Institution in their Millennium celebrations, and been the subject of print, radio, and TV programs in media including the New York Times, The Economist CNN, and PBS.

Dr. Gershenfeld has a B.A. in Physics with High Honors from Swarthmore College, was a member of the research staff at Bell Labs where he studied laser interactions with atomic and nuclear systems, received a Ph.D. in Applied Physics from Cornell

University for experimental tests of order in complex condensed matter systems, and was a Junior Fellow of the Harvard Society of Fellows where he ran an international study on prediction techniques.

8.5 Biography of Author



Figure 8-1: Benjamin Vigoda

Benjamin Vigoda is an PhD candidate and Intel Fellow in the Center for Bits and Atoms at the MIT Media Laboratory. His research has been at the boundary of machine learning and wireless communication systems.

While at the Media Lab, Vigoda helped found the Thinkcycle.org and the Design that Matters studio seminar, which have had great success bringing engineering students together to work on technical problems posed by NGO's serving under-served communities across the world. He also created a shadow juggling system which now tours on stage with a vaudeville juggling troupe, the Flying Karamazov Brothers as well as a number of other technologically enhanced musical instruments.

Ben earned his undergraduate degree in physics from Swarthmore College in 1996. He has worked at the Santa Fe Institute on alternative models of computation, and at Hewlett Packard Labs where he helped transfer academic research to product divisions. He won second place in the MIT \$50K Entrepreneurship Competition and first in the Harvard Business School Competition using a business plan based on this PhD research.

Bibliography

- [1] K. Abend and B. D. Fritchman (May 1970). Statistical Detection for Communication channels with intersymbol interference. *Proc. IEEE*, vol. 58, pp. 779–785
- [2] P. Bardell, W. McAnney, and S. Jacob (1987). *Built-In Test for VLSI: Pseudorandom Techniques*. New York, NY: John Wiley and Sons.
- [3] S. E. Bensley and B. Aazhang (1998). Maximum Likelihood Synchronization of a Single User for Code Division Multiple Access Communication Systems. *IEEE Transactions on Communications*, COM-46, no. 3, pp. 392–399
- [4] Rafael J. Betancourt-Zamora, Shwetabh Verma and Thomas H. Lee (2001). 1-GHz and 2.8-GHz CMOS Injection-locked Ring Oscillator Prescalers. *2001 Symposium on VLSI Circuits, Kyoto, Japan, June 14, 2001*, pp. 47–50
- [5] G. Cauwenberghs (1995). Micropower CMOS Algorithmic A/D/A Converter. *IEEE Transactions on Circuits and Systems I: Fundamental Theory and Applications*, Vol. 42, No. 11, pp. 913–919
- [6] H. C. Casey, Jr. (May 1998). Supplemental Chapter to Introduction to Silicon and III-V Compound Semiconductor Devices for Integrated Circuits. *Department of Electrical and Computer Engineering Duke University*
- [7] K. M. Cuomo and Alan V. Oppenheim (Jul. 1993). Circuit Implementation of Synchronized Chaos with Applications to Communications. *Physical Review Letters*, 1993, Vol. 71, No. 1.
- [8] Jie Dai (Aug. 2002). Doctoral Dissertation: Design Methodology for Analog VLSI Implementations of Error Control Decoders. Salt Lake City, Utah: University of Utah.
- [9] A. S. Dmitriev, A. I. Panas, S. O. Starkov (Oct. 2001). Direct Chaotic Communication in Microwave Band.
- [10] Andreas Demosthenous and John Taylor (Feb. 2001). A 100Mb/s, 2.8V CMOS Current-Mode Analogue Viterbi Decoder. *IEEE Trans. Inform. Theory*, vol. 47, pp. 520–548

- [11] Jose E. Franca and Yannis Tsividis (1994). Design of Analog-Digital VLSI Circuits for Telecommunications and Signal Processing, second ed. Englewood Cliffs, NJ: Prentice Hall.
- [12] M.A. Franklin and T. Pan (Nov. 1994). Performance Comparison of Asynchronous Adders. *Proceedings of the International Symposium on Advanced Research in Asynchronous Circuits and Systems, 1994*, pp. 117–125
- [13] G. D. Forney (Feb. 2001). Codes on Graphs: Normal Realizations. *IEEE Trans. Inform. Theory*, vol. 47, pp. 520–548
- [14] Neil Gershenfeld and Geoff Grinstein (1995). Entrainment and Communication with Dissipative Pseudorandom Dynamics. *Physical Review Letters*, 74, pp. 5024
- [15] Neil Gershenfeld (1999). *The Nature of Mathematical Modeling*. Cambridge, UK: Cambridge University Press.
- [16] T. R. Giallorenzi and S.G. Wilson (Sept. 1996). Suboptimum Multiuser Receivers for Convolutionally Coded Asynchronous DS-CDMA Systems. *IEEE Transactions on Communications*, 44, pp. 1183–1196
- [17] M.R. Greenstreet and P. Cahoon (Nov. 1994). How Fast Will the Flip Flop? *Proceedings of the International Symposium on Advanced Research in Asynchronous Circuits and Systems, 1994*, pp. 77–86
- [18] David J. Griffiths (1995). *Introduction to Quantum Mechanics*. Upper Saddle River, NJ: Prentice Hall.
- [19] J. Hagenauer (Feb. 1998). Decoding of Binary Codes with Analog Networks. *Proc. 1998 Information Theory Workshop, San Diego, CA, Feb. 811*, pp. 1314.
- [20] J. Hagenauer and M. Winklhofer (Feb. 1998). The Analog Decoder. *Proc. 1998 IEEE Int. Symp. on Information Theory, Cambridge, MA USA, Aug. 1621*, p. 145.
- [21] Gunhee Han and Edgar Sanchez-Sinencio (Dec. 1998). CMOS Transconductance Multipliers: A Tutorial. *IEEE Transactions on Circuits and Systems II: Analog and Digital signal Processing*, VOL.45, NO.12
- [22] Tom Heskes (2002). Stable fixed points of belief propagation are minima of the Bethe free energy. *Proceedings of Neural Information Processing, 2002*
- [23] Erika Jonietz (Dec. 2001). Community-Owned Wireless Networks Are Gaining Popularity and Could Help Bridge the Digital Divide. *Innovation: Unwiring the Web Technology Review, December 2001*
- [24] Tobias Koch. Advisor: Justin Dauwels, Matthias Frey and Patrick Merkli in collaboration with Benjamin Vigoda (Feb. 2003). Continuous-Time Synchronization. Zurich, Switzerland. Semester Project at Institute for Signals and Information (ISI), ETH.

- [25] Ed. H. S. Leff and A. F. Rex (Jan. 1990) *Maxwell's Demon: Entropy, Information, Computing* Washington State, USA: Institute of Physics Publishing.
- [26] H. Li (Mar. 2001). Building a Dictionary for DNA: Decoding the Regulatory Regions of a Genome. *Institute for Theoretical Physics (ITP) Program on Statistical Physics and Biological Information*
- [27] Douglas Lind and Brian Marcus (Dec. 1995). *An Introduction to Symbolic Dynamics and Coding*. New York, NY: Cambridge University Press
- [28] Frank R. Kschischang, Brendan J. Frey and Hans-Andrea Loeliger (Feb. 2001). Factor Graphs and the Sum-Product Algorithm. *IEEE Transactions on Information Theory*, 47:2, pp. 498–519
- [29] Felix Lustenberger (Nov. 2000) Doctoral Dissertation: On the Design of Analog VLSI Iterative Decoders Zurich, Switzerland: Swiss Federal Institute of Technology (ETH).
- [30] Soumyajit Mandal and Soumitro Banerjee (2003). Analysis and CMOS Implementation Of A Chaos-based Communication System. *IEEE Transactions on Circuits and Systems I*,
- [31] G. J. Minty. (1957). A Comment on the Shortest-Route Problem. *Operational Research*, vol. 5, p. 724
- [32] Andreas F. Molisch (2001). *Wideband Wireless Digital Communications*. Upper Saddle River, NJ: Prentice-Hall
- [33] S.V. Morton, S.S. Appleton, and M.J. Liebelt (Nov. 1994). An Event Controlled Reconfigurable Multi-Chip FFT. *Proceedings of the International Symposium on Advanced Research in Asynchronous Circuits and Systems, 1994*, pp. 144–153
- [34] Jan Mulder, Wouter Serdijn, Albert C. van der Woerd, Arthur H.M. van Roermund (1999). *Dynamic Translinear and Log-Domain Circuits*. Boston, Ma: Kluwer Press
- [35] Alison Payne, Apinunt Thanachayanont, and C. Papavassiliou (Sept. 1998). A 150-MHz Translinear Phase-Locked Loop. *IEEE Transactions on Circuits and Systems II: Analog and Digital signal Processing*, Vol.45, No.9
- [36] L. M. Pecora and T. L. Carroll (1990). Synchronization in Chaotic Systems. *Physical Review Letters*, vol. 64, pp. 821–824
- [37] John G. Proakis (2001). *Digital Communications*. Boston, MA: McGraw-Hill
- [38] L. R. Rabiner and B. H. Juang (Jan. 1986). An Introduction to Hidden Markov Models. *IEEE ASSP Magazine*, pp. 4-15

- [39] Mark C. Reed (Oct. 1999) *Doctoral Dissertation: Iterative Receiver Techniques for Coded Multiple Access Communication Systems* School of Physics and Electronics Systems Engineering, University of South Australia.
- [40] P. V. Rooyen, M. Lotter, D. v. Wyk. (2000). *Space-Time Processing for CDMA Mobile Communications*. Norwell, MA: Kluwer Academic Publishers.
- [41] Rahul Sarpeshkar. (Apr. 1997) *Doctoral Dissertation: Efficient Precise Computation with Noisy Components: Extrapolating From an Electronic Cochlea to the Brain* Pasadena, CA: California Institute of Technology (CalTech).
- [42] Evert Seevinck (1999). *Analysis and Synthesis of Translinear Integrated Circuits*. Amsterdam, Netherlands: Elsevier Press
- [43] M.H. Shakiba, D.A. Johns and K.W. Martin. (Dec. 1998). BiCMOS Circuits for Analog Viterbi Decoders. *IEEE Trans. on Circuits and Systems - II: Analog and Digital Signal Processing*, VOL.45, pp. 1527-1537.
- [44] S. Sheng and R. Brodersen. (1998). *Low-Power CMOS Wireless Communications: A Wideband CDMA System Design*. Boston, MA: Kluwer Academic Publishers.
- [45] Semiconductor Industry Association. (2002). International Technology Roadmap for Semiconductors, 2001. *SEMATECH* <http://public.itrs.net/Reports.htm>
- [46] A.C. Singer and A.V. Oppenheim. (1999). Circuit Implementations of Soliton Systems. *International Journal of Bifurcation and Chaos*, Vol. 9, No. 4, pp. 571–590.
- [47] Robert H. Walden.(Feb. 1999). Performance Trends for Analog-to-Digital Converters. *IEEE Communications Magazine*, pp. 96–101
- [48] Remco J. Wiegink (1993). *Analysis and Synthesis of MOS Translinear Circuits*. Boston, Ma: Kluwer Press
- [49] Sergio Verd.(Jan. 1986). Minimum Probability of Error for Asynchronous Gaussian Multiple Access Channels. *IEEE Trans. on Info. Theory*, pp. 85–96
- [50] Sergio Verd. (Jan. 1989). Computational Complexity of Optimum Multiuser Detection. *Algorithmica* Vol. 4, No. 3, pp. 303–312
- [51] Sergio Verd (1998). *Multiuser Detection*. New York, NY: Cambridge University Press
- [52] Benjamin Vigoda, Justin Dauwels, Neil Gershenfeld, and Hans-Andrea Loeliger. (In Press). Low-Complexity LFSR Synchronization by Forward-Only Message Passing. *Submitted to IEEE Transaction on Information Theory*
- [53] A.J. Viterbi (1995). *CDMA, Principles of Spread Spectrum Communication*. Reading, MA: Addison-Wesley Longman Inc.

- [54] Glenn Watanabe, Henry Lau and Juergen Schoepf. (Aug. 2000). Integrated Mixer Design. *Proceedings of the Second IEEE Asia-Pacific Conference on ASIC*
- [55] J. S. Yedidia, W. T. Freeman and Y. Weiss. (2001). Understanding Belief Propagation and Its Generalizations. *published as chapter 8 of 'Exploring Artificial Intelligence in the New Millennium eds. G. Lakemeyer and B. Nebel, pp. 239-269, Morgan Kaufmann 2003*
- [56] J. S. Yedidia, W. T. Freeman and Y. Weiss. (Apr. 2002). Constructing Free Energy Approximations and Generalized Belief Propagation Algorithms.